

Hydro- meteorological functioning of tropical montane cloud forests in the Orinoco River basin

Beatriz Helena Ramírez Correal

Propositions

1. The main hydrological impact of land-use change in tropical montane cloud forests is changing soil-water storage that originates from the organic layer removal.
(this thesis)
2. A decrease in fog persistence threatens tropical montane cloud forests by increasing potential evaporation and not by reducing water inputs by fog.
(this thesis)
3. Uncertainty estimates are the best allies when confronted with limited budgets for experimental studies in logistically complex areas.
4. Field work is not only about collecting data but also about experiencing and understanding the broader context in which research is embedded.
5. If lay-people misunderstand scientific uncertainties, scientific knowledge will remain equitable to alternative facts.
6. Nature conservation should focus on the right actions for the right reasons.

Propositions belonging to the thesis entitled:

'Hydro-meteorological functioning of tropical montane cloud forests in the Orinoco River basin'

Beatriz Helena Ramírez Correal
Wageningen, 30 January 2018.

**Hydro-meteorological functioning of tropical
montane cloud forests in the Orinoco River
basin**

Beatriz Helena Ramírez Correal

Thesis committee

Promotor

Prof. Dr R. Leemans
Professor of Environmental Systems Analysis
Wageningen University & Research

Co-promotors

Dr L.N. Ganzeveld
Assistant professor, Meteorology and Air Quality
Wageningen University & Research

Dr A.J. Teuling
Associate professor, Hydrology and Quantitative Water Management
Wageningen University & Research

Other members

Prof. Dr V. Geissen, Wageningen University & Research
Dr I. van Meerveld, University of Zurich, Switzerland
Prof. Dr J. Bendix, University of Marburg, Germany
Prof. Dr M. van Noordwijk, World Agroforestry centre (ICRAF), Bogor,
Indonesia

This research was conducted under the auspices of the Graduate School for
Socio-Economic and Natural Sciences of the Environment (SENSE)

Hydro-meteorological functioning of tropical montane cloud forests in the Orinoco River basin

Beatriz Helena Ramírez Correal

Thesis

submitted in fulfilment of the requirements for the degree of doctor
at Wageningen University
by the authority of the Rector Magnificus,
Prof. Dr A.P.J. Mol,
in the presence of the
Thesis Committee appointed by the Academic Board
to be defended in public
on Tuesday 30 January 2018
at 4 p.m. in the Aula.

Beatriz Helena Ramírez Correal
Hydro-meteorological functioning of tropical montane cloud forests in the Orinoco
River basin
210 pages

PhD thesis, Wageningen University, Wageningen, NL (2018)
With references, with summary in English

ISBN 978-94-6343-215-3

DOI 10.18174/424868

Table of contents

Chapter 1. Introduction	8
1.1. Hydrology under climate and land cover change	8
1.2. Why the Orinoco River basin?	10
1.3. Tropical Montane Cloud Forest hydrological functioning	12
1.4. Research objective and questions	17
1.5. Thesis outline	18
Chapter 2. Tropical Montane Cloud Forests: Hydro-meteorological variability in three neighbouring catchments with different forest cover	24
2.1 Introduction	26
2.2 Materials and Methods	31
2.3 Results	45
2.4 Discussion	59
2.5 Conclusions	67
Appendix 2A	69
Chapter 3. Tropical Montane Cloud Forests in the Orinoco River basin: The role of soil organic layers in water storage and release	72
3.1 Introduction	74
3.2 Materials and Methods	78
3.3 Results	86
3.4. Discussion	99
3.5 Conclusions	104
Chapter 4. Tropical Montane Cloud Forests in the Orinoco River basin: Inferring fog interception from through-fall dynamics	110
4.1. Introduction	112
4.2. Materials and methods	116
4.3. Results	132
4.4. Discussion	144
4.5. Conclusions	148
Appendix 4A	150
Chapter 5. Synthesis	154
5.1. Seasonal and spatial hydro-meteorological variability effects on streamflows	155
5.2. Land-cover effects on streamflows	157
5.3. Closing the water budgets	158
5.4. Dry season effects on moisture	160
5.5. Land-cover change impacts on streamflows	162
5.6. Conclusions	165
Chapter 6. Outlook	170
6.1. Future Research	170
6.2. Connecting with decision-making processes	174
Summary	181
References	185



CHAPTER 1

Introduction

Chapter 1

Introduction

1.1. Hydrology under climate and land cover change

Water fluxes across the Earth's surface-atmosphere interface are largely driven by the Earth's energy budget. Changes in this budget are mainly caused by atmospheric greenhouse gas accumulation and land-cover change. On the one hand, the accumulated greenhouse gases increase temperatures and this intensifies the global water cycle, expressed through more pronounced evaporation and precipitation patterns (Durack et al., 2012). On the other hand, land-cover changes affect surface-water fluxes as these are strongly controlled by vegetation. In this case, land-cover change includes both the changes caused by a shift in land-use and the changes derived from, for example, natural disturbances or natural regeneration. The changes in atmospheric temperature and land-cover affect water fluxes and biogeochemical cycles through multiple complex feedbacks (Alkama and Cescatti, 2016). In particular, forests regulate climate locally and regionally through a combined effect of higher net incoming radiation, due to lower albedo for forests compared to other vegetation types, and higher latent heat flux compared to other vegetation types (Anderson-Teixeira et al., 2012; Bonan, 2008; Ellison et al., 2012; Pielke et al., 2007; van der Molen et al., 2006). Forests likely also enhance cloud cover and precipitation (*e.g.* Ellison et al., 2012; Spracklen et al., 2012; Teuling et al., 2010). Some proposed mechanisms for this enhancement include cloud-formation effects by locally emitted aerosols (Khain, 2009), rain 'attraction' due to pressure changes over evaporating forests (the so-called 'Biotic pump' theory; Makarieva and Gorshkov, 2007; Sheil and Murdiyarso, 2009) and the forests' higher sensible and latent heat fluxes combined with developing meso-scale circulation patterns that favour cloud formation (Teuling et al.,

2017). In conclusion, changes in hydroclimatic patterns are caused by complex land-atmosphere interactions at various scales.

Changes in the hydroclimatic patterns and land cover can also shift species composition in ecosystems (Beniston, 2003; Eller et al., 2015; Walther et al., 2002) because these species depend on site-specific water, nutrient and energy conditions (Knapp et al., 2008; Reichstein et al., 2014). Simultaneously, vegetation controls water fluxes between the atmosphere and the soil (*e.g.* Teuling et al., 2017; Motzer, 2005). The initial short-term land-cover change impacts on hydro-climatic patterns are caused by structural and physical modifications of vegetation and soils (Zhao et al., 2012), while its long-term impacts depend on the emerging new equilibrium between soils, modified land covers and climate (Brown et al., 2005). Thus, water availability at variable spatial and temporal scales is vulnerable to climate and land-cover change. However, the magnitude and direction of these water-availability changes are highly uncertain and subject to considerable debate and research (*e.g.* Balthazar et al., 2015; Bonell, 2010; Ellison et al., 2012; Ellison et al., 2017). From a water-resource management perspective, strategically focused field studies to observe changes in hydrology and land-atmosphere interactions are crucial to avoid potentially harmful land-use decisions that can be further exacerbated by climate change (Malmer et al., 2010).

From a regional perspective, natural and anthropogenic water demands are supplied by hydrological processes that operate under specific environmental conditions (Vorösmarty et al., 2000). These hydrological processes are affected by both local and regional ecosystems and continental biomes, and by the direction and magnitude of climate change (Ellison et al., 2017; Jackson et al., 2001; Pielke et al., 2007). However, the hydrological functioning of many of these ecosystems is poorly understood and, consequently, scientific understanding is too limited to properly advice decision makers on resource

governance and management, and climate-change adaptation strategies. This knowledge gap also complicates the hierarchical decision making processes involving stakeholders ranging from land owners to national and international political institutions (McDonnell, 2008).

1.2. Why the Orinoco River basin?

One of the regions where hydro-climatological data is lacking to support such decision-making processes, is the Orinoco River basin (Latrubesse et al., 2005). The Orinoco River basin has the fifth largest streamflow and the third largest sediment load of all rivers worldwide (Meade, 1994). Furthermore, it has 175,000 km² of seasonally flooded savannahs exposed to extreme wet-dry climate conditions (Latrubesse et al., 2005). Although the Andean streamflow contributes less to the total Orinoco streamflow compared to other Andean basins (*e.g.* Río Negro), it buffers the extreme variability caused by the lowland's pronounced dry seasons (Viviroli and Weingartner, 2004). This buffer function is highly relevant for societal and economic activities (*e.g.* urban centres, rice paddies, oil-palm plantations and hydrocarbon extraction), because they concentrate in the transition area between the Andean foothills and the lowland savannahs. These activities require much water and therefore it is very relevant to assess future changes in the basin's hydrology as a function of anticipated climate and land-cover changes.

Multiple socio-economic factors make water use and availability contentious issues as they lead to multiple controversies and civil conflicts. The lack of hydro-meteorological data allow for many different opinions in a timely but complicated debate without any scientifically based support. Prolonging this debate hampers effective decision making processes on water governance and management, and climate-change adaptation plans. This bleak outlook can be averted by better understanding the Orinoco River basin's hydrology and how land-cover and climate change will impact it.

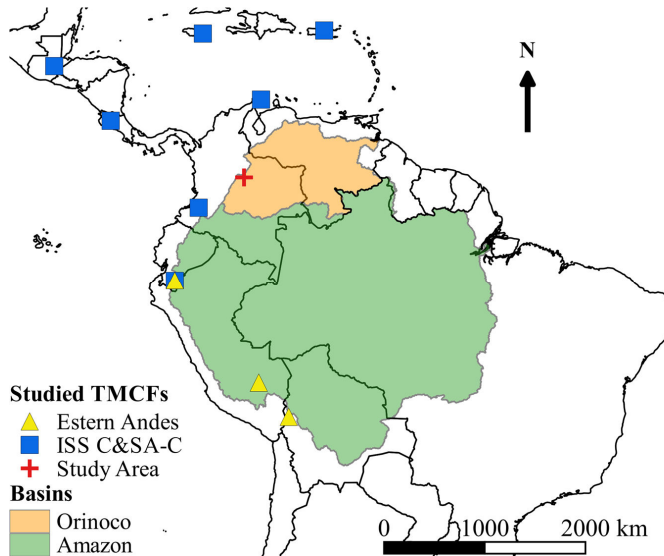


Figure 1.1. Tropical Montane Cloud Forests studied in Central and South America and the Caribbean. The study sites on the eastern Andes (triangles), the intensively studied sites in Central and South America and the Caribbean (ISS C&SA-C; squares; Jarvis and Mulligan, 2011), and the study site for this thesis (cross). The Orinoco and Amazon River basins are shown in orange and green, respectively.

From a broader scientific perspective, the lack of hydro-meteorological data in the Orinoco River basin contrasts the data availability for the more intensively used and investigated southern neighbour basin: the Amazon (Figure 1.1). The relevance of the Amazon basin in regulating climate is undisputed (Nobre et al., 1991; Shukla et al., 1990) and, consequently, the efforts to understand the climate and land-cover change impacts on its hydro-meteorology are well justified. Nevertheless, such interactions involving climate, land cover and hydrology, should also be studied for the Orinoco River basin, since its dominating lowlands are a unique naturally occurring low vegetation landscape characterized by pronounced seasonal moisture differences (Latrubesse et al., 2005). This low vegetation landscape contrasts with the tall forest and with the less variable moisture conditions of the Amazon Basin (Kim et al., 2012). However, both basins have their

headwaters sources in the Eastern Andes. In this regard, quantifying the forests' role in determining local and downwind climate (*e.g.* Khain, 2009; Makarieva and Gorshkov, 2007; Sheil and Mudiyarso, 2009) could be approached by studying the hydrological dynamics of the seasonally flooded savannahs, how they affect the downwind Andean ecosystems' hydrological dynamics, and how the lowland savannahs and the Andean region affect each other's hydrology (Poveda et al., 2006). To compare the hydrological dynamics between the Amazon and the Orinoco River basins more hydro-meteorological observations are required, especially in the Orinoco River basin. This would allow to compare some of the potential effects of the forested versus seasonally flooded savannahs on the downwind meteorological and hydrological conditions that prevail in the eastern Andean ecosystems.

1.3. Tropical Montane Cloud Forest hydrological functioning

Among the eastern Andean ecosystems, Tropical Montane Cloud Forests (TMCFs) are spatially restricted and play a key role in the regional hydrological cycle (Calder, 2002; Zadroga, 1981). Their hydrology is controlled by fog persistence, which depends on the temperature and moisture content of the incoming air masses (Scatena et al., 2011). This dependence leads to distinct hydro-meteorological spatio-temporal patterns in TMCFs as a function of their distance to the coast (Bruijnzeel et al., 2011b). However, most of the studied TMCFs are close to the coast (Figure 1.1; Jarvis and Mulligan, 2011) where, cloud-formation processes are deemed to be easier to characterize, whereas multiple feedbacks between land cover and meteorology are involved further inland (van der Molen et al., 2006). Furthermore, the climate data for the more continental TCMF sites included in the study by Jarvis and Mulligan (2011) were derived from the WorldClim data base. This data base is much less reliable in mountainous terrains due to data scarcity (Hijmans et al., 2005). Therefore, to better understand the actual hydro-meteorological

functioning of continental TMCs more data collection, analysis and modelling are required. Recently, the outcome of several studies on continental TMCs in the eastern Andes downwind from the Amazon basin have been published (*e.g.* Clark et al., 2014; Rapp and Silman, 2012; Schawe et al., 2011; Figure 1.1). In contrast to the intensively studied Central and South American and Caribbean TMCs (Jarvis and Mulligan, 2011), the eastern Andean TMCs are located at higher mean elevations (>1850m asl vs. 1747m asl), show higher annual mean precipitation (>2300mm vs. 1179mm) and lower mean temperatures (16.8°C vs. 17.5°C). Additionally, the eastern Andean TMCs show increasing rainfall at elevations higher than 1500m asl. This contradicts the conclusion by Jarvis and Mulligan (2010) that rainfall decreases above this elevation in large mountain systems. These contrasts indicate that climate variability in TMCs is likely caused by the diversity in orography, climatic settings, upwind land cover and land-use conditions in the Andes. In this regard, the hydro-meteorology of the eastern Andean TMCs in the Orinoco River basin are expected to differ from the TMCs in the Amazon basin due to their contrasting upwind land covers.

As mentioned previously, TMCs' hydrological functioning is largely determined by persistent fog conditions (Grubb, 1977). Fog reduces both incoming solar radiation and vapour pressure deficit, and increases canopy wetness. Therefore, fog reduces evapotranspiration (Eller et al., 2015; Letts and Mulligan, 2005, Reinhardt and Smith, 2008). Additionally, fog interception by the forest canopy and foliar water uptake represent an additional water source for the ecosystem besides rainfall (Eller et al., 2015; Zadroga, 1981). The reduced evapotranspiration plus the additional water inputs by fog, cause TMCs to have a higher throughfall (TF) compared to forests where fog is absent (Bruijnzeel et al., 2011a). Although the effect of fog on the canopy-water balance is

acknowledged, quantifying its precise influence remains challenging (Frumau et al., 2011).

Fog interception by the canopy is not only related to fog-water content but also to the canopy characteristics (Crockford and Richardson, 2000; Holwerda et al., 2010). A major challenge is the extrapolation of in-situ measurements of fog-water content and/or canopy characteristics to the topographically complex and highly diverse catchment areas. A common approach to study such fog and canopy interactions is to compare interception between areas or seasons with contrasting fog influence, and/or between different land-cover types (*e.g.* Brauman et al., 2010; Giambelluca et al., 2011; Ponette-González et al., 2010; Pryet et al., 2012). To quantify interception, precipitation should be measured above and below the canopy. This information allows to quantify the additional water input by fog reflected in a higher TF/rainfall ratio under fog influence compared to conditions without fog. However, fog occurrences are highly variable in time. Thus, its quantification is sensitive to the temporal resolution of the data, which varies considerably throughout the literature (*e.g.* weekly: Fleischbein et al., 2005; Gómez-Peralta et al., 2008; Wullaert et al., 2009; daily: Hölscher et al., 2004; and 10 minutes: Holwerda et al., 2010). These different temporal resolutions of the data also limit a direct comparison of the observed quantities of fog presence and interception between studies. Furthermore, the TF/rainfall ratio does not provide information on the relative contribution of fog water interception and fog affected evaporation, while both are necessary to quantify the water balance of the canopy. This is particularly relevant because each process is uniquely related to the local land-cover canopy characteristics and climate conditions. For example, the reduction in potential evaporation caused by fog is largely independent from land cover. In contrast, fog interception by the canopy strongly depends on land-cover

characteristics (e.g. Holwerda et al., 2010). Thus, these processes are expected to be differentially affected as a function of current and future land-cover and climate change.

The hydrology of TMCFs also involves water fluxes across their thick organic soil layers that can be up to 1 m deep (Hafkenscheid, 2000). Their hydrological dynamics are so far poorly studied but studies from other ecosystems with organic layers show that these layers have high water-retention capacities (Yang et al., 2014; Keith et al., 2010). In addition, these organic layers also generally have high infiltration rates that reduce surface runoff (Hartanto et al., 2003). Yet, infiltration rates are governed by saturated hydraulic conductivities, which are a strongly scale-dependent (Hu et al., 2012), especially in organic soils (Van der Ploeg et al., 2012). TMCFs' organic layers consist of decomposing organic material with dense fine root networks compared to those found in the underlying mineral soils (Hafkenscheid, 2000; Tanner et al., 1998). These high root densities in the top organic layer indicate that most of the water and nutrient uptake occurs in this layer (Leuschner et al., 2006). Water uptake in the root zone implies that the organic layer acts as a highly dynamic water-storage. Therefore, the removal of the organic layers by slash and burn practices, which are common in the Andes (Lambin et al., 2001), could potentially have a strong effect on TMCFs' hydrological functioning and, in particular, on rainfall-streamflow responses.

In relation to soil moisture dynamics, water logging rather than water deficit is generally considered to affect TMCFs' growth (Benner et al., 2010; Bruijnzeel and Veneklaas, 1998 and references therein). However, only few studies have evaluated seasonal dynamics of plant available water (see Kapos and Tanner, 1985). Plant available water is the amount of water that plants can extract from the soil column to fulfil their evapotranspiration demands and is estimated by the difference between the water content at field capacity (θ_{FC}) and at wilting point (θ_{WP}) over the root zone (Dunne and Willmott, 1996). θ_{FC} and

θ_{WP} are defined from water retention curves and these curves can be derived from the mineral soil texture using pedotransfer functions (Minasny and Hartemink, 2011; Wösten et al., 2001). However, this approach cannot be used to derive the curves for organic soil layers because these layers lack mineral soil particles. Hence, to evaluate climate and land-cover change impacts on TMCFs, the water retention curves of organic layers have to be established to improve our understanding on TMCFs' soil moisture dynamics and to evaluate the organic layers' potential role in sustaining plant transpiration during dry seasons.

The combined effect of fog interception and water storage in the organic soil layers on the streamflow of TMCF catchments is uncertain. Given that the presence of fog enhances TF and the organic soil layer potentially stores significant amounts of water that sustain baseflows, it could be hypothesized that catchment streamflow decreases with TMCF deforestation. However, the few studies that compare streamflow between forested and deforested catchments, do refute this hypothesis (*e.g.* Bruijnzeel, 2006; Muñoz-Villers, 2008). None of these studies, however, addressed the uncertainties involved in estimating hydrological fluxes in TMCFs. The apparent contradiction between the observations on specific hydrological processes (*i.e.* evapotranspiration, fog interception and soil water infiltration) and the catchment streamflow responses to deforestation are likely caused by the spatial variability of hydro-meteorological variables and land-cover distribution. This spatial variability likely stimulates different and contrasting fog-vegetation-soil interactions between multiple land covers, complex topography, local weather patterns and geological contrasts within and between focal catchments (Bruijnzeel, 2006; Muñoz Villers, 2008). Thus, defining the water balance of TMCF catchments is very challenging and the role of TMCFs in sustaining water yields depends on site-specific conditions.

The hydrological functioning of TMCFs present in the Andean part of the Orinoco River basin is expected to be affected by alterations on the upwind hydrological conditions due to land-use change, such as afforestation and reduction of flooded areas by artificial drainage systems (Pardo-Vargas et al., 2015). In addition, regional climate change is expected to increase the frequency of extreme dry events (Magrin et al., 2014). Therefore, the hydrological functioning of these TMCFs is likely highly vulnerable to climate and upwind land-cover changes. Still et al. (1999), for example, concluded from a study in Costa Rica that the cloud base can be lifted under the expected increase in temperature. Furthermore, Ray et al. (2006) showed by field data analysis and modelling that deforestation in the Costa Rican lowlands and premontane upwind areas increase the average cloud base and, consequently, decrease the extent of montane forests immersed in clouds. Their modelled surface and dew-point temperatures, and sensible and latent heat fluxes showed that over deforested areas the air masses were warmer and drier compared to those over intact forests. Such trends would push TMCFs upwards, as TMCFs' plant species are vulnerable to atmospheric drought due to hydraulic failure (Oliveira et al., 2014). These findings highlight the importance to continuously monitor TMCFs' hydro-meteorological variables and canopy and soil moisture dynamics, and include these observations in interpreting the potential role of changes in local and upwind land-cover and climate conditions.

1.4. Research objective and questions

This thesis aims to improve our understanding on TMCFs' hydrological functioning in the unique setting of the seasonal Orinoco River basin headwaters located in the Colombian eastern Andes. This understanding is fundamental to evaluate the potential impacts of land cover and climate changes on TMCFs' hydrology. To accomplish this, a hydro-meteorological monitoring system was setup in 2013. This system covered three

headwater TCMF catchments with contrasting land covers. The observational data that were collected, were analysed and used to parameterize suitable models to address the following research questions (RQs):

- RQ1. What is the hydro-meteorological spatio-temporal variability in the three neighbouring catchments with different forest covers?
- RQ2. To what extent can variations in streamflow between catchments be explained by the differences in forest cover?
- RQ3. What is the hydrological role of TCMFs' organic layers in water storage and release under land-use and climate changes?
- RQ4. What is the role of fog presence and interception on the canopy water balance on three successional TCMFs' regeneration stages?

The answers to these RQs will provide novel information on continental TCMFs' hydrology with a unique upwind land cover, while simultaneously providing valuable information to better guide further research and the decision-making processes in resource governance and management, and climate-change adaptation for the Orinoco River basin.

1.5. Thesis outline

The main objective and the research questions of this study are addressed in Chapters 2-4 (Figure 1.2). To set the stage of the study area, Chapter 2 describes the observed spatial and temporal variability in hydro-meteorological variables (RQ1) and provides a detailed analysis of the corresponding hydrological responses of soil moisture and streamflow in three neighbouring catchments with contrasting land cover (RQ2). The uncertainties associated with these RQs, their methods and setups are also assessed. A first-order comparison was also performed between the hydro-meteorological spatio-temporal

patterns found in the study area to those reported for eastern Andean TMCFs in the Amazon basin. From this Chapter, key processes that could potentially explain the seasonal contrasts between the water budgets of the studied catchments were identified.

Two of those identified key processes were water storage and release from TMCFs' organic layers. Therefore, Chapter 3 focuses on assessing the hydrological role of these organic layers for different land-cover and climate conditions (RQ3) by combining field and laboratory data with modelling. This allowed to quantify the organic layer's storage capacity and to evaluate the impact of actually observed and potential future dry season conditions on plant water availability. It also provides evidence to explain the observed differences in rainfall-streamflow responses between catchments found in Chapter 2.

Another key process identified in Chapter 2 was the potential fog influence on the catchments' water budgets through its effect on the canopy water budget. Therefore, Chapter 4 focuses on fog's effect on the canopy water budget of three TMCFs' successional stages (RQ4) by combining hydro-meteorological data with modelling. In this analysis, the reduction of incoming solar radiation and fog interception during fog-only and foggy rainfall events were explicitly considered. Contrasts in the canopy water budgets between successional stages linked to their distribution within the studied catchments provide information on the relative contribution of fog water inputs that could potentially explain the missing water sources in the studied catchments' water budgets found in Chapter 2.

Chapter 5 synthesizes this research by summarizing the main findings of the individual chapters and integrating the information gained in addressing the individual research questions to improve the understanding on TMCFs' hydrological functioning. Chapter 6 discusses the key challenges and solutions for further development and application of the monitoring system used in this PhD research. Finally, Chapter 6 also analyses how the

outcomes of this thesis, coupled with preliminary analyses on the main land-use change drivers in the recent past, can be used to scientifically support decision-making processes on resource governance and climate-change adaptation plans.

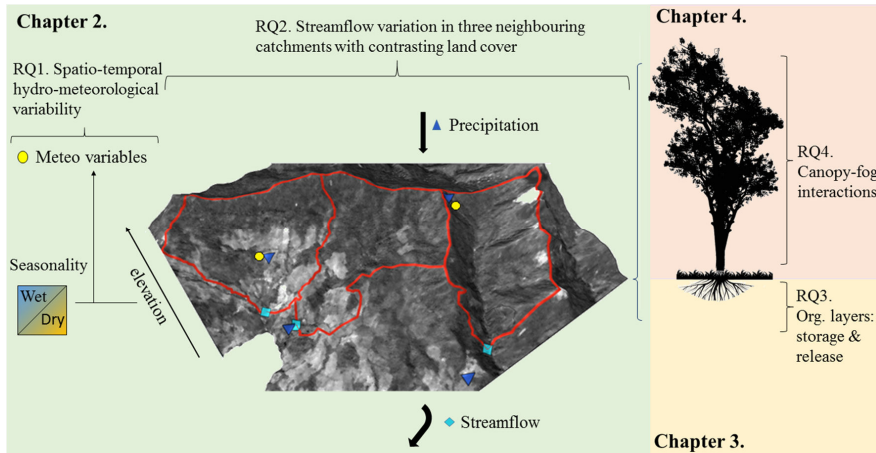


Figure 1.2. Schematic representation of the thesis outline with the research questions (RQs) and their corresponding chapters. The delineated study catchments (red) overlay a Landsat 2014 image. Dark areas are forests, whereas light areas are grasslands. The catchments' 3D view is based on the SRTM 30m resolution digital elevation model.



CHAPTER 2

Tropical Montane Cloud Forests:
Hydro-meteorological variability in three neighbouring catchments
with different forest cover

Chapter 2

Tropical Montane Cloud Forests: Hydro-meteorological variability in three neighbouring catchments with different forest cover¹

Mountain areas are characterized by a large heterogeneity in hydrological and meteorological conditions. This heterogeneity is currently poorly represented by gauging networks and by the coarse scale of global and regional climate and hydrological models. Tropical Montane Cloud Forests (TMCFs) are found in a narrow elevation range and are characterized by persistent fog. Their water balance depends on local and upwind temperatures and moisture, therefore, changes in these parameters will alter TMCFs' hydrology. Until recently the hydrological functioning of TMCFs was mainly studied in coastal regions, while continental TMCFs were largely ignored. This study contributes to fill this gap by focusing on TMCFs located on the northern eastern Andes at an elevation of 1550 to 2300 m asl, in the Orinoco River basin highlands. In this study, we describe the spatial and seasonal meteorological variability, analyse the corresponding catchment hydrological response to different land cover, and perform a sensitivity analysis on uncertainties related to rainfall interpolation, catchment area estimation and streamflow measurements. Hydrometeorological measurements, including hourly solar radiation, temperature, relative humidity, wind speed, precipitation, soil moisture and streamflow, were collected from June 2013 to May 2014 at three gauged neighbouring catchments with contrasting TMCF/grassland cover and less than 250 m elevation difference.

¹ This chapter has been published as: Ramírez, B.H., Teuling, A.J., Ganzeveld, L., Hegger, Z., and Leemans, R. (2017). Tropical Montane Cloud Forests: Hydro-meteorological variability in three neighbouring catchments with different forest cover. *Journal of Hydrology*, 552:151-167, DOI: 10.1016/j.jhydrol.2017.06.023

We found wetter and less seasonally contrasting conditions at higher elevations, indicating a positive relation between elevation and fog or rainfall persistence. This pattern is similar to that of other eastern Andean TMCs, however, the study site had higher wet season rainfall and lower dry season rainfall suggesting that upwind contrasts in land cover and moisture can influence the meteorological conditions at eastern Andean TMCs. Contrasting streamflow dynamics between the studied catchments reflect the overall system response as a function of the catchments' elevation and land cover. The forested catchment, located at the higher elevations, had the highest seasonal streamflows. During the wet season, different land covers at the lower elevations were important in defining the streamflow responses between the deforested catchment and the catchment with intermediate forest cover. Streamflows were higher and the rainfall-runoff responses were faster in the deforested catchment than in the intermediate forest cover catchment. During the dry season, the catchments' elevation defined streamflows due to higher water inputs and lower evaporative demand at the higher elevations.

2.1 Introduction

Climate change has intensified the debate on the regional and global roles of forests as carbon storage stands and climate regulators (Bonan, 2008; Ellison et al., 2012; Pielke et al., 2007; van der Molen et al., 2006). The combined effect of a higher net radiation due to lower forest albedo and a higher latent heat flux compared to other vegetation types affects global climate regulation (Anderson-Teixeira et al., 2012). Additionally, forest-atmosphere interactions and the precipitation enhancement by forests are currently debated (e.g. Ellison et al., 2012; Spracklen et al., 2012; Teuling et al., 2010). Some proposed mechanisms for forests to enhance precipitation include cloud formation effects by locally emitted aerosols (Khain, 2009) and rain ‘attraction’ due to pressure changes over evaporating forests (‘Biotic pump’ theory; Makarieva and Gorshkov, 2007; Sheil and Murdiyarso, 2009). It has also been argued that such forest-atmosphere interactions might impact the survival of seasonal cloud forests (Hildebrandt and Eltahir, 2008). Regardless of the mechanisms, wind largely defines where the precipitation will fall, implying that land-use decisions upwind from catchments are relevant for determining water inputs just as upstream land-use decisions are relevant for water availability downstream. Therefore, regional information is required to interpret, use and project local data for local and regional land-use management and climate change adaptation plans.

In contrast to the large-scale view that forests might increase water availability by enhancing precipitation, catchment-scale studies show that forest-water interactions cannot be generalized (Malmer et al., 2010). Deforestation/afforestation usually leads to an increase/decrease in annual streamflow because forests tend to use more water compared to lower vegetation (Andréassian, 2004; Calder, 2007; McVicar et al., 2007a; Zhang et al., 2001, and the references therein). However, other studies have shown that grasslands can have higher water use than forests (Teuling et al., 2010; van der Molen et

al., 2006; Williams et al., 2012). Overall, forest water use is determined by plant species, seasonality, soil depth and water content (Bruijnzeel, 2004; Eller et al., 2015; Zotz et al., 1998). Additionally, observations at intra-annual periods reveal an increase in streamflow variability following deforestation. This variability implies higher peak flows during heavy rainfall and lower base flows during dry spells that are likely more relevant for water resource management than annual mean streamflow (Bruijnzeel, 1989). What causes such flow variability is that land-use change (generally implying deforestation but not exclusively) usually deteriorates soil infiltration capacity (*e.g.* Chaves et al., 2008; Ghimire et al., 2014; Zimmermann et al., 2006). Low infiltration increases overland flow and leads to higher peak flows (Bruijnzeel, 2004; Suryatmojo et al., 2014). It also diminishes ground water recharge and thus reduces base flows, especially if the area experiences pronounced dry spells (Bruijnzeel, 2004; Roa-García et al., 2011). This indicates that soil hydraulic properties can greatly influence the land cover-water yield relation. Given these considerations on possible hydrological impacts following land-use change, land-use and water-resource management decisions have to be based on strategically focused field studies that reduce the policy-research gap and could avoid potentially disastrous hydrological consequences of land use decisions (Malmer et al., 2010).

Successful land-use and water-resource management depends on understanding local hydrological processes and their interactions within the larger hydrometeorological context. However, for many regions around the world, including tropical mountain systems, such understanding is severely limited by lack of data, as well as uncertainties associated with available data such as catchment area due to errors in digital elevation models (Weschler and Kroll, 2006). Tropical mountain systems play a crucial role in streamflow generation, mainly supported by glacier snowmelt and orographic induced

precipitation (Alpert, 1986, Céleri and Feyen, 2009; Viviroli et al., 2011; Viviroli and Dürr, 2007). Mountains are also characterized by a spatially dense succession of climates and ecosystems with a large heterogeneity in hydrological and meteorological conditions that are poorly represented by gauging networks (McVicar et al., 2007b; McVicar et al., 2010; Viviroli and Weingartner, 2004). Therefore, new data sets on tropical mountain catchments could help to improve our understanding on the meteorological, geomorphological and ecological interactions that define the mountain ecosystems' hydrological role (Buytaert et al., 2011; Crespo et al., 2011), and the representation of mountain ecosystems in climate and hydrological models (McInnes et al., 2011; McVicar et al., 2008; Viviroli and Dürr, 2007).

Tropical Montane Cloud Forests (TMCFs) are considered to play a key role in the hydrological cycle (Calder, 2002; Zadroga, 1981), largely due to the effects of fog persistence (Grubb, 1977). The most common TMCF classification (*sensu* Bruijnzeel, 2001) considers an increase in fog persistence with an increase in elevation that leads to distinct hydrological and ecological functioning. Fog reduces incoming solar radiation, increases leaf wetness frequency and decreases the atmospheric vapour pressure deficit, all of which reduce transpiration (Eller et al., 2015; Letts and Mulligan, 2005; Reinhardt and Smith, 2008). Simultaneously, fog interception by the forest and foliar water uptake can constitute relevant water sources to the system (Eller et al., 2015; Zadroga, 1981). Low TMCFs' transpiration and the water input by fog interception may support the idea that catchment streamflow decreases following TMCFs' deforestation. However, the few studies comparing streamflow between forested and deforested catchments showed no differences or even lower streamflow for forested catchments (*e.g.* Bruijnzeel, 2006 and Muñoz-Villers, 2008). It should be noted that none of these studies addressed uncertainty in estimates of hydrological fluxes. The mismatch between the observations on specific

hydrological processes (*i.e.* transpiration and fog interception) and the catchment streamflow responses to deforestation are likely caused by: 1) low cloud water inputs to the studied catchments; 2) high water interception by rough grasslands and shrubs that is comparable to those of forests; 3) the narrow distribution of high fog intercepting areas in contrast to the broader distribution of lower areas with no or low cloud water input; and 4) geological and topographical differences between forested and deforested areas (Bruijnzeel et al., 2011; Muñoz-Villers, 2008). These results highlight the difficulties in defining the hydrological functioning of TMCFs and suggest that their role in sustaining water yields depends on site-specific conditions.

TMCFs are also particularly vulnerable to upwind land cover changes because fog persistence depends upon the temperature and moisture content of the air masses (Scatena et al., 2011). Therefore, it is essential to distinguish between coastal and continental TMCFs, as coastal TMCFs' moisture conditions are determined by the ocean influence, whereas continental TMCFs' moisture conditions will mainly depend on the upwind land cover (Scatena et al., 2011). Additionally, the cloud formation processes are simpler under maritime conditions, whereas under continental conditions multiple feedbacks between land cover and meteorology are involved (van der Molen et al., 2006). However, continental TMCFs were underrepresented in the most recent effort to characterize TMCFs' climate and estimate TMCFs' distribution (Jarvis and Mulligan, 2011). Furthermore, the climate data for the TMCF sites included in the previously mentioned study were derived from the WorldClim data base, which has a high uncertainty for mountainous terrain due to data scarcity (Hijmans et al., 2005). Since the study by Jarvis and Mulligan (2011), other research on continental TMCFs on the eastern Andes, downwind the Amazon basin, have been published (*e.g.* Clark et al., 2014; Rapp and Silman, 2012; Schawe et al., 2011). In contrast to the intensively studied Central and

South American and Caribbean TMCs (C&SA-C; Jarvis and Mulligan, 2011), the eastern Andean TMCs are located at higher mean elevations (>1850 m asl vs. 1747 m asl), have higher annual mean precipitation (>2300 mm vs. 1179 mm) and lower mean temperatures (16.8° C vs. 17.5° C; Table 2.6). Additionally, in the eastern Andean TMCs rainfall increases at elevations higher than 1500 m asl, challenging the conclusions by Jarvis and Mulligan (2010) that rainfall decreases with elevation in large mountain systems, particularly above 1500 m asl. These contrasts show that climate variability in TMCs is caused by the diversity in orographic and climatic settings in mountainous South America. However, TMCs on the eastern slope of the north-eastern Andes belonging to the Orinoco River basin remain underrepresented, despite that this basin offers a unique combination of forested uplands and natural lowland savannahs that could provide valuable information on the effect of upwind lowland cover (*i.e.* forests vs. savannahs) on mountain climate. The lowland Orinoco River basin savannahs are exposed to wet-dry climate conditions characterized by pronounced seasonal moisture patterns (Latrubesse et al., 2005) that strongly contrast with the less variable moisture conditions of forested lowland areas (c.f. Amazon basin; Kim et al., 2012). Overall, it can be hypothesized that hydrometeorological conditions differ between coastal TMCs and continental TMCs, and in the latter, between forested and non-forested upwind conditions.

This chapter contributes to understand the hydrological role of TMCs in the Orinoco river basin and their vulnerability to climate change and upwind land-use change to support local and regional land-use management decisions. Here, we present our unique hydro-meteorological data set that covers three headwater catchments with contrasting land-cover conditions and seasonal fog conditions. Specifically, this chapter aims to answer the following three research questions: 1) What is the spatial and temporal

hydrometeorological variability in three neighbouring catchments? 2) How unique are these hydrometeorological patterns in comparison to other TMCFs with different upwind land covers? 3) To what extent can the effect of contrasts in TMCF cover be detected in streamflow observations in these neighbouring catchments? To answer the first question we analysed our meteorological dataset covering the 1600-2148 m asl elevation range. We address the second question by comparing our results to those reported for other TMCFs. To answer the third question we compared our observations on soil moisture and streamflow of three neighbouring catchments with contrasting TMCF/grassland cover. In contrast to previous studies on TMCF catchment hydrology (Bruijnzeel, 2006; Clark et al., 2014; Muñoz-Villers, 2008), we performed an extensive sensitivity analysis on uncertainties related to rainfall interpolation, catchment area estimation and streamflow measurements, allowing for a robust assessment of TMCF catchment hydrology.

2.2 Materials and Methods

2.2.1 Study Area

We collected data in three adjacent catchments located on the eastern slope of the eastern Andean Cordillera (Figure 2.1) at the municipality of Chámeza (Casanare, Colombia), from June 12 2014 to May 30 2015 (353 days). From a biogeographical perspective this study area belongs to the Andean region and from a hydrological perspective, it is part of the Orinoco river basin highlands. In contrast to the extensively studied Amazon basin (*e.g.* Bonan, 2008), the Orinoco basin is poorly gauged (Mejía et al., 1999) even though the Orinoco discharge is globally the third largest and its sediment discharge is the tenth largest (Meade, 1994). The Andean streamflow contribution to the total Orinoco streamflow is relatively small but it buffers the Orinoco seasonal streamflow variability caused by the lowland's pronounced dry season (Viviroli and Weingartner, 2004).

The three studied catchments drain to the Salinero River, a fourth order tributary of the Orinoco River. Although these catchments are located next to each other, they differ in their elevation (defined per McVicar and Körner, 2013) gradients and forest cover percentage (Table 2.1). To provide a more detailed description of the catchments, we estimated the grassland and forest cover percentage in two elevation ranges, defined by the elevation of our meteorological stations (see Section 2.2.2). We found clear differences between the catchments (Table 2.1). The forested catchment (FOR) has the largest forest cover at higher elevations (87%), whereas the deforested catchment (DEF) has the largest percentage of grassland cover at lower elevations (27%). The catchment with intermediate forest cover (INT) has 57% of its area at higher elevations compared to DEF which has 44% of its areas at higher elevations (Table 2.1). The low presence of grasslands at higher elevations is currently associated with human influence on the landscape; forests remain in steep remote areas while deforestation occurred in flatter and more accessible terrain (Sandel and Svenning, 2013). Slope is another relevant catchment (morphological) feature that can influence streamflow generation: steeper slopes promote a faster streamflow response to rainfall (Bruijnzeel, 2004). In our case, DEF and INT have similar slope values (1° difference), but are less steep than FOR (c. 8° difference; Table 2.1).

The eastern Andes are dominated by young mountains with steep slopes and sharp summits (Stallard et al., 1991). According to the Colombian Geographic Institute (IGAC), our study area is located on two formations belonging to the Caqueza Group (Cretaceous origin): Las Juntas and Macanal (IGAC, 2014). Las Juntas consists of black shales and sandstones, whilst Macanal consists of black shales and siltstones (Mejía, 2008). Soils in the study area are classified as a Lithic udorthents-Typic dystrodepts (LU-TD) association and Typic dystrodepts-Typic udorthents (TD-TU) association (IGAC, 2014). Note

however, that some profiles used by IGAC (2014) to characterize soil associations and create the soil map were collected in the municipality of Chámeza, located from 3 to 10 km from our study area, implying that this soil type may not represent the soil characteristics at our study site. The LU-TD association is characterized by shallow (35 cm) sandy soils found mainly on steep slopes, while the TD-TU association is characterized by deeper, silty-clay textured soils found on less steep slopes (IGAC, 2014; Rubio-Rivas, 2008). Soil analyses from the study area indicated that soils have a low clay content ($7.5\pm 3.7\%$) in contrast to sand ($47.9\pm 22.0\%$) and silt ($44.6\pm 18.6\%$), and that saturated hydraulic conductivities, inferred from soil texture by pedotransfer functions, are highly uncertain ($2.14\pm 1.44 \text{ cm h}^{-1}$; Chapter 3). According to the official soil map (1:500000), DEF soils belong to the TD-TU association, INT soils belong to the TD-TU association at elevations below the 1900 m asl, and to the LU-TD association at elevations above 1900 m asl. FOR soils belong to the LU-TD association (IGAC, 2014) implying a lower storage and faster drainage.

Table 2.1. Characteristics of the studied catchments: Coordinates (decimal degrees); elevation (m asl); mean slope estimated following Zevenbergen and Thorne (1987) (degrees); area (km^2); and forest (F) and grassland (G) cover percentage above and below 1900 m asl.

Catchment	Coordinates	Elev.	Slope	Area	<1900	>1900	<1900	>1900
					m asl G	m asl G	m asl F	m asl F
Deforested (DEF)	72.910E 5.230N	- 1575- 2241	18	3.7	27%	2%	29%	42%
Intermediate (INT)	72.900E 5.243N	- 1550- 2256	17	3.5	15%	1%	28%	56%
Forested (FOR)	72.889E 5.257N	- 1668- 2490	26	3.0	0%	1%	12%	87%

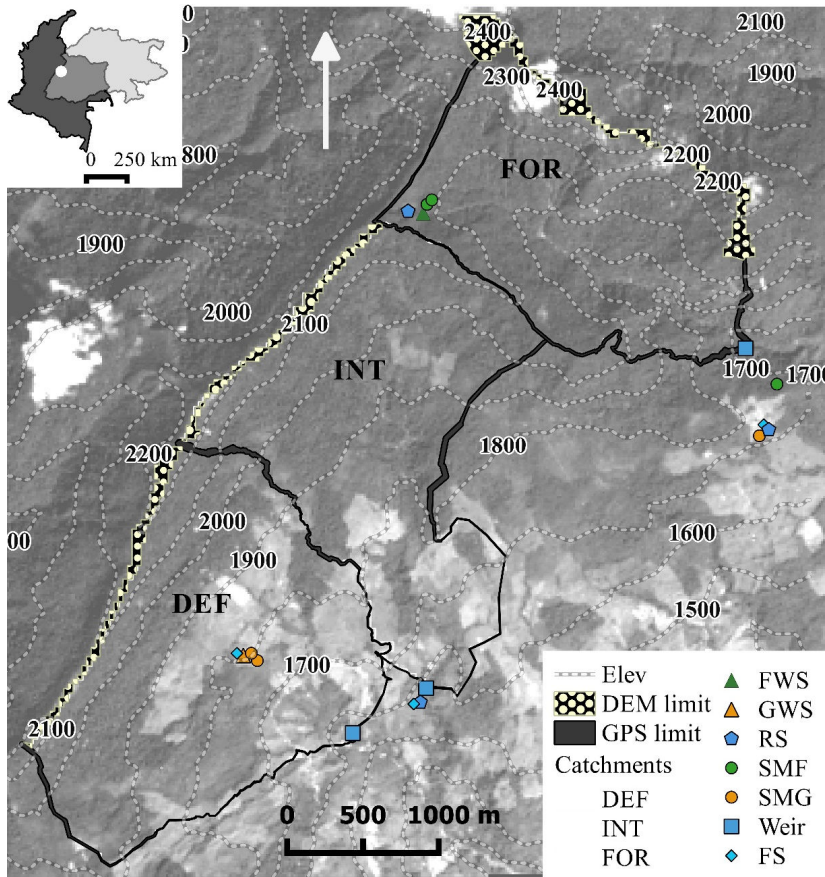


Figure 2.1. Map of the study region. The inset in the upper left corner shows a map of the Orinoco river basin (light grey) and Colombia (dark grey). The white dot represents the study area, magnified on the main map. The main map shows: 1) Elevation contours. 2) Catchment boundaries and their associated uncertainty; represented by white dotted areas (derived from SRTM Digital Elevation Models) and dark grey areas (derived from GPS data). 3) Study catchments: the less forested catchment (DEF), the intermediate forested catchment (INT); and the forested catchment (FOR).

The closest pluviometric station to our study area (c. 25 km) is located on the Cusiana River basin (Corinto at 1550 m asl) and this station is operated by the National Meteorology, Hydrology and Environmental Studies Institute. Mean annual rainfall at

Corinto is 3669 mm (Peralta and Ataroff, 2005). Here, seasonality is related to the southern displacement of the Inter-Tropical Convergence Zone (ITCZ) during the austral summer (Poveda et al., 2006) with the dry season dominated by the north-easterly trade winds occurring between December and March, and the wet season occurring from March to November.

The current landscape consists of mature forest, old secondary forest (>10 y), young secondary forest (<10 y), grasslands and small-scale agriculture areas. Most of the mature forests have been subjected to selective logging. As expected for TMCFs, epiphyte presence on the trees gradually increases with elevation. Above 1900 m asl, almost all of tree trunks are covered with mosses (bryophytes) and bromeliads. Mosses, whose presence and abundance are related to fog immersion (Frahm and Gradstein, 1991), are extremely abundant on the ridges around 2000 m asl and grow on various substrates (exposed roots, trunks, leaves, and rocks).

Our data collection covers both the expected fog persistence along the elevation gradient and its influence on hydrometeorological variables, and facilitates exploring how the land cover influences soil moisture and streamflow. The final distribution of study sites was also influenced by permits to access private lands and budget considerations to optimize data collection and site maintenance.

2.2.2. Catchment delineation

To delineate the catchments we used two sources of information: 1) Thirty meter resolution Shuttle Radar Topographic Mission Digital Elevation Model (DEM; USGS, 2014), and 2) Global Position System (GPS) field data. While the DEM based catchment delineation resulted in a high uncertainty for easy-access flat terrain, it provided robust results for terrain with inaccessible ridges. We included the DEM random error, which is correlated to topography, in the catchment delineation following the method by Wechsler

and Kroll (2006). Accordingly, we created a new DEM by adding to every pixel of the original DEM a random value from a uniform distribution of its error range. Given the complex topography of our study area, we chose the error reported for highly topographical complex areas (10 m; Rodríguez et al., 2006). We repeated this procedure until we obtained 250 new DEMs. For each DEM, sinks were filled with the *sinkfill* function (topmodel R-package). On each resulting map we performed an automatic catchment delineation with the single flow *subcatch* function (topmodel R-package). The catchment outlet was defined with field GPS coordinates. If the DEM derived stream channel did not coincide with the true outlet, then the *subcatch* function could not delineate the catchment. These results were therefore excluded from the analysis.

GPS delineation consisted of recording the track while walking on each accessible catchment water divide. The GPS error was recorded every 200 m or when grasslands shifted to forests. We assigned to each track segment the largest error between the two recorded points. This created boundaries with different widths which represented the delineation error (Figure 2.1). All DEM derived catchment areas were visually inspected. We excluded maps where the catchment area did not cover the full extent of the missing boundary between the two end points of the GPS derived limits (Figure 2.2). We extracted from each valid DEM map the fraction comprising the GPS missing border and added it to the GPS delineated area to obtain all possible catchment areas. The range in catchment areas were used to calculate uncertainty in catchment average rainfall and specific discharge (Appendix 2A).

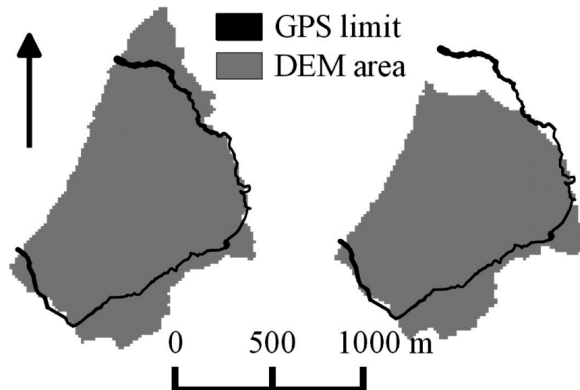


Figure 2.2. Illustration of the DEM exclusion procedure. Example of a valid DEF map (left) and an excluded DEF map (right). The grey areas represent the DEM estimated areas. The dark lines represent the GPS-derived boundaries. Note that the excluded map fails to cover the full extent between the GPS-delimited end-points.

2.2.3. Meteorological data

We recorded shortwave incoming radiation (Vantage-Pro2 6450 Solar pyranometer), relative humidity, air temperature, wind speed (large cup anemometer) and barometric pressure with two Davis Vantage Pro2-plus automated weather stations (AWS). One AWS was located on a grassland site in DEF at 2 m from the ground (72.907 E, 5.231 N; 1819 m asl; from now on referred to as GWS₁₈₁₉). The second AWS was located 17 m above the ground in a scaffolding tower surrounded by a forest canopy of c.16 m, therefore the meteorological station was 1 m above the surrounding canopy on FOR (72.897 E, 5.257 N; 2148 m asl; from now on FWS₂₁₄₈). Both stations recorded data on a Weatherlink datalogger at 10 minute intervals. To estimate cloud cover, we applied cloud transmissivity threshold values as proposed by Haurwitz (1948) distinguishing the presence of fog whenever transmissivity was <20% and presence of low clouds (nimbostratus, stratus and stratocumulus) for a transmissivity 20-35%. Cloud transmissivity is defined as the proportion of measured incoming solar radiation to expected solar radiation, the latter being inferred from extra-terrestrial solar radiation

derived from solar geometry (Donatelli et al., 2006), and clear-sky transmissivity through the Thornton and Running (1999) model. Whilst GWS₁₈₁₉ had clear-sky days (observed solar radiation resembled the expected solar radiation), FWS₂₁₄₈ did not have a single full clear-sky day. Thus, for FWS₂₁₄₈ we constructed a clear-sky day by selecting the maximum observed solar radiation for each daytime hour from the full time-series. The difference between a clear-sky day observed at GWS₁₈₁₉ and expected solar radiation was 0.5%, and the difference between the constructed clear-sky day at FWS₂₁₄₈ and expected solar radiation was 1.1%. Additionally, we evaluated the topographic shadowing on each AWS and each catchment following Corripio (2003), which combines solar geometry with topography.

We installed three Decagon ECRN-100 rainfall gauges at 2 m above the ground. Data from each gauge was recorded at 10 minute intervals on a Decagon EM50 data logger. One rainfall gauge was located at 2148 m asl on a large clearing (>900 m²) inside the forest at FOR (RS₂₁₄₈). The other two were located on grassland sites on the lower end of INT (1554 m asl; from now on RS₁₅₅₄) and FOR (1729 m asl; from now on RS₁₇₂₉) (Figure 2.1). Two wind correction models were applied on rainfall data: 1) the model by Førland and Hanssen-Bauer (1996) (hereafter referred to as *windcor_F*) that uses rainfall intensity and wind speed as input; and 2) the model by Yang et al. (1999) (hereafter, *windcor_Y*) that only uses wind speed. Wind speed data from the GWS₁₈₁₉ were used to correct rainfall data from RS₁₅₅₄ and RS₁₇₂₉. To correct RS₂₁₄₈ rainfall data we used the logarithmic wind profile (Sevruk and Zahlavova, 1994) to estimate wind speed at 2 m above the ground from FWS₂₁₄₈ measured wind speed data at 17 m above the ground. To consider under- or overestimation in wind speed used for rainfall correction due to contrasts in wind exposure between the rainfall gauges and the AWSs, we estimated and compared their wind exposure using the *wind effect* tool (Böhner and Antonic, 2009),

available in SAGA software v2.3.1 (Conrad et al., 2015). The topography was derived from the Shuttle Radar Topographic Mission Digital Elevation Model (DEM; USGS, 2014) and the wind exposure was estimated for the dominant day time and night time wind directions. The search distance to determine the topographical position was reduced to 0.1 km to emphasize local topography and the wind acceleration index was left as default (1.5). Due to the low number of rainfall gauges, we used the inverse distance and elevation weighting interpolation method (IDEW) following Masih et al. (2011) to estimate rainfall at each catchment. This method allows assigning different weights to the elevation and distance components. Given that we have no data to validate any specific weight selection we performed the interpolation with different contrasting weights, namely: 1) considering only distance; 2) considering only elevation; and 3) equal weight to both components. To include catchment area uncertainty in catchment rainfall estimation we applied the IDEW for all possible catchment areas (see Section 2.2) and for the raw and wind-corrected rainfall estimates (Appendix 2A).

We built three cylindrical Juvik type fog collectors (Juvik and Nullet, 1995) of 21 cm diameter and 60 cm of height with a circular greenhouse UV resistant plastic of 141 cm diameter on top to avoid rainfall but without avoiding wind driven drizzle (horizontal precipitation). Each fog collector had a funnel-hose-rubber lid connection to a Decagon ECRN-100 rainfall gauge. Data from each gauge was recorded at 10 minute intervals on a Decagon EM50 data logger. Fog collectors FS₁₅₅₄ and FS₁₇₂₉ were at 2.5 m distance from the corresponding rainfall gauges RS₁₅₅₄ and RS₁₇₂₉. The fog collector FS₁₈₁₉ was located at 3 m distance from the meteorological station GWS₁₈₁₉. All fog collectors were placed with the collecting surface perpendicular to the ground. In all cases we selected flat areas within the dominant slopes. Additionally, they were positioned with the top at

2 m and located on the side of the rainfall gauges avoiding up and downwind positions in relation to the rainfall gauges and GWS₁₈₁₉.

Several issues with the fog gauging systems (disconnection of the hoses, failures of the tipping buckets during the wet season and poor silicone sealing before the dry season) did not allow us to specifically quantify water inputs by fog and include them in the catchments' water budgets. However, we used the data to discriminate between hours without fog, with only fog and fog + rain following Tanaka et al. (2011). With this approach we established seasonal and elevation trends in fog frequency. To evaluate if the missing data could influence the observed patterns we first determined the length of the time-periods (in hours) with and without missing data and established the fog frequency only during the time-period with data. Then, we assumed that the fog frequency would remain the same during the periods with missing data and established the potential fog inputs for all gauges.

2.2.4. Soil moisture measurements and soil properties

Soil volumetric water content profiles (VWC cm³ cm⁻³) were measured at six locations within our study area using Decagon GS-3 frequency domain soil moisture sensors (Figure 2.1). Data from each sensor was recorded at 10 minute intervals on a Decagon EM50 data logger. Each soil moisture station (from now on SM) consisted of three sensors, which were inserted at depths of 0-10 cm, 20-30 cm and 40-50 cm in the mineral soil. Three SMs were located on grasslands (SMG). SMG₁₈₁₉ was located at 3 m distance from the GWS₁₈₁₉, in a relatively flat area. Another soil moisture sensor, SMG₁₇₈₉, was located 300 m downslope of SMG₁₈₁₉ on a hillslope (72.907 E, 5.230 N and 1789 m asl). Both SMG₁₈₁₉ and SMG₁₇₈₉ were in DEF. SMG₁₇₂₉ was located at 3 m distance from RS₁₇₂₉ in relatively flat terrain, 360 m outside FOR's limits. Three SMs were located in forested areas (SMF). SMF₁₉₇₃ (72.897 E, 5.258 N; 1973 m asl) and SMF₂₀₆₈ (2068m asl)

were located respectively at 150 and 200 m distance from FWS₂₁₄₈ in FOR. SMF₁₉₇₃ was located on relatively flat terrain, whereas SMF₂₀₆₈ was located on a hillslope. SMF₁₇₂₀ was located in the lower part of FOR on a hillslope (72.876 E, 5.246 N; 1720 m asl). Note that flat terrain or hillslopes refers here to landscape features at small spatial scales (<20 m). The error specified by the manufacturer for our soil moisture sensors for typical (mineral) soils is $\pm 0.03 \text{ m}^3 \text{ m}^{-3}$ (Campbell et al., 2009). For each SM we estimated the VWC weighted mean of the 50 cm deep soil profile. The top sensor data represented about 30% (0-15 cm) of the total soil moisture present in this 50 cm soil profile, the middle sensor about 40% (15-35 cm) and the bottom sensor about 30% (35-50 cm).

We assessed our soil moisture data from two perspectives 1) the water content, and 2) the soil moisture depletion rates during dry spells. While a limited number of sampling points cannot be used to estimate areal mean values, the soil moisture dynamics of point observations are typically very similar to that of the larger scale average following the concept of temporal stability (Vachaud et al., 1985), thus wetter soils and drier soils often remain consistent throughout time in their moisture patterns. Additionally, Vachaud et al. (1985) and others such as Gómez-Plaza et al. (2000), Penna et al. (2013) and Teuling et al. (2006) have proven that soil moisture values on any area are distributed around a mean soil moisture content and mean soil moisture variability, thus reflecting general soil moisture patterns. Once soils reach field capacity, typically after three days without water inputs (Cong et al., 2014; Veihmeyer and Hendrickson, 1931), percolation and lateral water flows have a smaller influence on the soil water balance compared to vertical flows driven mainly by evapotranspiration (Grayson et al., 1997). Here, we estimated the average loss rate of soil moisture storage over the top 50 cm during dry spells ($<0.5 \text{ mm d}^{-1}$) of different lengths (3, 5, 7 and 12 days).

2.2.5. Streamflow measurements

Water levels in the streams were measured on 10 minute intervals at each of the catchment outlets with Solinst level-logger pressure sensors (model 3001-M10-F30) which have a factory determined full-scale accuracy of 0.05% or 0.5 cm. For atmospheric pressure compensation we used data from a Solinst baro-logger installed next to INT's outlet. At FOR (72.878 E, 5.249 N; 1643 m asl) and DEF (72.902 E, 5.226 N; 1506 m asl) we built 90° V-notch weirs to obtain a better stage-discharge relation. At INT (72.897 E, 5.228 N; 1539 m asl) the weir was damaged before the onset of the study so we decided to gauge this catchment at a natural stable, narrow and deep channel that had a sudden river bed elevation, forcing/allowing critical flow.

While the uncertainty of streamflow observations is often neglected, it can significantly impact hydrological studies' results and models' predictive capacities (McMillan et al., 2012; Peña-Arancibia et al., 2015; Wechsler and Kroll, 2006). Here, we determined streamflow uncertainty by accounting for the three most likely sources of error: 1) individual stage-discharge estimates; 2) regression uncertainty; and 3) the catchment area estimation. Discharge from water levels was calculated by salt dilution measurements with constant flow injection at several times throughout the study period (Hudson and Fraser, 2002). An advantage of the salt dilution method is that it estimates streamflow independent from the weir. In this regard, the stage-discharge relation will already account for biases in stage measurements due to any infiltration occurring under the weir. The uncertainty estimate for every measured discharge was obtained by accounting for the uncertainties in each step along the salt-dilution process. The corresponding water level was obtained from the level loggers but was also corroborated with a metric tape.

To include the uncertainty estimates in determining the rating curves we performed a bootstrap sampling (n=1000) of the discharge measurements by choosing the same

number of discharge events with repetition (FOR=48, INT=63, DEF=57; Figure 2.3 and Appendix 2A). For each selected dilution exercise a discharge value was selected from a uniform distribution within the range of minimum and maximum estimated discharge. At the catchments with weirs (DEF and FOR), we employed a linear fitting procedure on the log value of the discharge to balance the weight to low and high flow conditions in the rating curve $Q = a \cdot h^b$. Both coefficients a and b were estimated (Figure 2.3). The expected b value for 90° V-notch weirs, like those in DEF and FOR, is 2.5, and for the natural channel at INT the b value should be close to 1.5 which corresponds to rectangular weirs (Bos, 1989). At INT, a break in the rating curve corresponded to the limitation of the natural channel where water above 1.5 m would overflow. Consequently, we employed a continuous segmented log model (Figure 2.3). We allowed the breaking point to move freely for each bootstrapped sample. We also constrained the maximum possible discharge by field data on the wetted area and possible flow velocities. From this exercise, we obtained 1000 possible sets for a and b values. The water level time series were translated to discharge using all rating curves. This approach was adapted from McMillan et al. (2010). We randomly selected one catchment area from the pool of possible catchment areas to estimate specific streamflow for each discharge time series (Appendix 2A).

We used discrete unit hydrographs to evaluate the catchments' rainfall-streamflow responses. This method is based on a multiple linear regression in which the first regression is calculated between the specific streamflow and rainfall time-series, and the following regressions are calculated by shifting rainfall one time-step forward in relation to streamflow for each regression. We analysed a 10 hour lag time period based on the observed maximum time within 48 hours after rainfall, before following storms influenced the hydrograph. The linear model was set to have a zero intercept. The

coefficients (slope) for each linear regression were plotted as a function of the time-step lag between the rainfall-streamflow time-series. The slope of the first linear regression (when lag=0) represents the runoff coefficient. The highest estimated slope from the evaluated lag-times corresponds to the moment when streamflow better reflects or expresses the rainfall inputs. The multiple linear regression R^2 reflects the stability of rainfall-streamflow relations throughout the time series. A low R^2 suggests a high variation of rainfall-streamflow responses within the time-series, whereas a larger R^2 suggests a higher homogeneity in rainfall-runoff responses in time.

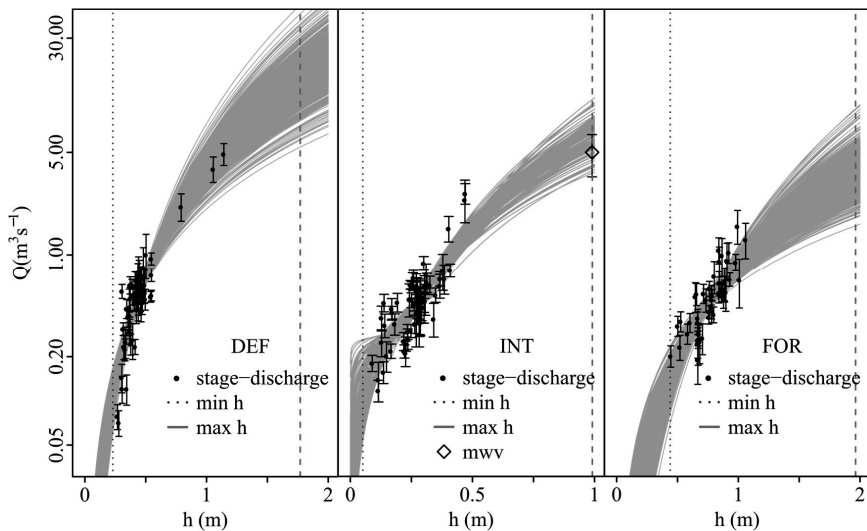


Figure 2.3. Rating curves for the three discharge stations. Stage (h) is plotted on the X-axis and discharge (Q) is plotted on the Y-axis. Note that the Y-axis is logarithmic. Dots and bars represent the stage-discharge measurements and their associated uncertainty, respectively. Plots include the minimum (dashed vertical lines) and maximum (dotted line) recorded stage values. For the deforested catchment (DEF; left panel) and the forested catchment (FOR; right panel) we used linear models. For the intermediate catchment (INT; central panel) we used a segmented model with a maximum water volume point (mwv) estimated from wetted area and flow.

2.3 Results

2.3.1 Meteorological conditions

Daily mean solar radiation at FWS₂₁₄₈ ($91 \pm 37 \text{ W m}^{-2}$) and at GWS₁₈₁₉ ($127 \pm 60 \text{ W m}^{-2}$) represented only ~28% and ~39% of the expected solar radiation under clear sky conditions (328 W m^{-2}). Estimated mean clear sky transmissivity at local noon was 0.89 ± 0.01 for both FWS₂₁₄₈ and GWS₁₈₁₉. Fog and clouds strongly reduce incoming solar radiation throughout the year, especially at higher elevations. Seasonal differences were less pronounced at FWS₂₁₄₈ (wet season: $90 \pm 35 \text{ W m}^{-2}$, dry season: $96 \pm 43 \text{ W m}^{-2}$) than at GWS₁₈₁₉ (wet season: $125 \pm 60 \text{ W m}^{-2}$, dry season: $134 \pm 61 \text{ W m}^{-2}$). In fact, fog and low cloud cover estimation derived from solar radiation data showed that at FWS₂₁₄₈ and GWS₁₈₁₉ low cloud/fog cover was reduced in the dry season compared to the wet season by c.2% and c.3%, respectively (Table 2.2). Diurnal patterns of solar radiation were asymmetrical with relatively high solar radiation in the mornings and less radiation in the afternoons peaking around 10 h (Figure 2.4), after which cloud (and fog) presence were more pronounced. Topographical shadowing on the AWSs only occurred in the late afternoon. FWS₂₁₄₈ was only shadowed during four days after 16:00 h throughout the study period. GWS₁₈₁₉ was shadowed after 17:00 h for 9 months (mean value 33 W m^{-2}), whilst FWS₂₁₄₈ was shadowed after 17:00 h for 6 months (mean value 26 W m^{-2}), in contrast to the expected solar radiation (184 W m^{-2}). Both stations were shadowed after 18:00 h during the period on which it is still daytime, however expected solar radiation at this hour is low (12 W m^{-2}). Therefore, topographical shadowing was not significantly different between stations or between the expected and the measured solar radiation. However, estimating topographical shadowing per catchment from 8 h to 16 h indicated that the catchments were partially shadowed by topography to different extents: the mean estimated shadowed area in DEF was 4%, in INT 9% and in FOR 24%.

Table 2.2. Estimated daytime hourly cloud cover percentage following Haurwitz (1948). SRm/SRcs: measured solar radiation over clear sky estimated solar radiation for FWS₂₁₄₈ and GWS₁₈₁₉.

	SRm/SRcs (%)	FWS ₂₁₄₈ (%)	GWS ₁₈₁₉ (%)
Wet season			
Fog	<20%	44	36
Low clouds	20% < and < 35 %	31	25
Dry season			
Fog	<20%	45	34
Low clouds	20% < and < 35 %	28	25

At FWS₂₁₄₈ the daily mean temperature was c. 2° C colder ($14 \pm 1^\circ \text{C}$) compared to the daily mean temperature measured at GWS₁₈₁₉ ($16 \pm 2^\circ \text{C}$). This represented a mean decrease of $0.6 \pm 0.3^\circ \text{C}$ per 100 m, which corresponded to a moist adiabatic lapse rate. Temperature differences between the relatively warmer dry season and the colder wet season at FWS₂₁₄₈ were 0.2°C and at GWS₁₈₁₉ 0.4°C (Figure 2.4). Such differences lead to a relatively drier adiabatic lapse rate in the dry season (wet season: $0.6 \pm 0.2^\circ \text{C}$, dry season: $0.7 \pm 0.2^\circ \text{C}$ per 100 m).

Mean and minimum daily relative humidity values were higher at FWS₂₁₄₈ ($97.0\% \pm 3.0\%$ min=80.0%) than at GWS₁₈₁₉ ($92.9\% \pm 4.2\%$, min=77.0%). Minimum values were close to the 80% condensation threshold value proposed by Slingo (2007) for low altitude cloud formation. Seasonal mean relative humidity differences are small at GWS₁₈₁₉ (wet= $93.8\% \pm 3.7\%$; dry= $90.6\% \pm 4.3\%$) and at FWS₂₁₄₈ they are negligible (wet= $97.2\% \pm 3.0\%$; dry= $96.6\% \pm 3.13\%$). Yet, on the diurnal relative humidity plots, seasonal differences were evidently stronger during day time (Figure 2.4).

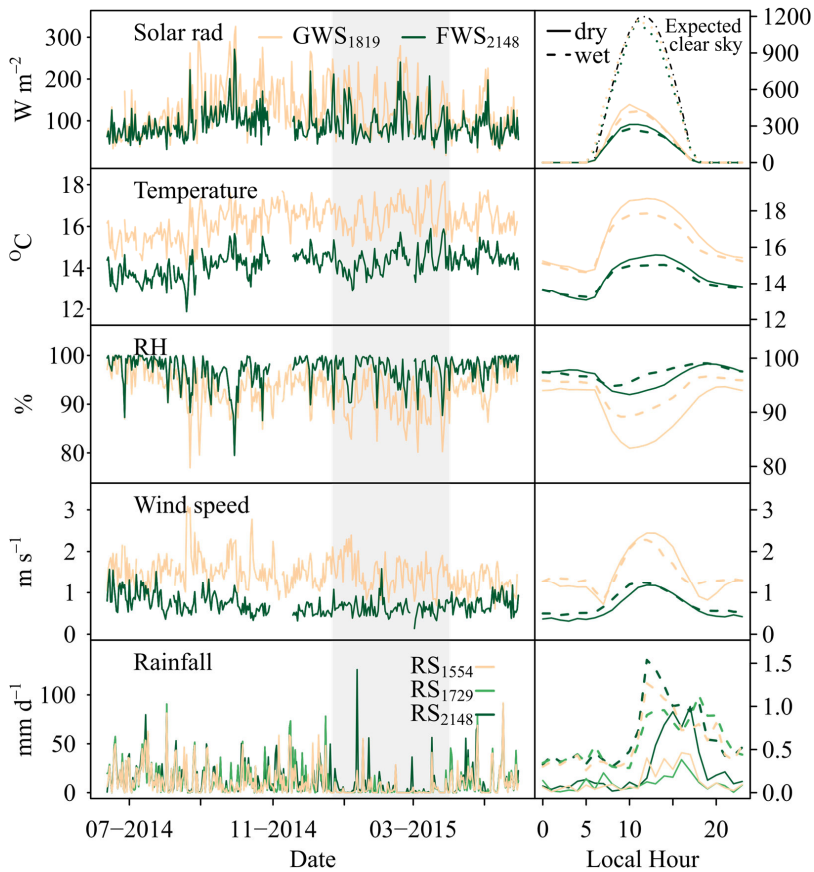


Figure 2.4. Meteorological variables measured at the grassland and forest weather stations GWS₁₈₁₉ and FWS₂₁₄₈. Left panels show the daily time series. The grey area represents the dry season. Right panels show the mean diurnal cycles. From top to bottom a) Solar radiation (W m^{-2}), b) Air temperature ($^{\circ}\text{C}$), c) Relative humidity (%), d) Wind speed (m s^{-1}), and e) Daily rainfall (mm). In the diurnal solar radiation plot the dotted black line represents the estimated expected solar radiation and the dotted coloured lines are the clear-sky solar radiation at each AWS.

Mean daily wind speed and maximum hourly values were higher at GWS₁₈₁₉ ($1.5 \text{ m s}^{-1} \pm 0.4 \text{ m s}^{-1}$, $\text{max}=7.3 \text{ m s}^{-1}$) than at FWS₂₁₄₈ ($0.7 \pm 0.2 \text{ m s}^{-1}$, $\text{max}=5.5 \text{ m s}^{-1}$; Figure 2.4). The dominant daytime winds were easterlies (68° to 113°), whilst night time winds were predominantly westerlies (270° to 293°). The FWS₂₁₄₈ daytime wind exposure index

(1.06) indicated lower exposure than GWS₁₈₁₉ (1.15). Night-time wind exposure followed the same pattern but values were lower (FWS₂₁₄₈= 0.95 and GWS₁₈₁₉= 1.06). Index values <1 indicate wind shadowing whereas values >1 indicate wind exposure (Böhner and Antonic, 2009). Regarding the use of wind speed data for correcting rainfall data, RS₂₁₄₈ (daytime= 1.02 and night time= 0.94) was less exposed than FWS₂₁₄₈. Therefore wind correction will result in a slight overestimation of rainfall at this site. This was also the case when contrasting RS₁₅₅₄ (daytime= 0.87 and night time= 0.81) and RS₁₇₂₉ (daytime= 1.08 and night time= 0.97) wind exposures to GWS₁₈₁₉. Catchment wise, the AWS exposure was highly similar to the mean values per catchment in both daytime and night time wind directions. Furthermore, the AWS wind exposure was similar to the mean catchments' wind exposure (DEF_{day}= 1.06 ± 0.09; DEF_{night}= 0.95 ± 0.09; INT_{day}= 1.03 ± 0.11; INT_{night}= 0.98 ± 0.11; FOR_{day}= 1.02 ± 0.11; FOR_{night}= 0.99 ± 0.12). Diurnal wind speed patterns followed those of solar radiation and temperature (Figure 2.4) and are consistent with an increase in surface temperature and atmospheric instability. Seasonal differences in wind speed at the two stations were very low (FWS₂₁₄₈ wet season: 0.74 ± 0.57 m s⁻¹, dry season: 0.63 ± 0.50 m s⁻¹; GWS₁₈₁₉ wet season: 1.47 ± 0.97 m s⁻¹, dry season: 1.46 ± 0.90 m s⁻¹).

Rainfall data after wind speed correction increased variably depending on the gauge and the wind correction method. Windcor_F led to small corrections (RS₂₁₄₈=1.3% to RS₁₅₅₄=2.9%), whilst windcor_Y led to larger corrections (RS₂₁₄₈=3.8% to RS₁₅₅₄=8.2%). As expected, the correction for RS₂₁₄₈ was smaller due to the lower wind speeds registered at FWS₂₁₄₈. Mean wind speed data for the wet and dry seasons at the most exposed GWS₁₈₁₉ is below 1.5 m s⁻¹ (Figure 2.4), and the rainfall gauges wind exposure was below those of the AWS. Low wind speeds at FWS₂₁₄₈ (17 m from the ground) also indicate that wind speeds at RS₂₁₄₈ (2 m above the ground) are small and hence a small effect of wind

driven throughfall is expected from the surrounding vegetation on the clearing where RS₂₁₄₈ was located.

Annual rainfall for the two rainfall gauges at the low elevation sites (RS₁₅₅₄ and RS₁₇₂₉ c.3900 mm) were similar but considerably lower than those observed at the high elevation station (RS₂₁₄₈ c.4700 mm; Table 2.3). Rainfall variation between the gauging stations was more pronounced during the dry season than during the wet season (Figure 2.4 and Table 2.3). Mean wet season daily rainfall was slightly higher at the higher elevation site RS₂₁₄₈ compared to RS₁₅₅₄ or RS₁₇₂₉, while in the dry season, it was over two times higher at the higher elevation compared to the lower sites (Table 2.3). The passage of the ITCZ above the study area's latitudes during the wet season leads to a widespread spatially homogeneous rainfall (Poveda et al., 2006). During the dry season, the ITCZ is located south of the study area and rainfall events therefore depend on orography and the condensation level defined by the air moisture brought by the north easterly trade winds. This favours rainfall at RS₂₁₄₈ as is illustrated by the contrasting seasonal difference in the percentage of days with recorded rainfall (>0.2 mm) between RS₂₁₄₈ (wet season: 96%, dry season: 93%), and RS₁₅₅₄ (wet season: 92.5%, dry season: 56%) and RS₁₇₂₉ (wet season: 88%, dry season: 51%). Note that in both seasons the intermediate elevation site RS₁₇₂₉ had c. 5% less days with rainfall than RS₁₅₅₄. Also, extreme daily rainfall values (<5% exceedance) at RS₂₁₄₈ were similar or stronger during the dry season than in the wet season (Figure 2.8). At RS₁₅₅₄ and RS₁₇₂₉ dry spells were longer during the dry season than during the wet season whereas this was not the case for RS₂₁₄₈ (Table 2.3).

The annual estimated rainfall per catchment varied according to whether the input data was wind corrected or not, to the different weights assigned to the distance and elevation components and uncertainties in estimated catchment area (Table 2.4). Differences between raw rainfall data and wind corrected rainfall for all assigned distance and

elevation weights was between 214-216 mm (5%) for FOR, 236-244 mm (6%) for INT and 256-282 mm (6-7%) for DEF. Differences in catchment rainfall between the different weights for distance and elevation were between 14-16 mm (0.3-0.4%) for FOR, 58-66 mm (1.3-1.5%) for INT and 100-126 mm (2-3%) for DEF. The low rainfall variation in FOR is caused by lower wind speeds at FWS₂₁₄₈ and because RS₂₁₄₈ and RS₁₇₂₉ were in or very close to this catchment and covered its elevation range. In contrast, raw and wind corrected data were more variable in DEF and INT compared to FOR because wind speeds were higher at GWS₁₈₁₉. Additionally, the highest catchment rainfall variation in DEF depends on the weights assigned to elevation and distance in the IDEW method because RS₂₁₄₈ is located furthest away from this catchment. Catchment area uncertainty had a comparatively smaller impact on total catchment rainfall increasing the total rainfall range by only a few millimetres (2 to 14 mm in DEF, 3 to 24 mm in INT and 3 to 12 mm in FOR; Table 2.4). Seasonal mean daily rainfall are also presented in Table 2.4.

Table 2.3. Summary of wind corrected rainfall (windcor_F - windcor_V) at each of the three rainfall stations. Annual rainfall, seasonal mean daily values, percentage of seasonal rainfall in relation to total rainfall and seasonal maximum duration of dry spells.

	RS ₁₅₅₄	RS ₁₇₂₉	RS ₂₁₄₈
Annual rainfall (mm y ⁻¹) (raw data)	3875-4073 (3765)	3869-4068 (3771)	4649-4761 (4588)
Rainfall increase after wind-cor (%)	2.9-8.2	2.6-7.9	1.3-3.8
Wet season mean daily rainfall (mm d ⁻¹)	14.3-15.0	14.0-14.7	15.8-16.2
Dry season mean daily rainfall (mm d ⁻¹)	2.6-2.7	3.3-3.5	6.5-6.7
Wet - dry season % of total rainfall	93% - 7%	92% - 8%	86% - 14%
Wet - Dry season longest continuous dry days (<0.2 mm d ⁻¹)	3.2 - 7.1	6 - 12.9	2.2 - 2.3

Diurnal rainfall during the wet season was similar for all gauges with a peak around noon and pronounced rainfall that decreased until the evening (21 h) followed by stable rainfall rates occurring throughout the night and the early morning. During the dry season, rainfall at the higher elevation site RS₂₁₄₈ peaked much higher than rainfall measured by the other gauges at 15 h with pronounced rainfall until 18 h. The dry season nocturnal rainfall was smaller compared to the wet season and similar for all gauges (Figure 2.4).

The total hourly fog events (only fog: fog + rain) registered at FS₁₅₅₄ were 178 h (54 h: 124 h), 227 h (59 h: 160 h) at FS₁₇₂₉ and 538 h (225 h: 313 h) at FS₁₈₁₉ (Figure 2.5). Therefore, fog increased with elevation and was more persistent at FS₁₈₁₉ compared to the other stations. Missing data for each gauge station were: 278 h for FS₁₅₅₄, 299 h for FS₁₇₂₉, and 440 h for FS₁₈₁₉. The percentage of hours with fog events for the time-periods with data were: 3.1% for FS₁₅₅₄, 3.9% for FS₁₇₂₉, and 9.6% for FS₁₈₁₉. These values are contrastingly low to the fog estimates derived from solar radiation (Table 2.2).

Table 2.4. Inverse distance and elevation weighting rainfall interpolation (in mm y^{-1}) per catchment for raw rainfall data and for the two wind correction models (raw-windcor_F - windcor_F) for the different weights assigned to distance (D) and elevation (Z). Total and seasonal rainfall mean and uncertainty includes the wind correction method, the weights assigned to IDEW and catchment area variability.

Weights (D/Z)	DEF	INT	FOR
1/0	3910-4009-4192	4175-4255-4411	4274-4344-4490
0.5/0.5	3973-4064-4242	4142-4222-4382	4282-4352-4497
0/1	4036-4121-4292	4109-4189-4353	4290-4360-4504
Rainfall mean and uncertainty (\pm sd)	4093 \pm 121 (3908-	4259 \pm 107 (4106-	4373 \pm 90 (4262-
(min-max)	4304)	4435)	4507)
Dry season mean			
daily rainfall (\pm sd)	3.8 \pm 0.4	4.6 \pm 0.1	5.2 \pm 0.1
Wet season mean			
daily rainfall (\pm sd)	14.7 \pm 0.4	15.0 \pm 0.4	15.2 \pm 0.3

Nevertheless, the underestimation of fog events by the fog collectors is expected as their efficiency depend on wind speed and fog water content (Villegas et al., 2008). If during the missing data time-periods fog frequency would remain constant then the total hours with fog would be: 187 h for FS₁₅₅₄, 239 h for FS₁₇₂₉ and 580 h for FS₁₈₁₉, therefore the observed trend with elevation would remain valid. The relative frequency of fog events during the wet season was higher compared to the dry season. Focusing on the diurnal pattern, daytime fog and rainfall events at FS₁₈₁₉ followed the rainfall diurnal cycle. The ‘fog-only’ events appeared to be particularly relevant during night time. Under such conditions, the collection of fog could have reflected radiation fog occurring for nocturnal low wind speed conditions.

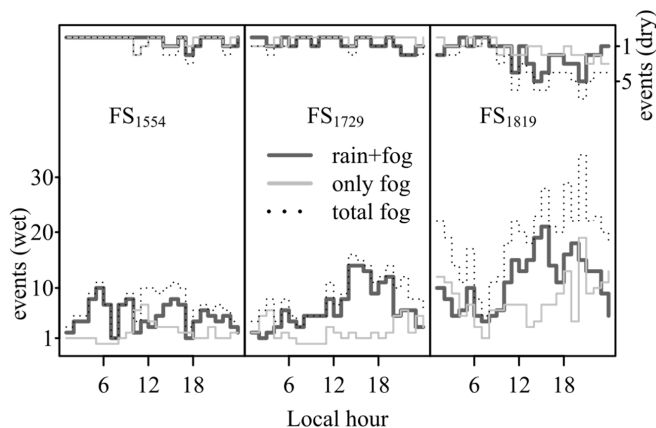


Figure 2.5. Total number of fog events at the three fog gauges stations (FS) in the dry (inverse right y-axis) and wet season.

2.3.2 Soil moisture dynamics

Seasonality in rainfall and other meteorological parameters reported in the previous section influenced the soil moisture dynamics in the study area. Soil moisture in the top 50 cm of mineral soils ranged between 165 mm up to 270 mm of water storage, depending on the soil texture. Soil moisture at the highest forest sites, SMF₁₉₇₃ and SMF₂₀₆₈, had the

lowest variability, remaining near saturation throughout the wet season and decreasing mainly at the end of the dry season (Figure 2.6). This soil moisture pattern reflected a higher rainfall frequency and likely reduced evapotranspiration at these higher elevations. Soil moisture on intermediate elevation grasslands (SMG₁₈₁₉ and SMG₁₇₈₉) was lower and more variable than for the higher elevation forest sites (Figure 2.6), likely due to lower rainfall inputs and higher evaporative demand. At the lowest elevation grasslands (SMG₁₇₂₉) and forests (SMF₁₇₂₀), soil moisture was most variable and reached the lowest levels during the dry season (Figure 2.6). These patterns were reflecting the potentially highest evaporative demand compared to the other sites.

Soil moisture decrease rates during dry spells varied between sites and between dry spells: from an elevation driven trend during the shortest evaluated dry spell (3-day; SMF₂₀₆₈ and SMF₁₉₇₃ = 1.1 mm d⁻¹, SMG₁₈₁₉ = 5.3 mm d⁻¹, SMG₁₇₈₉ = 4.4 mm d⁻¹, SMG₁₇₂₉ = 6.5 mm d⁻¹, SMF₁₇₂₀ = 6.5 mm d⁻¹); followed by a land cover trend with lower depletion rates in forest soils than in grassland soils during the 5- and 7-day dry spells (5-day: SMF₁₉₇₃ = 1.4 mm d⁻¹, SMF₁₇₂₀ = 2.3 mm d⁻¹, SMF₂₀₆₈ = 2.5 mm d⁻¹, SMG₁₈₁₉ = 2.8 mm d⁻¹, SMG₁₇₈₉ = 2.8 mm d⁻¹, SMG₁₇₂₉ = 4.0 mm d⁻¹; 7-day: SMF₁₉₇₃ = 1.4 mm d⁻¹, SMF₁₇₂₀ = 1.4 mm d⁻¹, SMF₂₀₆₈ = 1.8 mm d⁻¹, SMG₁₈₁₉ = 2.0 mm d⁻¹, SMG₁₇₈₉ = 2.9 mm d⁻¹, SMG₁₇₂₉ = 3.5 mm d⁻¹); to a depletion rate pattern independent from elevation and land cover in the 12-day dry spell (SMG₁₈₁₉ = 1.5 mm d⁻¹, SMF₁₉₇₃ = 1.7 mm d⁻¹, SMF₁₇₂₀ = 2.4 mm d⁻¹, SMF₂₀₆₈ = 3.0 mm d⁻¹, SMG₁₇₈₉ = 3.4 mm d⁻¹, SMG₁₇₂₉ = 4.7 mm d⁻¹).

2.3.3 Streamflow response

The streamflow estimates obtained from all the fitted rating curves strongly indicated that the median streamflow between catchments differed in both seasons (*sensu* Chambers et al., 1983) even though the error bounds were large and that the 95% data error bounds for the catchments overlapped (Figure 2.7). The highest total streamflow for the study period

was recorded in FOR (5018 mm; 2.5%=4535 mm; 97.5%=5535 mm; Table 2.5), as well as the highest mean daily streamflow per season: $FOR_{wet}=16.7 \text{ mm d}^{-1}$ (2.5%=14.9 mm d⁻¹, 97.5%=18.7 mm d⁻¹; Figure 2.7), and $FOR_{dry}=7.7 \text{ mm d}^{-1}$ (2.5%=6.4 mm d⁻¹, 97.5%=8.8 mm d⁻¹; Figure 2.7). A smaller total streamflow was recorded in DEF (4619 mm; 2.5%=4231 mm; 97.5%=5107 mm; Table 2.5). During the wet season DEF's mean daily streamflow was slightly smaller compared to FOR: $DEF_{wet}=16.0 \text{ mm d}^{-1}$ (2.5%=14.5 mm d⁻¹, 97.5%=17.9 mm d⁻¹; Figure 2.7), while in the dry season its mean daily streamflow was the lowest of the three catchments: $DEF_{dry}=5.8 \text{ mm d}^{-1}$ (2.5%=5.1 mm d⁻¹, 97.5%=7.0 mm d⁻¹; Figure 2.7). The lowest total streamflow was recorded in INT (4026 mm; 2.5%=3658 mm; 97.5%=4414 mm; Table 2.5), as well as the lowest mean daily values for the wet season: $INT_{wet}=13.1 \text{ mm d}^{-1}$ (2.5%=11.8 mm d⁻¹, 97.5%=14.6 mm d⁻¹; Figure 2.7). During the dry season it had an intermediate mean daily streamflow: $INT_{dry}=6.9 \text{ mm d}^{-1}$ (2.5%=5.9 mm d⁻¹, 97.5%=8.0 mm d⁻¹; Figure 2.7). Differences in dry season streamflows also reflected the larger fraction of the catchments' areas at higher elevations where rainfall was higher (Table 2.1).

The mean maximum error range of all the single stage-discharge measurements was similar between catchments (37-38%; Table 2.5 and Figure 2.3). The bootstrapped estimated level power values for FOR and DEF were close to theoretical values for V-notch weirs (*i.e.* 2.5; Table 2.5; Bos, 1989). The low flow segment exponent for INT represents a unique combination of streambed geometry and streamflow friction and the high flow segment resembles the theoretical value for a rectangular weir (*i.e.* 1.5; Table 2.5 and Figure 2.3; Bos, 1989). The adopted catchment delineation method combining the GPS+DEM error reduced the delineation uncertainty in comparison to only using the DEM error (Table 2.5).

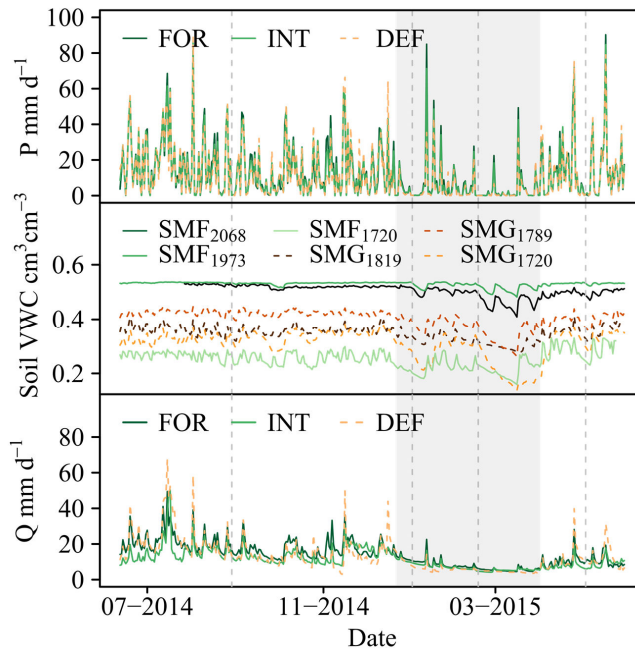


Figure 2.6. Hydrological dynamics over the observation period. Catchment interpolated rainfall (P ; mm d^{-1}), soil VWC weighted mean for 50 cm deep profiles ($\text{cm}^3\text{cm}^{-3}$) and runoff (Q ; mm d^{-1}) time series. The grey area represents the dry season. The vertical dotted grey lines mark the beginning of the four selected dry spells for soil moisture decrease analysis.

The total streamflow uncertainty ranges were similar for all three catchments (% of mean streamflow): DEF=876 mm (19%), INT=757 mm (19%), and FOR=1000 mm (20%; Table 2.5). These values were within the uncertainty range for total estimated discharges (20-40% uncertainty range; McMillan et al., 2012 and references therein). However, those studies were based on velocity area measurements and not on the salt dilution method that was employed in our study. Tomkins (2014) reported a considerable scatter at low stages far exceeding the 10% error bounds and showed that despite very careful weir constructions, stage-discharge relations in small headwater catchments are likely more variable compared to gauges located further downstream that collect water from a larger

area and have a higher discharge. This is potentially explained by the larger effect on the stage-discharge relation caused by small changes in the streambed. Furthermore, it was extremely difficult to keep the streambeds completely unchanged due to their loose-rock constitution despite our persistent efforts in maintenance.

Table 2.5. Estimated uncertainties: stage-discharge point data maximum error range (%), level power, catchment area estimations (ha) from the GPS+DEM approach and the DEM-only approach, and total streamflow (mm).

	Stage-discharge	Level power mean (min-max)	DEM-only areas (+/-)	GPS+DEM areas (+/-)	Streamflow (2.5%-97.5%)
DEF	37%	2.4 (1.7-3.3)	425 (20/100)	373 (5/5)	4619 (4231-5107)
INT	37%	Low segment: 0.8 (0.2e ⁻³ - 1.3) High segment: 1.40 (0.5e ⁻³ - 2.3)	306 (40/10)	300 (8/6)	4026 (3658-4414)
FOR	38%	2.1 (1.4 - 3.3)	297 (30/90)	348 (7/8)	5018 (4535-5535)

When comparing the mean daily streamflow values with rainfall for DEF and FOR we found that streamflow exceeded rainfall (Figure 2.7). During the wet season the inferred missing water inputs at DEF and FOR, based on the observed differences between mean rainfall and streamflow, ranged from 1.3 mm d⁻¹ up to 1.5 mm d⁻¹, respectively. During the dry season the missing water inputs were 2.0 mm d⁻¹ in DEF, 2.3 mm d⁻¹ in INT and 2.5 mm d⁻¹ in FOR.

Streamflow exceedance probability curves provide insights to the differences in the hydrologic behaviour of the catchments (Figure 2.8). During the wet and dry seasons there were similar patterns between INT and FOR. In contrast, there was a stronger inter-seasonal variation in DEF. During the wet season, when rainfall was evenly distributed throughout the study area (see Section 2.3.1), DEF maximum streamflows were higher than those of the other catchments. This indicated a higher streamflow sensitivity to

extreme rainfall events. During the dry season the lowest streamflow was recorded in DEF. The hydrograph results, expressed by the R^2 values of the multilinear regression model and the slopes of the individual regressions with various lag times, complemented the analyses from the streamflow exceedance probability curves by explicitly including rainfall in the analysis (Figure 2.9). The higher rainfall-streamflow multilinear model correlation values for all catchments during the wet season ($R^2_{DEF}=0.59$, $R^2_{INT}=0.48$ and $R^2_{FOR}=0.54$), compared to the dry season ($R^2_{DEF}=0.22$, $R^2_{INT}=0.24$ and $R^2_{FOR}=0.30$) reflected that the catchments were (nearly) saturated during the wet season when incoming rainfall is directly translated into streamflow. Comparing the three catchments, during the wet season all peak responses were at similar lag times (60 minutes), but DEF had the highest rainfall-streamflow slope (coefficient from the linear model). During the dry season, the correlation of the multilinear model (R^2) decreased for all catchments (Figure 2.9). In terms of the timing of streamflow responses to rainfall, in DEF the lag time in streamflow to rainfall response increased from 60 min during the wet season to 150 min in the dry season while for FOR and INT it remained the same (50 to 60 min). In addition, DEF's linear model coefficients dropped between the wet (maximum slope = 0.027) and dry season (maximum slope = 0.011), whereas, these remained relatively constant in FOR (wet and dry season maximum slope = 0.014) and in INT (wet season maximum slope = 0.012; dry season maximum slope = 0.010; Figure 2.9).

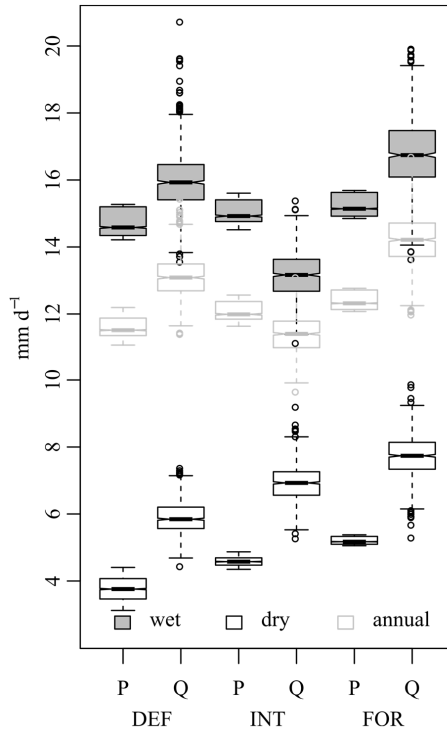


Figure 2.7. Comparison of water balance components. Total and seasonal rainfall (P) and specific runoff (Q) notched boxplots per catchment.

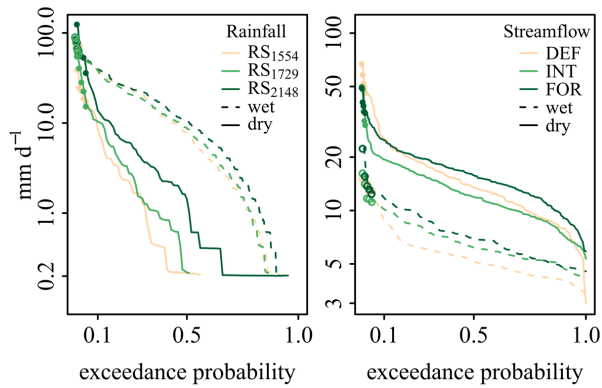


Figure 2.8. Exceedance probability curves for rainfall and streamflow. Left: seasonal rainfall. Right: Streamflow. Lines are shown per catchment with y-logarithmic axes. Circles show the 10 most extreme data points.

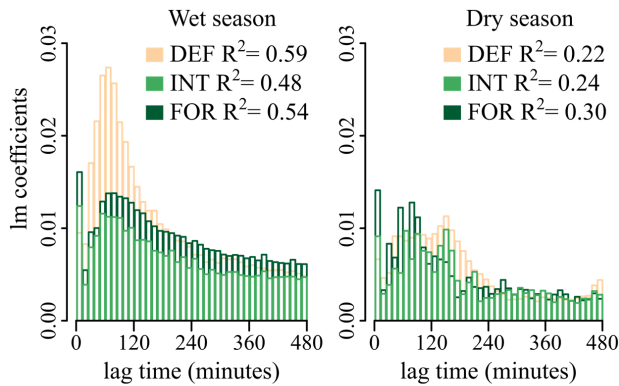


Figure 2.9. Seasonal discrete unit hydrographs per catchment. On the y-axis the regression slope for each time lag between rainfall and streamflow. The R^2 values are derived from the multilinear model.

2.4 Discussion

2.4.1 Meteorological spatial and temporal variability

The spatio-temporal meteorological patterns at our study area follow the trends of other TMCFs on the eastern Andes in Bolivia (Schawe et al., 2011), Ecuador (Emck, 2007); and Peru (Rapp and Silman, 2012; Table 2.6). At all eastern Andean sites solar radiation and air temperature decreased with elevation whereas cloud cover, relative humidity and precipitation increased with elevation. This pattern, as well as the observed diurnal pattern in precipitation, are related to the regional orographic effects in which cloud/fog cover increases with elevation (Bendix et al., 2008b). An exception is the observed precipitation trend in Peru (Rapp and Silman, 2012). Our annual and wet season rainfall measurements at the sampled elevations were generally larger than those reported at other sites. During the wet season the wettest month was recorded in Ecuador (950 mm) followed by Colombia (689 mm), Bolivia (650 mm) and Peru (410 mm). The reported rainfall in Ecuador at 2930 m asl was particularly high after wind correction due to mean wind speeds of 6 m s^{-1} (Emck, 2007). Other methods that consider the catchment's wind

exposure can also lead to correction factors of 5 for extreme wind speeds (monthly mean values $>5 \text{ m s}^{-1}$), leading to a large rainfall increase after wind correction (Mulligan and Burke, 2005). However, wind speeds at the study area were comparatively low. Furthermore, mean wind speed was higher at GWS₁₈₁₉ than at FWS₂₁₄₈ (Figure 2.4). These differences do not agree with the wind-speed-ups expected with an increase in elevation (*e.g.* Miller and Davenport, 1998). However, the change in the speed-up ratio is dependent on surface roughness (Miller and Davenport, 1998). In our case, GWS₁₈₁₉ is located downwind from grassland dominated areas, whereas FWS₂₁₄₈ is located downwind from forest dominated areas. In this regard two data points within such complex terrain both topographically and in surface roughness (land cover) are not enough to define wind-speed patterns along the elevation gradient.

Despite the proximity to the equator, the observed solar radiation at our sites was lower than the solar radiation measured at the other TMCFs at similar elevation ranges (Table 2.6). Overall, observed rainfall and solar radiation as well as inferred cloud cover at our study area indicated a stronger fog influence at lower elevations compared to other eastern Andean areas (Table 2.6). This larger fog influence and the higher rainfall at our study sites could be partially caused by the eight month period in which a vast area of upwind savannahs are flooded ($107,530 \text{ km}^2$; Hamilton et al., 2002). A higher evaporation is expected from an upwind open water source than from a forested system and this would enhance precipitation downwind in the Andes. Regarding dry season rainfall, our study site had the driest month (38 mm) compared to Peru and Bolivia (both 50 mm), and Ecuador (150 mm). Furthermore, our data also showed that the fog influence at lower elevations appears to be more limited whereas at the higher elevations it is more persistent, suggesting a seasonal upward shift in cloud cover. This might reflect the dry

soil moisture conditions prevailing in the upwind savannah region during the four month dry season.

Table 2.6. Meteorological variable mean values for eastern Andean TMCFs in Colombia (this study), Bolivia, Ecuador and Peru, contrasted with the Central and South American and the Caribbean (C&SA-C) TMCFs' climate characterization.

Country	Latitude	Elevation (m asl)	Solar rad. (MJ d ⁻¹)	Temp (°C)	RH (%)	Precipitation (mm)	Cloud cover (%)
Bolivia	16°S	1850	15.5	16.8	90	2310	37
		2600	10.4	12.8	96	3970	58
		3050	9.9	10	97	5150	62
Ecuador	4°S	1970	11	15.4	90	3061	60
		2930	9.5	9.3	96	3898 (wcor 6152)	67
Peru	13°S	1840	c. 11.7	16.5	82	4200	60-80
		2720	c. 10.1	11.8	92	3000	
Colombia	5°N	1850	11.0	16.3	93	3950 (at 1550m asl)	75
		2148	7.9	14.2	97	4700	87
C&SA-C	23.5°N- 35°S	1747	NA	17.5	NA	1779	NA

We are aware that the application of only two AWS and a year of field observations pose limitations on this comparative assessment. Longer and simultaneous meteorological time-series are required to test our hypotheses on the drivers of the meteorological contrasts between the Amazon and Orinoco river basins' TMCFs. Nevertheless, our field data analysis and interpretation are supported by other studies that aimed to assess the causes of observed shifts in the condensation level at TMCF sites (*e.g.* Ray et al., 2006 in Costa Rica). Ray et al. (2006) showed by modelling and field data analysis that deforestation in the lowlands and premontane upwind areas increase the average cloud base and, consequently, decrease the extent of montane forests immersed in clouds. Their modelled surface and dew-point temperatures, and sensible and latent heat fluxes in the

premontane and lowland areas had warmer and drier air masses occurring over deforested areas compared to intact forests. The moisture content of the air masses carried by the easterly trade winds to the Orinoco River basin TMCs would be affected by the seasonal changes in the sensible and latent heat fluxes on the upwind savannahs. In contrast, the upwind forest cover for the other eastern Andean sites is relatively more homogeneous and seasonally stable, with even higher evapotranspiration during the dry season (Kim et al., 2012).

Whilst the upland-lowland hydrological feedbacks have been analysed in the Amazon basin (e.g. Poveda et al., 2006), the Orinoco basin feedbacks have not been explored. In the Amazon basin, feedbacks between the lowlands and the Andes are recognized in precipitation recycling and fluxes (energy, water, sediments, nutrients and pollutants; Poveda et al., 2006). Understanding these feedbacks becomes highly relevant in a changing climate and when the Orinoco river basin lowlands' land cover will be shifted from the savannahs (low vegetation) to plantations for biofuel or wood-pulp production (Pardo-Vargas et al., 2015).

2.4.2 Meteorological effects on catchment hydrology

Despite the relative small size of the catchments (3.0-3.7 km²), the clear elevation gradients, expressed by wetter atmospheric conditions at the higher elevations and drier atmospheric conditions at the lower elevations, are also reflected in the catchments' hydrology (Figure 2.4 and Figure 2.7). Whereas wet season rainfall inputs were fairly similar between elevations, the atmospheric demand driven by solar radiation, temperature and relative humidity was more variable (Figure 2.4). During the dry season, contrasts in meteorological parameters became larger with pronounced differences in rainfall amounts and rainfall frequency, similar to what has been described in Costa Rica (Goldsmith et al., 2013). While at the low elevations rainfall was reduced from ~14.5 to

~3 mm d⁻¹ and the rainfall frequency (days with rainfall) decreased from 96% to 53%, at the high elevations rainfall decreased from 16.0 to 6 mm d⁻¹ and the rainfall frequency from 96% to 93% (Table 2.3). The atmospheric evaporative demand also increased but for the high elevations the dry season incoming solar radiation ($96 \pm 43 \text{ W m}^{-2}$) and relative humidity (97%) remained higher than those measured at the low elevation in the wet season (solar rad= $125 \pm 60 \text{ W m}^{-2}$, RH= 94%; Figure 2.4). Therefore, at the high elevations the dry season is much milder compared to the lower elevation. In fact, the soil moisture levels at the high elevation remained relatively high during the dry season in contrast to soil moisture levels at the low elevations. Nevertheless, soil moisture depletion rates during dry spells did not persistently responded to the meteorological elevation gradients, suggesting an additional land cover influence. A plausible reason why in some cases water uptake was lower in TMCFs is their tendency to close stomata under high atmospheric vapour pressure deficits (Motzer et al., 2005). This observed higher water use by grasslands compared to forests has been reported previously (e.g. van der Molen et al., 2006; Williams et al., 2012). The observed contrasts in soil moisture decrease between sites and between dry spell lengths reflect the complex interactions between plant species, soil moisture dynamics, and atmospheric water demand, which have only been recently addressed in more detail for TMCFs (Eller et al., 2015 and Chapter 3).

The differences in seasonal streamflow between catchments can be partially explained by the catchments' contrasting elevations. FOR, mainly located at the higher elevations had higher streamflow values during both the wet and the dry season than INT and DEF, located mainly at the lower elevations (Table 2.1 and Figure 2.7). During the dry season the elevation contrasts between catchments (FOR higher than INT and INT higher than DEF) were reflected in the dry season streamflows (Figure 2.7). This confirms that dry season streamflows were largely modulated by the higher water inputs at the higher

elevations. FOR's higher rainfall-streamflow responses during the dry season compared to those of the other two catchments, are consistent with the milder dry season conditions at the higher elevations that lead to higher soil moisture and likely higher antecedent canopy wetness in contrast to lower antecedent moisture conditions occurring at the drier low elevations. In addition, DEF's delayed response in streamflow to rainfall likely reflected a drier system that during dry season rainfall events will first fill its water storages before reaching the streambed. During the wet season, the faster rainfall-streamflow responses observed in DEF did not agree with what was expected from the catchments' elevation differences (Table 2.1 and Figure 2.9). If the higher elevations tended to be more saturated, FOR should have had higher rainfall-streamflow responses which was not the case according to the discrete unit hydrograph (Figure 2.9). Also, during the wet season INT had the lowest streamflow among the studied catchments but this behaviour could not be explained by the elevation moisture gradient alone. These contradicting results might be a consequence of differences in land cover between catchments.

2.4.3. Land cover effects on stream flow

Isolating the land cover effects on streamflow from spatial variations in meteorology, soils and topography is challenging. However, the information derived from the soil maps of the national geographic institute (IGAC) provide valuable information to describe soil contrasts between catchments. The steep slopes have the shallower LU-TD soil association while the less steep slopes have the deeper TU-TD soil association. This implies that LU-TD is mainly found at the higher elevations of DEF and INT and in most of FOR's area. TU-TD is mainly found at DEF's and INT's lower elevations. From this description, the shallower soils and steeper slopes in FOR compared to DEF and INT would lead to faster rainfall runoff responses in this catchment, especially in the wet

season but this was apparently not the case (Figure 2.9). Furthermore, the role of soil water storage to support the dry season base flow would also be less in FOR than in the other two catchments but this does not agree with the observations of having higher dry season streamflows at FOR (Figure 2.7). This suggests that slope and mineral soil depth are not the main dominant factors explaining streamflow for this TMCF site.

From a land cover perspective, forests have more complex canopies with a larger canopy water storage capacity than grasslands. A larger canopy water storage means more water being intercepted and evaporated from the canopy, and implies reduced water inputs to the ground and to streamflow. It also means that even if the canopy storage is saturated it will take longer for the water to reach the ground delaying the rainfall-streamflow responses (Keim et al., 2006). TMCFs also have a deep organic layer above the mineral layers (Roman et al., 2011) while grasslands tend to have, if any, thinner organic layers. Furthermore, grasslands used for cattle ranching will tend to have lower infiltration capacities and hence more overland flow (Tobón et al., 2011). In this regard, it is expected that FOR and INT would have slower and less pronounced rainfall-streamflow responses whilst DEF would have faster and more pronounced rainfall-runoff responses. This is in agreement with the results of the discrete unit hydrographs for the wet season (Figure 2.9) and with reports from other forests around the world, including TMCFs, where deforested catchments have faster rainfall-streamflow responses given the relation between antecedent wetness. (e.g. TMCFs: Muñoz-Villers and McDonnell, 2012; Muñoz-Villers and McDonnell, 2013; Roa-García et al., 2011; Other forests: Bruijnzeel, 2004; Zhao et al., 2012). This also suggests that the soil-water interactions in the top layer largely define the rainfall-streamflow responses. INT's lower streamflow compared to DEF's during the wet season could also be related to land cover. INT has the largest low elevation forest cover whereas DEF has the largest low elevation grassland cover and therefore, INT

would have the largest canopy interception capacity. Forests at the lower elevations intercept more water as the water stored in the canopy evaporates faster at these low elevations compared to the forests at the higher elevations. Additionally, transpiration is also higher given that leaf wetness is likely less frequent compared to the higher elevations. This might all together explain that this catchment had the lowest wet season streamflow.

The estimated missing water inputs obtained by comparing rainfall and streamflow (Figure 2.7) are not unique to the study area. This issue has also been reported in several other TCMF studies (e.g. Clark et al., 2014; Zadroga, 1981). Zadroga (1981) concluded that streamflow excess in a Costa Rican TCMFs was related to underestimation of rainfall at the highest elevations of the catchment. However, Bruijnzeel et al. (2011b) suggested that Zadroga did not consider cloud water input. In our case, the rainfall gauge distribution covered most of the elevation range of the study area, although elevations above 2148 m asl were not represented. This has potentially a stronger effect on FOR with c. 26% of its area above this elevation whilst for DEF and INT have <3.5% of their area above this elevation. Fog inputs at our study area are also possible, especially at higher elevations which are mainly covered by forests (Figure 2.5, Table 2.1). In fact, missing water inputs (Figure 2.7) agree with fog inputs reported for TCMFs (between 0.5 mm d⁻¹ and 3.3 mm d⁻¹; Giambelluca and Gerold, 2011) but the conflict between the relatively low fog frequency observed in the dry season (Figure 2.5) in contrast to the higher estimated fog frequency by solar radiation (Table 2.2), suggests that there might be other water sources in addition to fog. Clark et al. (2014), who also reported missing water inputs in a Peruvian TCMFs during the dry season, estimated that the mean daily fog inputs could be 0.9 mm d⁻¹ whereas the dry season inferred contribution from soil water storage was 65 mm. However, these were not enough to explain all the missing water and so they

concluded that ground water, which was not monitored during their study, could be an important component to consider in the water balance. We estimated soil moisture storage in the study area (165 mm to 270 mm) but we cannot directly translate this water storage to soil moisture contribution to discharge because we were not monitoring lateral flows and did not measure deeper soil moisture dynamics. Nevertheless, soil moisture represents a likely important water reserve that could contribute to sustain baseflows. Isotope or chemical analyses (*e.g.* Mosquera et al., 2016; Scholl et al., 2011) could help confirming this hypothesis.

2.5 Conclusions

Results based on a year of dedicated field observations in three small neighbouring headwater catchments in the eastern Andes reveal a strong spatial and temporal variability in hydro-meteorological conditions along the TMCFs' elevation range and related to the amount of TMCF cover. Higher canopy and soil water storages in the more forested catchments compared to the less forested catchment potentially reduce rainfall-runoff responses during the wet season, when rainfall was found to be relatively homogeneous throughout the study area. In contrast, during the dry season the higher elevations receive larger water inputs than the lower elevations. We found the highest average streamflow in the catchment with largest TMCF cover, but its higher average elevation prohibited direct attribution of streamflow to TMCF cover. Overall, we were unable to close the catchment water budgets even after careful consideration of all relevant uncertainties including uncertainties in rating curves and catchment areas, and found higher streamflow than rainfall in all three catchments. This suggests a potential important role for additional water inputs by fog and soil water contributions that were not considered in this work. From a broader perspective, meteorological conditions as a function of elevation at our field site were quite similar to the conditions found at other eastern Andean TMCFs.

However, seasonal contrasts suggest that these TMCs in the Orinoco River basin are subjected to upwind moisture dynamics. Thus, they might be vulnerable to changes in the upwind hydrology associated with land use change. This description and analysis of the hydro-meteorological patterns in Orinoco River basin TMCs provides new information on the hydrology of continental TMCs with a unique upwind land cover that constitutes an opportunity to better understand the feedbacks between the lowlands and mountain systems that support regional water dynamics.

Appendix 2A

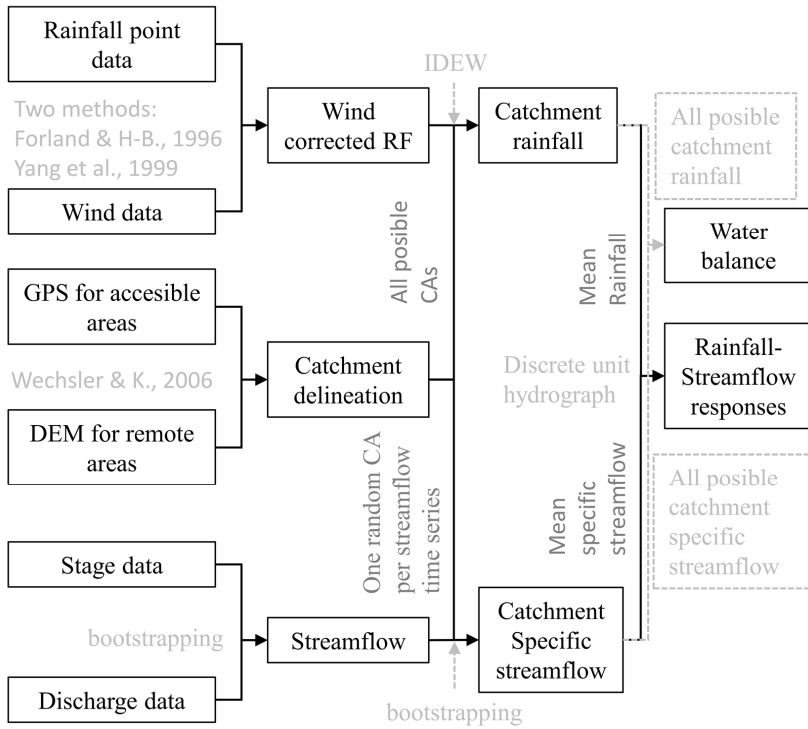
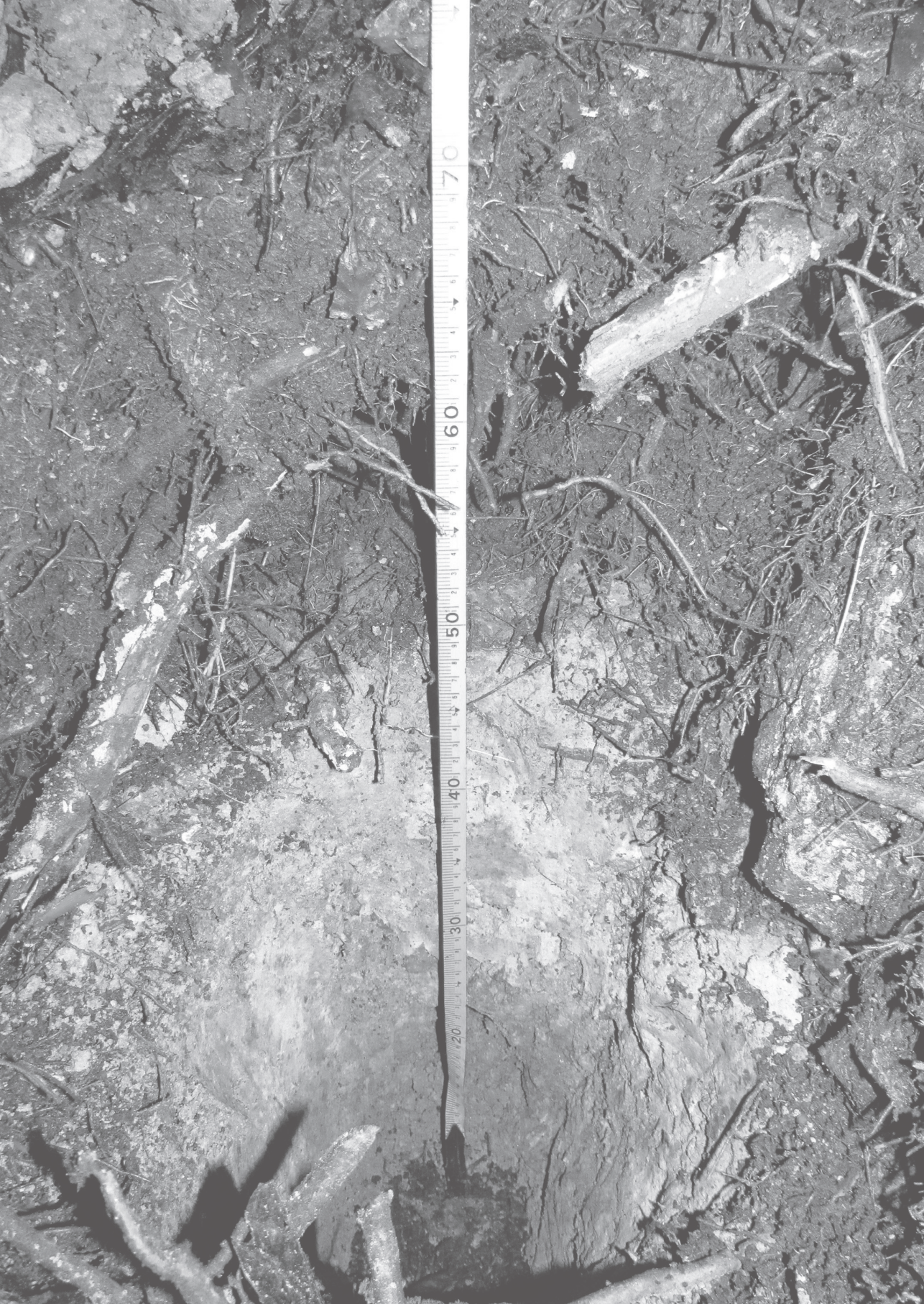


Figure 2.A. Flowchart with the methods to estimate the water balance and the rainfall-streamflow responses. Boxes show data and results. In light grey, clarification of the chosen data inputs. In dark grey, methods. The dotted lines and boxes on the right side indicate the data used to estimate the water balance.



CHAPTER 3

Tropical Montane Cloud Forests in the Orinoco River basin:
The role of soil organic layers in water storage and release

Chapter 3

Tropical Montane Cloud Forests in the Orinoco River basin: The role of soil organic layers in water storage and release²

The Tropical Montane Cloud Forest (TMCF) is a hydrologically unique and highly vulnerable ecosystem to changes in land-use and climate. Assessing the impacts of these changes needs to consider soil-water dynamics. In particular, the organic layer and its functioning requires attention because its difference in water retention characteristics and root density compared to the underlying mineral soils. A higher root density and a higher water storage capacity of the organic layer compared to the mineral soils suggests that most nutrient and water uptake occurs in this layer. However, hydraulic properties of mineral soils and their impact on hydrology of TMCFs have been poorly studied. Here we provide organic layer water retention curves for TMCFs' soils that were measured in the laboratory. With these data we assessed the potential land-use and climate change impacts on TMCFs' soil moisture dynamics. From the land-use change perspective, we estimated the water storage capacity loss by slash-and-burn deforestation practices. These estimates show that the storage loss ranges from 35 to 59 mm when TMCFs are converted to pastures. This is several times higher than the estimated TMCFs' canopy storage capacity (2 to 5 mm). Therefore, the higher peak flow observations in deforested catchments might not only be explained by a decreasing canopy water storage but also likely due to a decreasing soil water storage. From the climate change perspective, we evaluated the effect of contrasting dry season conditions on soil moisture and transpiration using a 1-D water-flow model, and assessed the sensitivity of these hydrological variables to uncertainties in saturated hydraulic conductivity. Although

² This chapter has been published as: Ramírez, B.H., van der Ploeg, M., Teuling, A.J., Ganzeveld, L., and Leemans, R. (2017). Tropical Montane Cloud Forests in the Orinoco River basin: The role of soil organic layers in water storage and release. *Geoderma*, 298:14-26, DOI: 10.1016/j.geoderma.2017.03.007

transpiration was not limited by soil moisture during the mild dry season, it was affected during the severe dry season and continued to decline under expected climate change with the prolongation of dry spells. Our results show that the organic layer is a key element in TMCFs' hydrological functioning and call for an increased focus on the role of organic soils when evaluating effects of land-use change.

3.1 Introduction

Understanding the consequences of changes in land-use and climate for hydrologic processes is a major scientific challenge (DeFries and Eshleman, 2004; Hooke and Martín-Duque, 2012; Wagener et al., 2010). The implications of these changes on the water cycle and ultimately water availability at variable spatial and temporal scales are subject to much debate and research (*e.g.* Bonell, 2010; Ellison et al., 2012). From an ecological perspective, native vegetation which is a unique species assemblage, is well adapted to site-specific water, nutrient and energy availability (Knapp et al., 2008; Reichstein et al., 2014). Simultaneously, this vegetation dynamically controls water fluxes between the atmosphere and the soil (Rodríguez-Iturbe, 2000). Both vegetation and its hydrology are affected in the short and the long-term by changes in land-use and climate. The initial short-term hydrological land-use change impacts are caused by structural and physical modifications of vegetation and soils (Zhao et al., 2012), while the long-term impacts depend on a new equilibrium between the interacting soils, the modified land covers and the atmosphere (Brown et al., 2005). Climate change alters the water-energy balances and plant-water processes and these eventually cause shifts in species composition (Beniston, 2003; Eller et al., 2015; Walther et al., 2002). In order for land-use and water resource management plans to be sustainable, these plans have to consider land-use change and climate change impacts.

Tropical Montane Cloud Forest (TMCF) is a hydrologically unique but highly vulnerable ecosystem to both climate and land-use changes (Scatena et al., 2011). TMCFs' hydrology is tightly linked to the occurrence of fog and its effect on: 1) reducing evapotranspiration (Eller et al., 2015; Letts and Mulligan, 2005; Reinhardt and Smith, 2008), 2) adding a source of water to the system through fog interception (Zadroga, 1981), and 3) enabling foliar water uptake (Eller et al., 2013; Gotsch et al., 2014). Therefore, an

increase in cloud-base altitude (Still et al., 1999) and in the frequency of extreme dry events (Magrin et al., 2014) due to climate change could severely affect TMCFs' hydrology. Oliveira et al. (2014) showed that TMCFs' species are vulnerable to atmospheric drought due to hydraulic failure. However, seasonal TMCFs' soil moisture dynamics and the potential impacts on root water uptake by soil moisture deficits are poorly understood. TMCFs can be found on various soil types (Roman et al., 2011), but regardless of the soil type they often have thick top organic soil horizons that can be more than 1 m deep. These layers consist of decomposing organic material with a dense fine root network (Hafkenschied, 2000; Tanner et al., 1998). Root density is typically higher in this organic horizon than in the underlying mineral horizon, indicating that most of the water and nutrient uptake occurs in this layer (Leuschner et al., 2006). Therefore, understanding the organic layer's hydrological dynamics is important to assess potential climate-change impacts on TMCFs.

In addition to climate-change impacts, land-use change also poses a major threat as more than half of TMCFs world-wide were converted to other land use types by the year 2000 (Mulligan, 2011). Studies assessing the deforestation impact on the rainfall-streamflow responses in TMCF catchments, have shown higher peak flows in deforested catchments (*e.g.* Muñoz-Villers and McDonnell, 2013; Roa-García et al., 2011). These increases are generally attributed to a reduced rainfall canopy interception and reduced infiltration rates in grasslands compared to TMCFs. However, the impact of the loss of the organic during and after deforestation has not been considered yet. After deforestation, the organic layer and its water storage capacity are irreversibly lost. This occurs rapidly in areas, like the Andes, where slash-and-burn practices are common (Lambin et al., 2001). Data on the water storage capacity of these organic layers have only been established in Jamaican TMCFs (Kapos and Tanner, 1985).

Organic layers have high water retention capacities (Yang et al., 2014) and likely are the major source for transpiration. Transpiration and wet canopy evaporation tend to equally contribute to the total evaporative water loss in TMCFs (Bruijnzeel et al., 2011a). Water uptake in the root zone area implies that the organic layer acts as a highly dynamic systemic water storage component. The organic layers generally also present high infiltration rates that reduce runoff (Hartanto et al., 2003). Yet, infiltration rates are governed by the saturated hydraulic conductivity (K^*), which is a strongly scale-dependent variable (Hu et al., 2012), especially in organic soils (Van der Ploeg et al., 2012). Additionally, K^* depends on its quantification method (Fodor et al., 2011; Schellekens et al., 2004). This means that K^* variability needs to be considered when evaluating the organic layer's role in TMCFs' soil moisture dynamics. The vegetation's water use is constrained by the soil plant available water (PAW), the amount of water that plants can extract from the soil column to fulfil evapotranspiration demands. PAW is estimated by the difference between the water content at field capacity (θ_{FC}) and at wilting point (θ_{WP} ; Dunne and Willmott, 1996) over the root zone. θ_{FC} and θ_{WP} are defined from water retention curves (WRC) and to estimate the WRC from soil texture by using pedo-transfer functions is well possible because large data sets are available for mineral soils (Minasny and Hartemink, 2011; Wösten et al., 2001). However, K^* values can be underestimated due to preferential flows caused by gravel content in the soils and biological activity (Beckers et al., 2016; Bogner et al., 2008; Ravina and Magier, 1984). In contrast, such pedo-transfer functions cannot be used to estimate the organic layer's WRC because these layers consist of decomposing organic material that lack mineral soil particles. Hence, to evaluate climate and land-use change impacts on TMCFs we need to obtain data on the WRC of organic layers and improve our understanding on TMCFs' soil moisture dynamics.

Our study area, located in the northern eastern Andes (Colombia) provides a unique opportunity to evaluate land-use and climate change impacts on TMCFs. First, it comprises three neighbouring catchments with contrasting TMCF covers. The catchment with larger grassland extents generates stronger wet season rainfall-streamflow responses. This likely reflects a reduction in its water storage capacity. Second, our observations show that during the dry season rainfall at the low elevation (1554 m asl) was lower (2.7 mm d^{-1}) than at the high elevation (2148 m asl: 6.5 mm d^{-1}), suggesting that dry season rainfall at the higher elevation is very important in sustaining high soil moisture levels and streamflow. Therefore extreme dry seasons could potentially lead to soil moisture deficits.

The characteristics of our study area enabled us to pursue the following objectives: 1) quantify the loss of water storage due to organic layer removal and 2) evaluate seasonal TMCFs' soil moisture dynamics under observed and hypothetical extreme dry seasons. We measured the organic layers' WRC in the laboratory from core samples and inferred the mineral layer WRC from their soil texture. We also measured in the field the organic layers' K^* . To achieve the first objective we determined the organic layer PAW and its water storage capacity. We then estimated the total water storage loss in a per catchment basis based on the extent of their deforested areas. To achieve the second research objective we analysed soil moisture data and parameterized the Hydrus1D water-flow model (Šimůnek et al., 2013) to simulate soil moisture dynamics under several observed contrasting dry seasons, including one influenced by the record 2015 El Niño (Jiménez-Muñoz et al., 2016), and under a hypothetical longer dry season. We also assessed the sensitivity of these hydrological parameters to uncertainties in K^* .

3.2 Materials and Methods

3.2.1 Study area

The three neighbouring catchments that we studied are located on the eastern slope of the eastern Andean Cordillera (Figure 3.1) at the municipality of Chámeza (Colombia). These catchments are fourth-order tributaries of the Orinoco River, and have different forest cover percentages: a deforested catchment (DEF) with 71% forest cover; an intermediate catchment (INT) with 84% forest cover; and a forested catchment (FOR) with 99% forest cover. Table 3.1 provides an overview of the catchments and their main characteristics.

Table 3.1. Catchment characteristics.

Catchment	Coordinates (decimal degrees)	Elevation range (m)	Size (km ²)	Forest cover	Grassland cover
Deforested (DEF)	72.910 E-5.230 N	1575-2241	3.71	71%	29%
Intermediate (INT)	72.900 E-5.243 N	1550-2256	3.50	84%	16%
Forested (FOR)	72.889 E-5.257 N	1668-2490	3.02	99%	1%

The eastern Andes are dominated by young mountains with steep slopes and sharp summits (Stallard et al., 1991). Our study area is located on two formations belonging to the Caqueza Group of Cretaceous origin: Las Juntas formation and Macanal formation (IGAC, 2014). The Las Juntas formation consists of black shales and sandstones, and the Macanal formation consists of black shales and siltstones (Mejía, 2008). Soils at the study area are classified following USDA (2010) into two associations: Typic dystrodepts-Typic udorthents (Entisol) and Lithic udorthent (Entisol)-Typic dystrodept (Inceptisol; IGAC, 2014). Lithic refers to shallow soils (<50 cm of depth) limited by bedrock contact (USDA, 2010). Inceptisols and Entisols generally undergo weak or very weak soil formation processes, respectively (Bockheim and Gennadiyev, 2000). The study area's current land cover consists of mature and old growth secondary forests (>10 y) and grasslands (Table 3.1). Most forests in the region are subjected to selective logging. Slash-

and-burn is the common local technique to transform these forests, first into annual crops and then into permanent grasslands (Lambin et al., 2001).

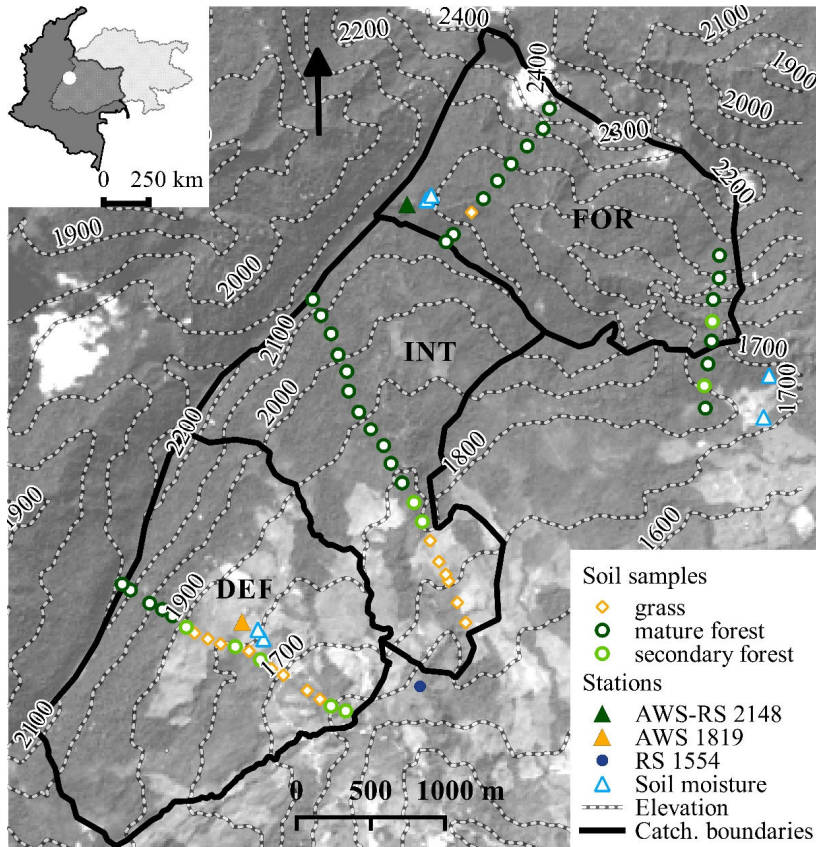


Figure 3.1. Map of study area and data collection setup. The upper left corner map shows the Orinoco river basin (light grey) and its overlap with Colombia (dark grey). The white dot represents the study area, enlarged on the main map. This map shows: 1) Elevation contours. 2) Catchment boundaries. 3) Study catchments: the less forested catchment (DEF), the intermediate forested catchment (INT); and the forested catchment (FOR). 4) Location of the collected soil samples classified according to the present land cover (grasslands, mature forest and secondary forest). 5) The data collection setup: Automated weather station (AWS) and rainfall gauging station (RS) at 2148 m asl; AWS at 1819 m asl; RS at 1554 m asl; and soil moisture sensors (SM). The background image is a Landsat 8, band 8 (15m resolution) from December 25th, 2013. Dark areas are forested whilst lighter areas represent low vegetation.

Climate data from April 2014 to April 2016 showed a mean daily temperature of 16.5°C and 14.5°C at 1819 m asl and at 2148 m asl respectively. Mean annual rainfall ranged between 4283 mm at 1554 m asl and 4966 mm at 2148 m asl. The mono-modal rainfall regime has a dry season from December to March during which less than 16% of annual rainfall occurs. Fog inputs have not been directly quantified at the study area given the difficulties to measure fog and to translate fog data into the amount of water that is actually intercepted by the canopy (Frumau et al., 2011). However, the measured mean solar radiation from June, 2014 to May, 2015, is below 20% of the expected clear sky solar radiation during 44% and 36% of the time at 2148 m asl and 1819 m asl, respectively. According to Haurwitz (1948), solar radiation below 20% of the expected solar radiation under clear skies indicates fog. Expected solar radiation under clear skies is estimated from extra-terrestrial solar radiation derived from solar geometry (Donatelli et al., 2006) and clear sky transmissivity through the Thornton and Running (1999) model. Furthermore, above 1900 m asl, almost all of tree trunks are covered with mosses (bryophytes) and bromeliads. Mosses, whose presence and abundance are related to fog immersion (Frahm and Gradstein, 1991), are extremely abundant on the ridges around 2000 m asl and grow on every substrate (exposed roots, trunks, leafs, and rocks).

3.2.2 Soil data collection and soil moisture

We collected samples from both the organic and the mineral horizon in these three catchments. Samples from the mineral horizon were used for texture analysis and combined with pedo-transfer functions (Schaap et al., 2001) to provide a good approximation of their hydraulic properties. In contrast, few observations regarding the hydraulic properties of organic layers and their pedo-transfer functions are available. These are required to establish hydraulic properties (Rudiyanto et al., 2016). Given the few available observations to infer those pedo-transfer functions, such as those reported

by Kapos and Tanner (1985) for Jamaican TMCFs, our collected soil core samples of the organic layers provide a unique data source on their hydraulic properties.

Fifty five soil samples were collected along four transects every 150 m in the INT and FOR catchment (19 and 17 samples, respectively) and every 100 m in the DEF (19 samples; Figure 3.1) during two field campaigns that took place from October to November 2013 and from April to September 2015. Differences in the sampling distances between catchments are explained by a higher land-cover heterogeneity in DEF in contrast to INT and FOR. At each site we sampled the organic layer (if present) and the top of the mineral horizon. Soil samples were collected with 5.08 cm diameter and 5 cm high PVC rings. Mineral samples were removed from the ring, placed in aluminium containers, oven dried at 70°C and manually ground with a ceramic mortar. During this grinding process we extracted roots. Finally, samples were sieved using a 2 mm copper sieve. Roots, coarse fragments (>2 mm) and fine soil material (<2 mm) were weighed and stored separately. Texture was determined for the fine soil material with a Coulter Beckman laser diffractor type LS230 following the standardized procedure (Arriaga et al., 2006). We used the neural network analysis of the software package Rosetta (from now on Rosetta; Schaap et al., 2001) imbedded in RETC software package (van Genuchten et al., 1991), to estimate the following hydraulic parameters: residual water content (θ_r), saturated water content (θ_s), the empirical α (cm^{-1} ; whose inverse value is often referred to as the bubbling pressure), the empirical parameter n and saturated hydraulic conductivity (K^*_{min} ; cm h^{-1}) all as a function of the particle size distribution per sample (van Genuchten, 1980). The pore connectivity term (l) was assigned a value 0.5 according to Mualem (1976).

Additionally, we quantified Organic Matter Content (OMC) by weight differences before and after placing the samples in a combustion oven at 550°C. For the organic horizons

we first performed at each sample point an infiltration test using the mini-disk infiltrometer (Decagon Devices Inc.) with a suction of -2 cm, on a thin layer (<5 mm) of siliceous sand. We estimated the saturated hydraulic conductivity by applying the Zhang function on the infiltration data (Zhang, 1997). We then collected the soil samples inserting the PVC ring and subsequently extracting the ring with the sample from the ground. Once the sample was out we used pruning scissors to cut the material protruding out of the ring. Samples were tightly packed with plastic wrap and transported to the laboratory where WRC were estimated using the sand box methods for head pressures between -0.49 kPa and -9.8 kPa, and the pressure cells for -98 kPa and -1554 kPa (Dane and Hopmans, 2002). We employed the RETC software package (van Genuchten et al., 1991) to infer from the measured WRC the organic horizon hydraulic parameters, except for K^*_{org} , which was measured at the field sites, and the dimensionless pore connectivity term l , which was set at a fixed value of 0.4 following Wösten et al. (1999) for European organic soils. We weighed the samples after they were oven dried at 105°C to estimate dry bulk density and porosity. OMC was determined with the same method used for the mineral soil samples. From the WRC we estimated gravitational water capacity and PAW for the organic layer in each of the catchments.

Soil volumetric water content (VWC, $\text{cm}^3 \text{cm}^{-3}$) was measured, from June 12, 2014 to April 15, 2016, at six locations within our study area using GS-3 frequency domain soil moisture sensors (Decagon Devices Inc.). Data from each sensor was recorded at 10 minute intervals on an EM50 data logger (Decagon Devices Inc.). Each soil moisture station (SM) consisted of three sensors inserted in the mineral soil at 10, 30 and 50 cm depths respectively. Three SMs were located on grasslands ($\text{SMG}_{\text{elevation m asl}}$): SMG_{1819} and SMG_{1789} (72.907E, 5.230N), which were 150 m apart and SMG_{1729} (72.877E, 5.245N). Three SMs were located in forested areas ($\text{SMF}_{\text{elevation}}$): SMF_{1973} and SMF_{2068}

(72.897E, 5.258 N), which were 200 m apart, and SMF₁₇₂₀ (72.876 E, 5.246 N) (Figure 3.1). The error specified by the manufacturer for the soil moisture sensors, which have been calibrated for typical (mineral) soils, is $\pm 0.03 \text{ m}^3 \text{ m}^{-3}$ (Campbell et al., 2009).

3.2.3 Hydrus1D modelling experiments: parameterization, input data and scenario study

The modelling component allowed us to integrate the observed soil moisture dynamics in the mineral layers and to explore the relevance of the organic horizon in the TMCFs' soil-water dynamics. We conducted model experiments with the Hydrus-1D (v4.16) modelling system for observed and hypothetical dry season conditions and also assessed the large uncertainty involved in TMCFs' K^*_{org} estimates, as well as the likely underestimation by Rosetta of K^*_{min} . Hydrus-1D is a software package that can simulate water movement in one-dimensional variably saturated media (Šimůnek et al., 2013). It solves the Richards's equation for variably saturated water flow and incorporates a sink term to account for root water uptake. We simulated water flow with root water uptake using the Mualem (1976) and van Genuchten (1980) single porosity model.

We implemented the Penman-Monteith approach (Monteith, 1981) in Hydrus1D to estimate potential evapotranspiration. Data used to parameterize the Penman-Monteith model were collected with two Vantage Pro2-plus automated weather stations ($\text{AWS}_{\text{elevation m asl}}$; Figure 3.1; Davis Instruments Corp.) These AWS were equipped with sensors that measured: shortwave incoming radiation (Vantage-Pro2 6450 Solar pyranometer), relative humidity, air temperature, wind speed (large cup anemometer) and barometric pressure. The low elevation AWS_{1819} was located on a grassland site in the DEF catchment at 2 m above the ground (72.907 E, 5.231 N). The high elevation AWS_{2148} was located 17 m above the ground in a scaffolding tower surrounded by a c.16 m forest canopy at FOR (72.897 E, 5.257 N; Figure 3.1). Both stations recorded data on a Weatherlink datalogger at 10 minute intervals which were then aggregated to one hour

time resolution. Cloudiness was estimated from an inferred transmission coefficient and clear sky solar radiation rates (see Section 2.1.). We verified these estimates of the maximum solar radiation by comparing them with the observed maximum radiation for the few days of clear skies recorded at each station. We applied a leaf-area index (LAI) of $4 \text{ m}^2 \text{ m}^{-2}$ and an albedo of 0.12 to represent the TMCFs' canopy (Bruijnzeel et al., 2011a). We used the S-shape root water uptake routine (van Genuchten, 1985) to allow for root water uptake under wet conditions. We set the pressure head value for halving the transpiration to -1000 cm, which corresponds to -98 kPa (or pF 3). This pressure head value was selected from the inspection of the WRC and represents the switch from a water content driven system to a pressure driven system when soils become drier (Minasny and McBratney, 2003). All other values required for the Penman-Monteith model and the S-shape root water uptake routine were as default values (see Šimůnek et al. (2013) for the default values).

We collected rainfall data, from June 12, 2014 to April 15, 2016, using two ECRN-100 rainfall gauges (Decagon Devices, Inc.) at 2 m above the ground. Data from each gauge was recorded at 10 minute intervals on an EM50 data logger. One rainfall gauge was located on a large clearing ($>900 \text{ m}^2$) inside the forest at FOR at 2148 m asl. The other was located on the grassland site at the lower end of INT at 1554 m asl (referred to as RS in Figure 3.1). To correct for wind effects on rainfall data we applied the wind correction model proposed by Førland and Hanssen-Bauer (1996). We used the equation in Feddes et al. (1976) that uses relative humidity and temperature to define the absolute value of the minimum allowed pressure head at soil surface, required to estimate the actual surface water flux.

Each soil sample was represented in the model by two different 100 cm deep soil profiles: one that included the organic layer and another one without this layer. The profiles with

the organic layer were divided in two layers: organic and mineral. Each of these layers was parameterized using the corresponding data for each sample: organic layer depth, root distribution and hydraulic parameter data from the organic and mineral layers (see Section 2.2). The percentage of roots in the organic horizon was evenly distributed along the layer's depth, while the remaining percentage of roots linearly decreased along the mineral layer's depth. We also conducted a sensitivity experiment using a range of K^*_{org} values within the reported range for TMCs' organic layers, given that K^*_{org} values can be expected to be highly variable in these organic soils (see: Van der Ploeg et al., 2012 for peat soils), and that they strongly depend on the method used to measure it (Fodor et al., 2011, Schellekens et al., 2004; Tobón et al., 2011). Additionally, we assessed the likely underestimation by Rosetta of K^*_{min} by running the simulations for the Rosetta estimated K^* (K^*_{minR}) and by increasing such estimate by a factor of 10 ($K^*_{minR \times 10}$). Evidence for the K^*_{minR} underestimation by Rosetta is presented in Section 3.1. The spatial discretization along the profile was set from 0.1 cm on the top profile to 1 cm at the bottom of the profile to facilitate numerical stability. The profiles without organic layer had only the mineral material, but the root distribution and the vertical profile discretization remained the same as in the simulations that included the organic layer. The selected lower boundary condition was free drainage, as no information on the water table is available. To evaluate the model experiments we compared the simulated soil moisture outputs with observed soil moisture time series. We used meteorological data collected from the AWS at the two different elevations (1819 and 2148 m asl) to account for the elevational rainfall gradient.

To evaluate the effects of observed and hypothetical extreme dry seasons in soil moisture dynamics, we selected two cases from the observed meteorological data of each AWS during the two contrasting dry seasons (2014-2015 and 2015-2016). The mild dry season

case corresponded to data collected at the high elevation site from December 1, 2014 to April 15, 2015. The total rainfall for this period was 1081 mm. The driest months were February (128 mm) and March (121 mm). The longest dry spell, defined as continuous days with rainfall less than 1 mm d^{-1} , lasted for six days and the median dry spell duration was two days. The severe dry season case corresponds to data collected at the low elevation site from December 1, 2015 to April 15, 2016, reflecting conditions of a strong El Niño year. The total rainfall for this period was 802 mm. The driest months were January (23.3 mm) and February (119.4 mm). The longest dry spell lasted for twenty days and the median dry spell duration was 3.5 days. Besides conducting model experiments with the observed temporal variability in meteorological parameters, we also evaluated an extreme dry season scenario to evaluate soil water behaviour as a function of potential future climate conditions. To develop the input data for this hypothetical scenario study, we applied the diurnal hourly mean values from meteorological data during 39 days with rainfall lower than 1 mm d^{-1} that occurred during the El Niño dry season. These mean values were then used to replace the measured values from the El Niño dry season from Day 50 until the end of the dry season for a total of 100 days without rainfall.

3.3 Results

3.3.1. Description of the mineral horizon

We collected 55 samples of mineral soils that were classified following USDA (2010) (Figure 3.2). Mean $>2 \text{ mm}$ gravimetric fraction for the collected samples was $31 \pm 23\%$ (range 0-83%), suggesting stony soils. This mean value lies within the range reported in the neighbouring Sumapaz area (range: 17-50%; Rubio-Rivas, 2008), but it is higher than the 11% mean value reported by Roman et al. (2011) for Puerto Rican TMCFs and the c.10% median value (range: 0-50%) for the A horizon in Ecuadorian TMCFs (Huwe et al., 2008).

Particle size distribution indicated a low clay content ($7.5\pm 3.7\%$) in contrast to sand ($47.9\pm 22.0\%$) and silt ($44.6\pm 18.6\%$). There were no significant differences in clay, silt or sand content in the top mineral soils between land covers (old growth TMCF, secondary TMCF or grasslands; Anova: $p > 0.05$). The Rosetta-RETC hydraulic parameters, inferred from particle size distribution, are shown in Table 3.2 except for $\alpha = 0.020 \pm 0.014$ and $n = 1.553 \pm 0.160$. From these parameters, we derived the WRC (van Genuchten, 1980; Figure 3.3) and estimated the PAW per unit depth as $0.237 \pm 0.071 \text{ cm}^3 \text{ cm}^{-3}$. In comparison to other TMCFs' soils in the region, soils from our study area had the lowest clay contents (c.f. Table 3.2 and references therein). Low clay contents are reflected by low θ_r values and high estimated K^*_{minR} values, which are similar to the neighbouring Sumapaz study area (Table 3.2). However, our estimated K^*_{minR} values ($2.14 \pm 1.44 \text{ cm h}^{-1}$) fall within the K^*_{min} data range for top soils from Ecuador (0.42 to 4.2 cm h^{-1} ; Huwe et al., 2008) and Costa Rica (1.5 to 3 cm h^{-1} ; Tobón et al., 2011), but are much lower than the K^*_{min} data range in Jamaica (57.5 to 375 cm h^{-1} ; Hafkenschied, 2000). The fact that these K^*_{min} data values in Ecuador, Costa Rica and Jamaica are higher than those estimated by Rosetta, suggest that our estimated K^*_{minR} values could also be underestimated, which motivates our experimental approach of increasing K^*_{minR} by a factor of 10. The variations in hydraulic parameters between TMCFs in the region imply differences in soil moisture dynamics, and thus, limit generalizations.

3.3.2. Description of the top organic horizon

We collected 34 samples of organic layers that had a mean depth of $15.5 \pm 7.5 \text{ cm}$ with a maximum depth of 38 cm at the mature forest sites (Table 3.2). The range and mean depth values agreed with reported values for other TMCFs (e.g. Girardin et al., 2010; Grieve et al., 1990; Schellekens et al., 2004; Schawe et al., 2007) and were much higher than those reported for European forests (i.e. 4 to 6 cm; Ilek et al., 2015; Keith et al., 2010). Variable

organic horizon depth was not significantly related to slope or elevation nor with forest age (Anova: $p > 0.05$).

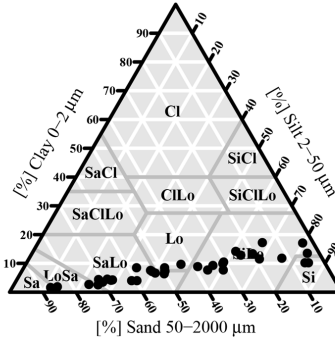


Figure 3.2. Textural classification (USDA, 2010) of the 55 soil samples. The samples fall in the following classes: Sandy (SA), Loamy Sand (LoSa), Sandy Loam (SaLo), Loamy (Lo), Silty Loam (SiLo; covered by the points) and Silty (Si).

Table 3.2. TMCFs' organic and mineral top layer soil characteristics. Clay content (%), organic matter content (OMC; %) and hydraulic parameters: Residual soil moisture (θ_r), saturated soil moisture (θ_s), saturated hydraulic conductivity (K^* ; cm h^{-1}). The hydraulic parameters for mineral soils were estimated from soil texture (Rosetta software package; Schaap et al., 2001) and for the organic layer from the water retention curves. When OMC was not available we present the carbon and nitrogen fraction (C+N). ND is no data available.

	Elevation (m asl)	Clay (%)	OMC (%)	θ_r	θ_s	K^* (cm h^{-1})
Mineral soils						
Colombia (this study)	1550-2300	7.5±3.7	8.1±4.1	0.041±0.012	0.410±0.030	2.14±1.44
Colombia- Sumapaz ¹	1700-2100	9.3±0.9	C+N 4.2 ±3.8	0.043±0.002	0.385±0.002	2.31±0.92
Ecuador ²	1960-2450	14.7±6.7	ND	0.062±0.006	0.414±0.012	0.69±0.12
Bolivia ³	1700-3300	22.3±2.9	C+N 8.1±2.4	0.071±0.004	0.429±0.005	0.61±0.06
Costa Rica ⁴	1450-1600	Loam	16.2±2.3	0.061	0.399	0.50
Jamaica ⁵	1809-1824	24.2±4.6	19.7±6.4	0.075±0.008	0.47±0.101	4.86±7.65
Organic layer						
Colombia (this study)	1550-2300	NA	69±26	0.042±0.051	0.600±0.093	1.45±1.93

¹Rubio-Rivas, 2008; ²Wilcke et al., 2008; ³Schawe et al., 2007; ⁴Tobón et al., 2011; and ⁵Hafkenscheid, 2000.

Therefore its variability was likely due to differences in topographic heterogeneity, tree species distribution and anthropogenic or natural land-cover disturbances (Bussmann et al., 2008; Roman et al., 2011; Wilcke et al., 2003). Mean porosity of 0.61 ± 0.1 was within the range reported for the top soil layer in Puerto Rican TMCFs (0.53-0.74; Schellekens et al., 2004), but it was lower than those reported for organic layers for northern latitudes (*i.e.* 0.84-0.98; Ilek et al., 2015; Keith et al., 2010). Bulk density ($0.19 \pm 0.12 \text{ g cm}^{-3}$) is within the range reported for Ecuadorian TMCFs (0.08-0.23 g cm^{-3} ; Wilcke et al., 2008) and Jamaican TMCFs (range: 0.07 to 0.48 g cm^{-3} ; Hafkenschied, 2000). OMC was high with a mean value of $69 \pm 26\%$, strongly contrasting with that found in the mineral layers ($8 \pm 4\%$; Table 3.2). The values for OMC were higher than those reported for other TMCFs: Costa Rica (37.2 to 40%; Grieve et al., 1990), Ecuador (44 to 47%; Wilcke et al., 2008) and south of the study area in Colombia (29 to 31%; Rubio-Rivas, 2008), but they were lower compared to those reported in Jamaican TMCFs (74-96%; Tanner, 1977). The organic layer had $77 \pm 22\%$ of the profiles' root biomass, which is comparable to the 80% reported by Hertel et al. (2003) for TMCFs in Costa Rica. Except for OMC, the organic layers at our study area appear to have similar properties as other TMCFs implying that the hydraulic parameters of our study site appear to be quite representative for TMCFs.

The organic layer had a higher θ_s compared to the mineral horizon (Table 3.2). The α and the n mean values were 0.037 ± 0.037 and $1.543 \pm 0.186 \text{ cm}^{-1}$, respectively. The organic layers contained more than twice the amount of water than the mineral horizons at field capacity (pF2), but the water content at -98 kPa (pF3) and at -1554 kPa (pF4.2) was similar (Figure 3.3). In addition, the catchments showed significant differences in porosity (ANOVA: $p=0.04$ $F=7.85$) and θ_s (ANOVA: $p=0.04$ $F=3.665$). INT presented a lower mean porosity (0.5 ± 0.06) and θ_s (0.53 ± 0.09) than DEF (porosity= 0.7 ± 0.07 , θ_s

=0.67±0.10) and FOR (porosity=0.6±0.10, θ_s =0.61±0.10). This potentially reflects differences in topography, species distribution or land cover/use history.

From the WRC and mean organic layer depth we estimated for each catchment the organic layer PAW (Table 3.3). The organic layer PAW per unit of depth (0.24 to 0.36 $\text{cm}^3 \text{cm}^{-3}$) at our study area is slightly higher than reported for Jamaican TMCs' organic soils (range: 0.17 to 0.23 $\text{cm}^3 \text{cm}^{-3}$; Kapos and Tanner, 1985) and was in between that of European organic soils (0.37 $\text{cm}^3 \text{cm}^{-3}$; Wösten et al., 1999) and Canadian hemic peat soils (0.14 $\text{cm}^3 \text{cm}^{-3}$; Letts et al., 2000; Figure 3.3). FOR had the highest gravitational water capacity and PAW in contrast to INT and DEF, due to its higher mean organic layer depth (Table 3.3)

Table 3.3. Estimated water storage for each catchment: Deforested (DEF), Intermediate (INT) and Forested (FOR). Forest-Deforested estimated area per catchment (For-Def), mean organic layer depth, mean water content at field capacity (θ_{FC} at 9.8 kPa), and at wilting point (θ_{WP} at 1554 kPa), stored water volume, gravitational water (GW), PAW and estimated total water storage loss in the deforested areas per catchment.

	For-Def area (km^2)	Organic layer depth (m \pm sd)	$\theta_{FC} \pm \text{sd}$ ($\text{cm}^3 \text{cm}^{-3}$)	$\theta_{WP} \pm \text{sd}$ ($\text{cm}^3 \text{cm}^{-3}$)	GW (mm)	PAW (mm)	Storage loss (m^3)
DEF	2.63–1.08	0.123 \pm 0.09	0.46 \pm 0.07	0.10 \pm 0.04	25.8	44.0	47,376
INT	2.94–0.56	0.148 \pm 0.06	0.34 \pm 0.05	0.10 \pm 0.05	28.1	35.2	19,725
FOR	2.99–0.03	0.176 \pm 0.09	0.45 \pm 0.09	0.11 \pm 0.11	28.1	59.1	1,786

Deforestation in the catchments implied a total water storage loss due organic layer removal. In DEF the total water storage loss in the 1.08 km^2 of deforested areas could be up to 47,376 m^3 . In INT the 0.56 km^2 of deforested areas represented a potential loss of 19,725 m^3 , while in FOR the 0.03 km^2 of deforested areas represented a potential loss of 1,786 m^3 (Table 3.3). The largest water storage loss in DEF likely affects the rainfall-runoff responses during the wet season. Through the modelling approach, we will further

investigate if the higher PAW of the organic layer in contrast to the mineral soil PAW ($0.127 \text{ cm}^3 \text{ cm}^{-3}$), provides an advantage to sustain transpiration during the dry season.

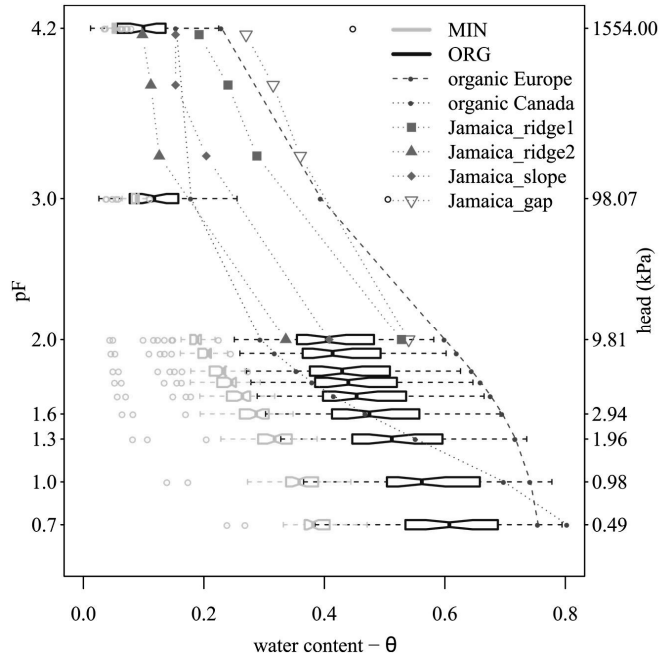


Figure 3.3. Boxplot displaying estimated water retention curves for the mineral (yellow) and organic horizons (brown), and the retention curves for: 1. four Jamaican TCMF sites: ridge1 (square), ridge2 (filled triangle), slope (diamond) and gap (unfilled triangle) from field capacity (pF2) to wilting point (pF4.2; Kapos and Tanner, 1985); 2. Organic soils in Europe (dashed line; Wösten et al., 1999); and 4. Hemic horizon of peat soils in Canada (dotted line; Letts et al., 2000). Boxplots show the median values with the vertical line, the first and third quartiles on the top and bottom box edges and the whiskers represent maximum and minimum values that do not exceed more than 1.5 times the inter-quartile range. Points outside that range are plotted as outliers. The notches extend to ± 1.58 Inter Quartile Range over the square root of the number of samples, following Chambers et al., 1983.

Measured K^* values for the organic layer ($1.45 \pm 1.97 \text{ cm h}^{-1}$) were variable and had a lower mean than those estimated of the mineral layer ($2.14 \pm 1.44 \text{ cm h}^{-1}$; Figure 3.4). We compared our measurements with those reported in the literature (Letts et al., 2000;

Schellekens et al., 2004; Wilcke et al., 2008; Wösten et al., 1999) and found that K^*_{org} values differed up to five orders of magnitude (mean range: 0.007 cm h^{-1} to 180 cm h^{-1} ; Figure 3.4). The impact of this variability on hydrological processes was investigated by a model sensitivity analysis (see Section 3.4).

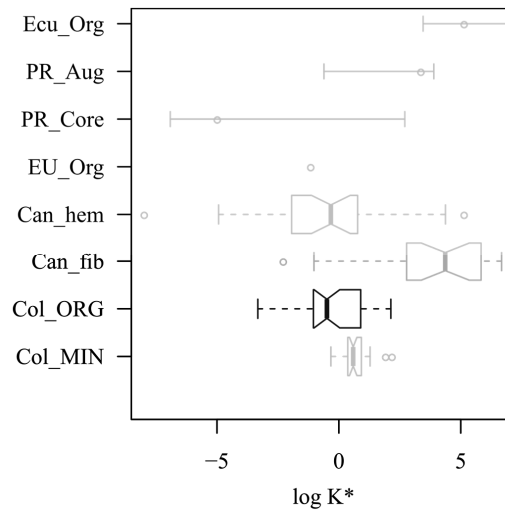


Figure 3.4. Comparison of the measured saturated hydraulic conductivity of organic and mineral horizons (Col_ORG and Col_MIN), with the estimated log transformed K^* (cm h^{-1}) of the underlying mineral horizon and the K^* reported for Canadian fibric and hemic peat soils (Letts et al., 2000: Can_fib and Can_hem), European organic soils (Wösten et al., 1999: EU_Org), TMCFs in Puerto Rico by auger and core methods (Schellekens et al., 2004: PR_Aug and PR_Core) and TMCFs in Ecuador organic layer (Wilcke et al., 2008: Ecu_Org). The notches extend to ± 1.58 Inter Quartile Range over the square root of the number of samples, following Chambers et al., 1983.

3.3.3 Observed soil hydrological dynamics

The soil moisture measurements specify the temporal mineral soil moisture variations under forests and grasslands along the elevation gradients at the study area (Figure 3.5). During the wet seasons, mineral soils appear to be saturated but fluctuations increased with decreasing elevation, similar to what has been reported for Bolivian TMCFs (Gerold

et al., 2008). This is likely related to a lower fog and rainfall frequency at the lower elevations and to the variability in soil hydraulic properties. For instance, soil moisture measurements at the lower elevations showed larger oscillations at all depths indicating higher permeability and less water retention. In contrast, the soils under forest at the higher elevations showed lower permeability suggesting either higher clay contents, a reduction of K^*_{\min} with depth, a shallower water table or a combination of all. Since we have only soil texture for the top 10 cm of mineral soils, and we did not find significant differences between clay content and land cover, we need to consider all potential explanations. However, TMCFs having a higher clay content with depth and presenting a reduction in K^*_{\min} have been reported in some but not all Jamaican TCMF sites (Hafkenscheid, 2000). The variation between dry seasons in terms of dry spell length was also reflected in the soil moisture observations with a much more pronounced decrease in soil moisture during the more severe dry season. At all sites except for SMF₁₇₂₀, the decrease in soil moisture during the dry season was stronger in the top 10 cm (Figure 3.5) similar to what was found in Bolivian and Mexican TMCFs (Gerold et al., 2008; Muñoz-Villers and McDonnell, 2012). Soil moisture measurements at 30 and 50 cm depth during the dry seasons showed smaller fluctuations at the high elevation forests (SMF₂₀₆₈ and SMF₁₉₇₃) compared to mid elevation grasslands (SMG₁₈₁₉ and SMG₁₇₈₉) (Figure 3.5). From only these soil moisture data it is impossible to determine if the dry season soil moisture decrease would translate in a reduction of root water uptake and transpiration. Soils at the study area are, however, clearly not continuously saturated.

3.3.4 Impact of organic topsoil on soil moisture dynamics

Simulated soil moisture dynamics showed similarities and differences with the observed soil moisture depending also on K^*_{\min} . The increase by $K^*_{\min R \times 10}$, caused a lowering in the simulated profile mean water content in comparison to $K^*_{\min R}$. However, this

lowering of the mean water content was more pronounced in the 30 and 50 cm deep simulations, and in the top 10 cm of profiles without organic layer. In some cases, it increased the difference between the observed and simulated soil moisture (c.f. Figure 3.5d and 5g), whereas in other cases it reduced the differences (c.f. Figure 3.5h). These contrasting responses suggested that K^*_{\min} is very variable and in some cases Rosetta's estimation is appropriate and in others can underestimate or even overestimate K^*_{\min} . Furthermore, similarities between observed and simulated soil moisture corroborated that the soil types at the measurement sites were properly represented by the soil samples on which the simulation profiles were based on. For example, soils under forests at low elevations were successfully represented at all depths (c.f. Figures 3.5b, 3.5e and 3.5h). On the other hand, differences showed that in some cases the soil moisture sensors were located in soil types that were not represented in our soil samples. For example, the soils at 30 and 50 cm depth under forests at high elevations presented a much higher water content than any of the profiles, suggesting a higher clay content or lower K^*_{\min} or a shallow water table (c.f. Figures 3.5d and Figure 3.5g). Additionally, the low soil moisture fluctuations recorded by these sensors can also reflect lateral flows in these extremely wet conditions or be caused by additional fog inputs that can occur in TMCFs (range: 1.6 mm d⁻¹ to 4.0 mm d⁻¹; Giambelluca and Gerold, 2011). Nevertheless, mean simulated soil moisture showed similar soil moisture decreases especially at the top 10 cm (c.f. first row in Figure 3.5), supporting the use of the model as an approximation to the top soil hydrologic dynamics. However, simulated soil moisture dynamics in the top 10 cm for specific profiles with organic layers were extreme and not recorded in the field (c.f. first row Figure 3.5c). These profiles likely reflect the heterogeneity in overlying organic layers as was shown by their measured WRC (Figure 3.3). This overview indicates that the simulations allow to analyse if soil moisture deficits were reached under the observed

mild and severe dry season and what could be the potential soil moisture impacts of longer dry spells. Since K^*_{org} was identified as a large uncertainty source and that Rosetta likely underestimates K^*_{min} , we conducted a sensitivity analysis with the model focussing on changes in simulated runoff as a function of K^* . Through the impact of K^* on infiltration, one would expect an increase in runoff with a decrease in K^* (Figure 3.6). We ran the simulations with K^*_{org} values that covered the range reported in the literature ($K^*_{0.1}$: 0.1cm h^{-1} ; K^*_{1} : 1cm h^{-1} ; K^*_{10} : 10cm h^{-1} ; K^*_{100} : 100cm h^{-1} ; Figure 3.4) and with the measured K^* values (K^*_{data} ; Table 3.2).

Additionally, we also ran the simulations for the profiles with and without the organic layer using the Rosetta estimates of K^*_{min} (K^*_{minR} ; Table 3.2) and those estimates increased by a factor of 10 ($K^*_{minRx10}$). For the runs with K^*_{minR} the low values of $K^*_{0.1}$ median runoff ranged from c.40% to 50% of incident precipitation, whilst for K^*_{10} and K^*_{100} median runoffs were close to zero. The profiles without organic layer showed also a low median runoff below 5% of incident precipitation. The simulations for the profiles including the organic layer and measured K^*_{org} (K^*_{data}) had high variability and median runoff ranged from c.15% to 25% of incident precipitation. Additionally, as K^*_{org} increased the runoff variability decreased, implying that the other hydraulic parameters became less important in determining runoff. The increase in $K^*_{minRx10}$, reduced the runoff compared to that simulated using K^*_{minR} and for all K^*_{org} values, except for profiles with organic layer and $K^*_{org} >$ than 10cm h^{-1} in the severe and hypothetical dry season in which runoff was not affected by K^*_{min} . However, the decrease in runoff was more pronounced for the mild dry season in the profiles without organic layer and with organic layer and $K^*_{0.1}$, and K^*_1 . The runoff decrease in the profile with K^*_{data} was similar for all dry season intensities. The variability in the decrease in runoff depending on K^*_{min} highlights the interactions between the organic and underlying mineral layers.

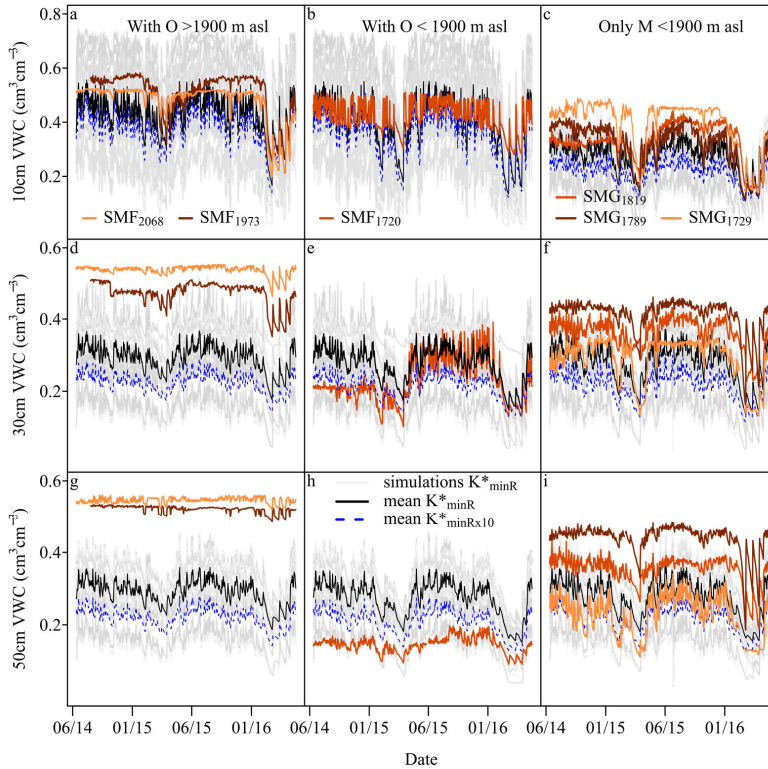


Figure 3.5. Observed and simulated soil moisture daily time series. Each panel shows the simulated soil moisture for each of the 36 sampled profiles (grey lines), the mean simulated soil moisture for all profiles with mineral layer K^* estimated by Rosetta (K^*_{minR} ; thin black lines), the mean simulated soil moisture for all profiles with mineral layer K^* estimated by Rosetta increased by a factor of 10 ($K^*_{\text{minRx}10}$) and the observed soil moisture for the different sites: Soil moisture under forests-SMF_{elevation} and Soil moisture under grasslands-SMG_{elevation}. The left column (a, d and g) shows soils with organic layer under high elevation climate conditions (With $O > 1900$ m asl). The central column (b, e and h) shows soils with organic layer under lower elevation climate conditions (With $O < 1900$ m asl). The right column (c, f and i) shows soils without organic layer under lower elevation climate conditions (Only $M < 1900$ m asl). From top to bottom, the first row (a, b and c) shows the sensors in the mineral layer (10 cm deep). The second row (d, e and f) shows the sensors in the mineral layer (30 cm deep), and the last row (g, h and i) shows the sensors in the mineral layer (50 cm deep).

After exploring the sensitivity of soil moisture and surface runoff to K^* uncertainty, we focused on assessing the potential effect of dry season soil moisture dynamics on the actual transpiration (T_{act}) and potential transpiration (T_{pot}) ratio (T_{act}/T_{pot}). Soil moisture simulations for the mild dry season and K^*_{minR} showed that profiles without organic layer reached lower soil moisture levels ($\theta=0.28 \text{ cm}^3 \text{ cm}^{-3}$) compared to the profiles with an organic layer (from $0.33 \text{ cm}^3 \text{ cm}^{-3}$ to $0.38 \text{ cm}^3 \text{ cm}^{-3}$ depending on K^*_{org}).

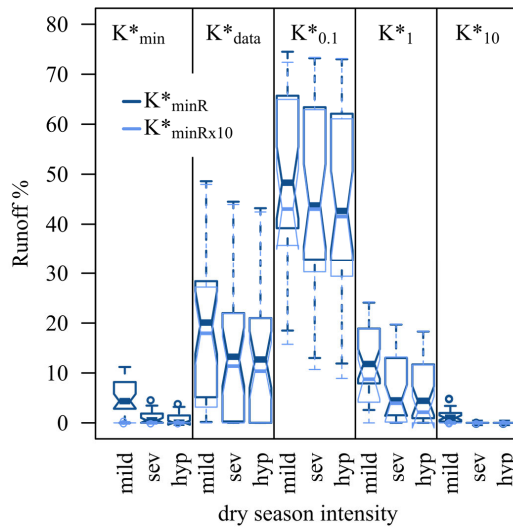


Figure 3.6. K^* (cm h^{-1}) effect on simulated runoff percentage under different dry season intensities: mild, severe (sev) and hypothetical longer dry season (hyp). Mineral layer K^* of the profiles corresponded to either Rossetta estimated values (K^*_{minR} ; light blue) or to 10 times the Rossetta estimated values ($K^*_{minRx10}$; dark blue). For profiles with organic layer, the K^* corresponded to either measured K^* (K^*_{data}), or to K^* values of 0.1, 1 or 10 cm h^{-1} .

However, these values were not low enough to induce a significant decrease in T_{act}/T_{pot} in most profiles. Therefore, the longest dry spell experienced during the mild dry season (six days) at the higher elevations does not lead to soil moisture deficits under the assumption that the K^*_{min} estimated by Rossetta is correct. If the true K^*_{min} is closer to

K^*_{minRx10} , then even the mild dry season can reduce soil moisture enough to reduce the $T_{\text{act}}/T_{\text{pot}}$ to median values between 0.9 and 0.95. This is particularly pronounced for profiles without organic layer and for profiles with an organic layer with K^*_{100} .

Simulations for the severe dry season and K^*_{minR} showed a decrease in soil moisture at the end of the 20-day dry spell ($<0.05 \text{ mm d}^{-1}$) that caused a significant effect on $T_{\text{act}}/T_{\text{pot}}$ (median values < 0.5 ; Figure 3.7). Additionally, the decrease in $T_{\text{act}}/T_{\text{pot}}$ also changed as a function of the K^*_{org} values (Figure 3.7). The profiles without organic layer showed the lower variability, whereas the soils with organic layer were highly variable implying that some profiles could still sustain $T_{\text{act}}/T_{\text{pot}}$ close to one. However, median $T_{\text{act}}/T_{\text{pot}}$ values were similar to profiles with organic layer and K^*_{10} . For the smallest and largest values of K^*_{org} (0.1 and 100 cm d^{-1}), median $T_{\text{act}}/T_{\text{pot}}$ was the lowest. Profiles with the organic layer and measured K^*_{data} showed the lowest median decrease in transpiration, but differences were relatively small (Figure 3.7). For the observed severe dry season conditions and using K^*_{minRx10} , the simulated decrease in soil moisture can further reduce $T_{\text{act}}/T_{\text{pot}}$ compared to that simulated using K^*_{minR} by c. 0.2 or slightly more for the profiles without organic layer.

We also assessed θ and $T_{\text{act}}/T_{\text{pot}}$ for hypothetical longer dry periods that can likely occur under progressing climate change (Figure 3.7). As the severe dry spell was forced to extend to 27 days and K^*_{min} was K^*_{minR} , $T_{\text{act}}/T_{\text{pot}}$ decreased, yet the magnitude of the decrease varied depending on whether an organic layer was included or not, and if included, on the assumption on K^*_{org} . Overall the lowest median $T_{\text{act}}/T_{\text{pot}}$ occurred in the profiles with an organic layer and $K^*_{0.1}$ and K^*_{100} followed by profiles with an organic layer and K^*_{10} and profiles with no organic layer. The profiles with an organic layer and K^*_{data} showed the lowest $T_{\text{act}}/T_{\text{pot}}$ decrease. If the dry spell is further prolonged for an additional 15 days, profiles with organic layer and K^*_{data} continued having a lower

median T_{act}/T_{pot} decrease compared to the other profiles. For the longest hypothetical dry season (50 days) all profiles had a median T_{act}/T_{pot} below 0.2 (Figure 3.7). The most interesting result is that the organic layers with a K^*_{org} lower than 100 cm d^{-1} , presented a higher variability in the T_{act}/T_{pot} decrease. The simulated decrease in T_{act}/T_{pot} for the hypothetically longer dry season conditions and $K^*_{minR \times 10}$, compared to K^*_{minR} becomes lower with the prolongation of dry spells as the soils reach critical soil moisture regardless of K^*_{min} variation. Overall the impact of the severe and hypothetically longer dry season conditions is stronger if K^*_{min} is larger than the one estimated by Rosetta. This is not only corroborated by the median T_{act}/T_{pot} values but also by the decrease in T_{act}/T_{pot} variability among the different soil profiles.

3.4. Discussion

The characterization of the organic layers is an important contribution to better understand the soil-water dynamics in TMCFs. In particular, the organic layer at our study area shared several characteristics (depth, porosity, bulk density and high root density) with organic layers in other TMCFs (Table 3.2). Furthermore, the range of organic layer WRC in our study area encompasses the different WRCs estimated for Jamaican TMCFs (Kapos and Tanner, 1985). This means that the data on the organic layer's WRC can be used in TMCFs' hydrological modelling and in evaluating the impacts of land-use and climate change. In contrast, the underlying mineral soils had relevant differences in texture that lead to comparatively higher Rosetta estimated K^*_{min} at our study area compared to other TMCF sites (Table 3.2), but lower than the measured K^*_{min} in other TMCFs. Nevertheless, this was expected as TMCFs do not occur on a specific soil types (Roman et al., 2011) and K^* is a highly variable parameter with a strong effect on soil moisture dynamics (Hu et al., 2012; Fodor et al., 2011; Schellekens et al., 2004; Van der Ploeg et al., 2012) specially in humid climates (Teuling et al., 2009). The variability of

mineral soil characteristics in TMCFs limit the extrapolation of our simulation results to other TMCFs.

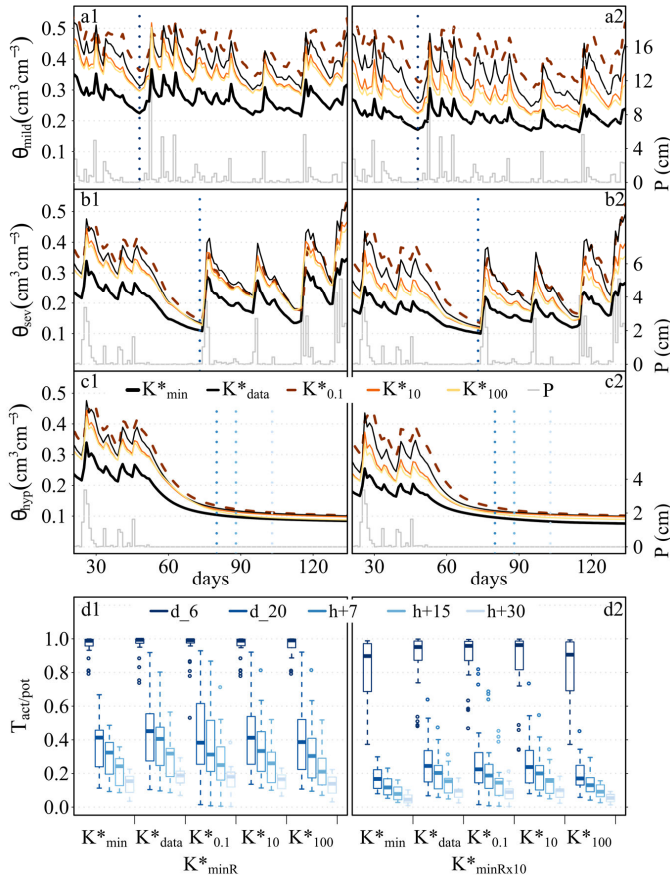


Figure 3.7. Dry season effects on top soil moisture and $T_{\text{act}}/T_{\text{pot}}$, under the potential variability of mineral and organic layer K^* . Simulated top soil moisture and rainfall time series for the observed mild (a1 and a2), the severe dry seasons (b1 and b2), the hypothetical extreme dry season (h; c1 and c2), and the effect on the $T_{\text{act}}/T_{\text{pot}}$ ratio (d1 and d2) for two potential values of mineral layer K^* : K^* estimated by Rossetta (K^*_{minR} ; left column) and 10 times the estimated values by Rosetta (K^*_{minRx10} ; right column). The bottom panels (d1 and d2) show the $T_{\text{act}}/T_{\text{pot}}$ ratio for profiles without organic layer and for the profiles with organic layer and different K^* after different dry spell durations: 6, 20, 27(h+7), 35(h+15) and 50(h+30) days, shown by dotted vertical lines in the soil moisture time series.

PAW estimates of the organic layer showed that its loss due to slash-and-burn practices reduced the water storage in the catchments (Table 3.3). When considering the deforestation effects on catchment hydrology there is usually an emphasis on changes in the canopy storage or on the deterioration of soil infiltration capacities due to compaction (e.g. Muñoz-Villers and McDonnell, 2013; Roa-García et al., 2011), but the change in water storage loss by the organic layer removal is seldom recognized. This despite that typical TMCFs' canopy storage (2 to 5 mm; Veneklaas and Van Ek, 1990) is much lower than the organic layer PAW (35.2 to 59.1 mm) and than the gravitational water content (25.8 to 28.1 mm; Table 3.3). In addition, the organic layer is a highly dynamic water storage component in the system that has water withdrawal by transpiration rates that tend to equally contribute with wet canopy evaporation to the total evaporative water loss (Bruijnzeel et al., 2011a), and it also has lateral flows due to the sloping soils (Bonell, 2005; Wilcke et al., 2011). As these dynamics are largely dependent on soil moisture, the impacts of the organic layer removal will vary according to the season. During the wet season, rainfall-streamflow responses of the catchment with a larger deforested area are more pronounced compared to the forested catchment as has been reported in other TMCFs (Muñoz-Villers and McDonnell, 2013; Roa-García et al., 2011), and can be the result of the lack of the organic layer and its large and dynamic water storage. Affirmation of this important role of the organic layer, however, depends on the actual value of K^*_{org} , which also largely determines the infiltration capacity and runoff generation (Figure 3.6; the specific role of K^* will be further discussed below). During the dry season, the removal of the organic layer leads to reduced PAW, which could be relevant for TMCFs' restoration processes if limited by low soil moisture in cleared areas (Muñiz-Castro et al., 2015). The organic layer's water storage is therefore a component that should be

considered in assessing hydrological impacts of land-use change to support land-use and water resource management decisions.

TMCFs are considered highly vulnerable to climate change but this perception is mainly based on studies with a focus on atmospheric dryness (*e.g.* Motzer, 2005). From the soil perspective, TMCFs' soil moisture deficits were generally discarded as limiting plant growths (*e.g.* Gerold et al., 2008; Hafkenscheid, 2000; Roman et al., 2011). However, our soil moisture data and the simulations show that such limitations will likely occur. Under mild dry seasons, soil moisture is surely not limiting, but the recently experienced severe dry season (with a dry spell of 20 days) reduced soil moisture enough to reduce T_{act}/T_{pot} (Figure 3.7). A large variation in T_{act}/T_{pot} between the evaluated profiles indicates that soil heterogeneity, which is not particularly relevant during the mild dry season, might become increasingly important during longer dry seasons. This can ultimately define the plant species distribution under a climate-change scenario (Esquivel-Muelbert et al., 2016).

Simulations also allowed us to evaluate if the organic layer provides an advantage for sustaining T_{act}/T_{pot} close to one during the dry season and in potentially longer dry periods. Our results suggest that the organic layer can have a potential role in buffering dry spells, especially if K^*_{min} values are closer to K^*_{minR} rather than to $K^*_{minR \times 10}$. The profiles with the organic layer K^*_{data} factually presented the lowest T_{act}/T_{pot} reduction supporting a relevant buffering capacity although with large uncertainty (Figures 3.4 and 3.7). In addition, any dry spell longer than the one observed during the 2015 El Niño could possibly have serious implications for root water uptake and the survival of the most drought vulnerable TMCFs' species.

Our results regarding soil moisture reduction with K^*_{minR} and its effect on T_{act}/T_{pot} during a mild dry season agree with those reported by Hafkenscheid (2000) for a dry season in

Jamaican TMCFs. In the Jamaican TMCFs' case, they reported high K^*_{\min} values (see Section 3.3.1), and showed that soil moisture tension did not reach pF3 values, which implies that the dry season was not strong enough to reduce $T_{\text{act}}/T_{\text{pot}}$. Furthermore, they also used modelling to determine that 37 and 117-day dry spells were needed for soil moisture tension to reach pF3 and pF4.2, respectively. In our case, the 20-day dry spell observed during the severe dry season, already caused median $T_{\text{act}}/T_{\text{pot}}$ values to drop below 0.5, and for the hypothetical extreme case of a 56-day dry spell, median $T_{\text{act}}/T_{\text{pot}}$ values dropped below 0.1, suggesting that forests in our study are more susceptible to drought than Jamaican TMCFs.

Both, in the land-use change (*i.e.* removing the organic layer) and climate change analyses, uncertainties in K^* 's quantification evidently appear to be the main source of uncertainty on TMCFs' soil moisture dynamics. This variable is difficult to measure because it depends on both the method used and the scale at which it is evaluated (Hu et al., 2012; Schellekens et al., 2004). We only employed one method for determining K^*_{org} and estimated K^*_{\min} by Rosetta due to budget and logistic restrictions. The mini-disk infiltrometer used for determining K^*_{org} has as a main limitation its sensitivity to the uniform contact between the mini-disk surface and the soil (Ronayne et al., 2012). This is difficult to guarantee in highly porous and irregular surfaces, such as the organic horizon, even when using silica sand as a contact surface. Those areas that lack contact, reduce the infiltration surface and thus underestimate K^*_{org} . The difficulties in properly characterizing K^*_{org} were reflected in the high variation of reported K^*_{org} values for TMCFs (Figure 3.4). Such high variation prevents evaluating the consistency of our K^*_{org} data. Additionally, we did not consider preferential flow in the model, which also affects infiltration, and hence runoff generation (Beven and Germann, 1982). Our field observations of low or no runoff under forests during heavy rainfall events confirm the

likely K^*_{data} underestimation. If K^*_{org} in the study area is closer to 10 mm h^{-1} , the organic layer would reduce runoff. This is also reported for organic layers elsewhere (e.g. Hartanto et al., 2003). Regarding K^*_{min} estimates we showed evidence from other studies that Rosetta tends to underestimate their value. In our case, a possible reason for K^*_{min} underestimation can be the high stone content. Evidence from an experimental approach in Ecuadorian mountain forest soils indicates that rock fragments increase preferential flows (Bogner et al., 2008).

The coupling of soil moisture with transpiration and meteorological data would allow developing an integrated analysis on the plant transpiration and carbon fixation effects of expected longer dry seasons. TMCFs' high vulnerability to hydraulic failure (Oliveira et al., 2014) suggest that these effects can be quite large. To assess the expected changes in the dry season frequency and intensity (Magrin et al., 2014), it is essential to continue the meteorological and soil moisture monitoring. This is crucial from a physiological perspective: if TMCF trees experience drought conditions that result in cavitation, forest die-off probably occurs and then drastic hydrological changes will follow (Hu and Riveros-Iregui, 2016).

3.5 Conclusions

We evaluated the land-use and climate change impacts in TMCFs from a soil moisture perspective. The organic layer characteristics for the studied TMCFs and their water retention curves are comparable to those described in Jamaican TMCFs, however, we have moved one step forward by estimating the storage loss due to organic layer removal on a catchment basis. Our results quantitatively demonstrate that the TMCFs' organic layers represent a large water storage compartment in the system. Water storage in the organic layer is up to 15 times higher than the water storage of the canopy. Therefore, organic layer loss due to land-use change has important consequences on TMCF

catchment hydrology. The organic layer's removal following land-use change will affect catchment rainfall-runoff processes and reduce PAW. We consequently emphasize that organic layer removal and not only canopy loss should be considered in water resource and land-use management plans. For example, when evaluating deforestation impacts in stream flow regulation and in designing reforestation or restoration plans, which should consider moisture limitations in seasonal areas with degraded or no organic layer.

Climate change impacts on TMCFs' soil moisture dynamics have also been studied by combining field data with modelling. Our simulation results showed that whilst the mild dry season conditions had a minor or no effect on the T_{act}/T_{pot} ratio, the severe dry season conditions did show a decrease in the T_{act}/T_{pot} ratio, highlighting that current extreme el Niño events (like the one on 2015-2016; Jiménez-Muñoz et al., 2016) represent a threat to TMCFs. This finding contrasts with observations from other TMCF sites, where dry seasons were not severe enough to reduce soil moisture to levels that affected transpiration. Thus, TMCFs on high precipitation areas ($>4000 \text{ mm y}^{-1}$) exposed to pronounced seasonality can experience water stress under severe dry seasons. With the expected longer dry spells under climate change the simulated decrease in T_{act}/T_{pot} reached critical levels. Given the large uncertainty in K^*_{org} we evaluated multiple K^*_{org} values. Very low K^*_{org} values ($<0.1 \text{ cm h}^{-1}$) enhance runoff and thus reduce soil moisture. Very high K^*_{org} values (close to 100 cm h^{-1}) poorly retain water showing similar behaviours to soils without the organic layer. Intermediate K^*_{org} values (close to 10 cm h^{-1}) sustained a higher soil moisture. Nevertheless, independent of the K^*_{org} value, the profiles with organic layer had larger variability in the T_{act}/T_{pot} ratios than soils without the organic layer. This suggests a buffering role of the organic layer on soil moisture reduction, and thus, in having higher water availability for plants. This buffering capacity, however, cannot sufficiently compensate for the prevailing conditions in extreme dry

seasons, when soil moisture levels reach extremely low levels. In contrast to the organic layer, mineral layer characteristics vary among TMCFs. However, the K^*_{\min} uncertainty assessment showed that at higher K^*_{\min} values the top soil moisture (organic or not) will decrease faster under already observed dry season conditions. Therefore, soils with organic layer and underlying mineral soils with larger clay contents or other characteristics that reduce the K^*_{\min} values, will likely sustain larger $T_{\text{act}}/T_{\text{pot}}$ ratios than very sandy soils or soils with other characteristics such as high gravel content that increase their K^*_{\min} . Soil heterogeneity within the catchments will surely define, under a future climate change scenario, the distribution and survival of TMCFs' species.



CHAPTER 4

Tropical Montane Cloud Forests in the Orinoco River basin:
Inferring fog interception from through-fall dynamics

Chapter 4

Tropical Montane Cloud Forests in the Orinoco River basin: Inferring fog interception from through-fall dynamics³

The interaction between vegetation and the atmosphere is highly complex in fog affected ecosystems like Tropical Montane Cloud Forests (TMCFs). Despite acknowledging fog effects on the canopy's water balance, quantifying their influence remains challenging. While the reduction in potential evaporation that is caused by fog presence, is largely independent of land cover, fog interception itself strongly depends on the land-cover's vegetation characteristics. A better understanding of how these two fog related processes affect the water balance is highly relevant under current land-use and climate-change pressures. In this study, we evaluate the different fog effects on TMCFs' canopy interception combining modelling and high temporal resolution (10 minute) observations that were collected in different TMCFs' regeneration stages and at two different elevations. We also analyse the limitations in closing catchment water balances caused by limitations on the measurements to properly represent these fog effects.

Results show that different fog frequencies along elevation affect potential evaporation. The higher elevation old-growth TMCFs have a lower simulated evaporation and a lower dry canopy frequency than the low elevation secondary and early succession forests. Furthermore, we show that fog water inputs during fog-only events, even though higher at the higher elevation, are probably insignificant (from 0.8% to 1.6% of measured rainfall), but this input of fog water can become more relevant during foggy rainfall events (from 5.8% to 12.8% of measured rainfall). Additional to the fog trends along the elevation, we also uncover variable fog-vegetation interactions controlled by differences

³ This chapter is in preparation as: Ramírez, B.H., Melsen, L.A., Teuling, A.J., Ganzeveld, L., and Leemans, R. (2017). Tropical Montane Cloud Forests in the Orinoco River basin: Inferring fog interception from through-fall dynamics.

in canopy water storages as a function of forest cover. Each evaluated process has associated uncertainties, which together cumulatively explain why closing a water budget in TCMF catchments is limited by data collection methods that probably do not capture all relevant fog effects. In addition, this study also indicates that the temporal resolution of measured rainfall and through-fall and compensating effects of canopy parameters that are estimated by the commonly used Rutter canopy-rainfall interception model, pose an additional challenge to understand and quantify fog effects in the water budgets of TCMFs.

4.1. Introduction

Understanding the consequences of land-use and climate change for hydrologic processes is a major scientific challenge (DeFries and Eshleman, 2004; Hooke et al., 2012; Wagener et al., 2010). The implications of these changes on the water cycle, and ultimately water availability at variable spatial and temporal scales, are subject to considerable debate and research (e.g. Balthazar et al., 2015; Bonell, 2010; Ellison et al., 2012). Canopy interception is a relevant water-balance component that is potentially affected by land-use and climate change (Piao et al., 2007). Interception can strongly affect water yields (Van Dijk and Peña-Arancibia, 2012) and also precipitation through intensified land-atmosphere interactions (Guillod et al., 2014). Deforestation and subsequent forest recovery induce changes in canopy characteristics that determine the canopy's water storage and drainage rates (Holwerda et al., 2010; Ponette-González et al., 2010; Pryet et al., 2012), while changes in rainfall (P) and potential evaporation (PE) affect the input and losses of water from the canopy (Crockford and Richardson, 2000). The interaction between the vegetation and the atmosphere is even more complex in fog affected ecosystems like Tropical Montane Cloud Forests (TMCFs; Chu et al., 2014; Dietz et al., 2007).

Fog affects evapotranspiration and thus plant-water relations by reducing incoming solar radiation, increasing leaf wetness frequency and decreasing atmospheric vapour pressure deficit (Eller et al., 2015; Letts and Mulligan, 2005; Reinhardt and Smith, 2008). Reduced transpiration results in less water uptake from the soils and reduced canopy evaporation can increase through-fall, both sustaining higher moisture conditions in the system. Furthermore, fog interception by the canopy provides an additional water input to rainfall (Zadroga, 1981) and potentially induce foliar water uptake (Eller et al., 2015; Goldsmith et al., 2013). Although the effect of fog on the canopy water balance is acknowledged,

quantifying its influence remains challenging (Frumau et al., 2011). Several measurement methods have been employed to quantify fog's liquid water content including passive or active fog collectors, fog detectors and fog/cloud droplet spectrometers. However, they all have their caveats concerning, for example, the discrimination between fog and wind-driven rainfall, minimum water content thresholds and fog droplet size distribution. These caveats are discussed in detail by Bruijnzeel et al. (2006). Additionally, these methods are point measurements and this limits their spatial representativeness. Furthermore, quantifying fog's liquid water content alone is insufficient to determine the canopy's fog interception rates. The fog-vegetation interaction also depends on wind speed and vegetation characteristics, like canopy roughness and canopy Leaf Area Index (LAI), leaf surface texture (*e.g.* hydrophilic hairs or hydrophobic waxes), leaf inclination and exposition to wind direction (Crockford and Richardson, 2000; Herwitz, 1985). The required information on canopy characteristics is already overwhelming, but determining all these features is impossible in montane (>1000 m asl) tropical forest contexts, where plant diversity can reach up to 100 *spp* per 0.1 ha (Gentry, 1988). A more practical approach is to evaluate the fog/vegetation interaction at the catchment scale with effective parameters that represent the high spatial variability within the canopy.

A common approach to study fog and canopy interactions is to compare interception and through-fall (hereafter TF) between areas or seasons with contrasting fog influence, and/or between different land-cover types (*e.g.* Brauman et al., 2010; Giambelluca et al., 2011; Ponette-González et al., 2010; Pryet et al., 2012). To quantify interception, precipitation above and below the canopy (*i.e.* TF) is measured. These comparisons allow to quantify the additional water input by fog reflected in additional TF. However, given the high temporal variability of fog occurrence at daily or shorter timescales, this quantification is likely sensitive to the temporal measurement resolution, which varies

considerably throughout the literature (*e.g.* weekly: Fleischbein et al., 2005; Gómez-Peralta et al., 2008; Wullaert et al., 2009; daily: Hölscher et al., 2004; and 10 minutes: Holwerda et al., 2010). Furthermore, the rainfall-through-fall approach does not provide information on the relative contribution of the multiple processes affected by fog that control the net water inputs. For example, evaporation that varies between very high levels under clear skies to very low levels under cloud/fog influence (Hidalgo et al., 2005), translates into variable canopy drying times.

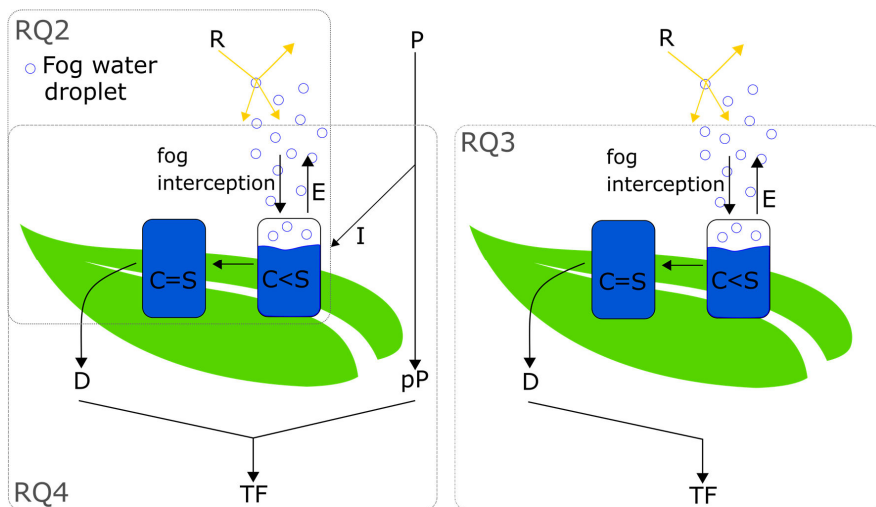


Figure 4.1. Conceptualization of processes related to canopy interception and the research questions addressed in this study (RQ2 to RQ4). The conceptualization represents canopy interception (I) and the effects of fog in partially reflecting and scattering radiation (R) and reducing evaporation (E; RQ2), filling the canopy water storage (C) and draining (D) during fog only events (RQ3), and enhancing through-fall (TF) during events with both fog and rainfall (P; RQ4).

At the same time, fog interception by the canopy fills the canopy water storage (Figure 4.1). The reduction in potential evaporation caused by fog is largely independent of land cover, whereas fog interception by the vegetation depends on vegetation characteristics associated with land cover (*e.g.* Holwerda et al., 2010). Thus, a better understanding of

how the two processes of reduced evaporation and fog interception affect the water balance of ecosystems, such as TMCFs, is highly relevant under current land-use and climate change pressures.

Canopy interception models allow to integrate the through-fall/rainfall (TF/P) processes by considering rainfall, evaporation, drainage outputs and canopy characteristics. Muzylo et al. (2009) review canopy interception models and their use worldwide. The two most commonly used interception models are the Rutter model (Rutter et al., 1971; Rutter et al., 1975; Rutter and Morton 1977) and the Gash model (Gash, 1979). The Rutter model is a process-based continuous water-balance model with two empirical drainage parameters. The Gash model is the analytical version of the Rutter model with reduced data requirements and it is thus more widely used (Muzylo et al., 2009). The Gash model partitions individual rainfall events into three stages: wetting up, saturation and evaporation after rainfall ceases, but it requires the discretization of rainfall events assuming to have a dry canopy preceding each event. The validity of this assumption is questionable in fog affected forests where fog is not detected by rain gauges. The continuous Rutter model does not rely on the assumption of a dry canopy. Furthermore, the continuous water-balance calculation provides insights in the water stored in the canopy in-between rainfall events and this allows to determine the dry/wet canopy frequency. Hence, the Rutter model is best suited to integrate meteorological data with TF data to understand the fog effect on the canopy water balance in TMCFs.

In this chapter, we aim to estimate the multiple fog effects on the canopy water budget in three successional TMCF stages. Our analyses are based on through-fall and meteorological data coupled with canopy interception modelling. To achieve our aim we will address the following research questions (RQs; see also Figure 4.1):

- RQ1. How does the temporal resolution of measured rainfall and through-fall affect the estimates of additional water inputs by fog?
- RQ2. What is the potential effect of different fog intensities on evaporation and how does this affect the partitioning of rainfall between through-fall and evaporation for the three main forest covers in our study area?
- RQ3. How (seasonally) relevant are the fog water inputs during fog-only events in the three main forest covers in our study area?
- RQ4. What is the fog effect on through-fall during rainfall in the three main forest covers?

To answer the research questions we monitored at a 10 minute time resolution for more than a year, three neighbouring catchments on the Colombian Orinoco River basin with different land covers: old-growth TMCFs (OGFs), secondary (SECFs) and early successional stages (EARFs) and grasslands. Previous studies on these catchments have shown that there are missing sources of water to close the water budgets (Chapter 2). A positive correlation between fog/clouds and elevation suggests that fog interception at the higher elevations could contribute to streamflows (Chapter 2). Another contribution could come from the soil water storage. So far, we have also identified an important role in water storage and release from the soil organic layer in TMCFs (Chapter 3). However, until this study, neither differences in Potential Evaporation (PE) nor fog inputs along elevations and/or between seasons for this specific area had been assessed.

4.2. Materials and methods

4.2.1 Study area

We collected data from August 1st 2014 to June 12th 2016 in three adjacent headwater catchments that are located on the eastern slope of the eastern Andean Cordillera (72.900 E-5.243 N; Figure 4.2), in the municipality of Chámeza (Casanare, Colombia). The

eastern Andes are dominated by young mountains with steep slopes and sharp crests (Stallard et al., 1991). From a biogeographical perspective this study area belongs to the Andean region, while hydrologically, it is part of the Orinoco River basin highlands. The catchments have a total area of 10.2 km², cover an elevation range between 1550 and 2490 m asl and are located windward. Climate data from April 2014 to April 2016 showed a mean daily temperature of 16.5°C and 14.5°C at 1819 m asl and at 2148 m asl, respectively. Mean annual rainfall ranged between 4283 mm at 1554 m asl and 4966 mm at 2148 m asl. Its mono-modal rainfall regime has a dry season from December to March during which less than 16% of annual rainfall occurs (Chapter 2). Mean observed daily wind speed and maximum hourly values were higher at 1819 m asl ($1.5 \text{ m s}^{-1} \pm 0.4 \text{ m s}^{-1}$, $\text{max}=7.3 \text{ m s}^{-1}$) than at 2148 m asl ($0.7 \pm 0.2 \text{ m s}^{-1}$, $\text{max}= 5.5 \text{ m s}^{-1}$; Chapter 2). The dominant daytime winds were easterlies (68° to 113°), whilst night time winds were predominantly westerlies (270° to 293°; Chapter 2). Previous fog event analyses revealed a positive relation between fog occurrence and elevation, and less fog events during the dry season compared to the wet season. Diurnal fog patterns in both seasons showed an increase of fog events during the afternoon until 20 h (Chapter 2). The study area's current land cover consists of evergreen old-growth TMCFs (OGFs), secondary TMCFs (>10 y; SECFs), young secondary forest (<10 y; EARFs), grasslands and small-scale agricultural areas.

In our analyses, we will assess canopy interception on different forest covers. OGFs are mainly found at the higher elevations on the steeper slopes in contrast to SECFs and EARFs, and according to local inhabitants, they have never been cleared. However, OGFs are occasionally subjected to selective logging. OGFs are characterized by emergent trees (>30 m) and a lower more homogeneous canopy (*i.e.* 15 to 20 m) with a high epiphyte cover (bromeliads and mosses) on tree trunks and branches, and a relatively open

understorey. *Cyathea sp.*, *Alchornea sp.*, *Hedyosmum sp.* and *Weinmannia sp.* were identified as dominant tree species according to a preliminary inventory (Stevenson and Casas, 2008). LAI was measured with a LAI-2000 Plant Canopy Analyzer (LI-COR) and calculated by employing the LAI-2000 computing method programmed in the Li-Cor's FV2000 software (<http://envsupport.licor.com/docs/FV2000Manual.pdf>). Mean OGFs' LAI was $4.8 \pm 1.0 \text{ cm}^2 \text{ cm}^{-2}$ ($n=186$). This is similar to the lower montane cloud forest mean values ($4.7 \pm 1.1 \text{ cm}^2 \text{ cm}^{-2}$; Bruijnzeel et al., 2011a). SECFs are found mainly on the edges of OGFs. They were OGFs before being cleared through slash-and-burn for agriculture or grasslands. These areas were afterwards abandoned and allowed to regenerate. SECFs have tall trees (up to 20 m) but not emergent ones as in OGFs and even though they also present a high epiphyte cover, it is comparatively lower than in OGFs. SECFs' understorey can vary from very open to very close due to the presence of broad banana-leafed Zingiberales clusters. Mean measured SECFs' LAI was $4.9 \pm 0.8 \text{ cm}^2 \text{ cm}^{-2}$ ($n=182$), similar to OGFs. EARFs are in the earliest forest succession stage. They were previously grasslands or croplands but they were abandoned (<10 years) as part of the local rotational agricultural practices. Trees can reach up to 10 m of height and most of them are early succession taxa such as *Cecropia*, *Siparuna* and *Vismia*. Below them, there is a dense canopy of other woody species shorter than 8 m and an even denser shrubby understorey with spiny ferns and various Zingiberales species. Epiphyte cover is less developed than in the other two forest types, mainly due to less trunk and branch surface area given the fairly young stand age. Mean measured EARFs' LAI was $4.0 \pm 0.8 \text{ cm}^2 \text{ cm}^{-2}$ ($n=117$) being slightly lower than OGFs' and SECFs' LAI. This similarity in LAI estimates between OGFs and SECFs is a common observation in tropical forests (e.g. Brown and Lugo, 1990), including TMCFs, where LAI recovery can be relatively fast

attaining 50% of the original forest LAI values after only three years (Lawton and Putz, 1988).

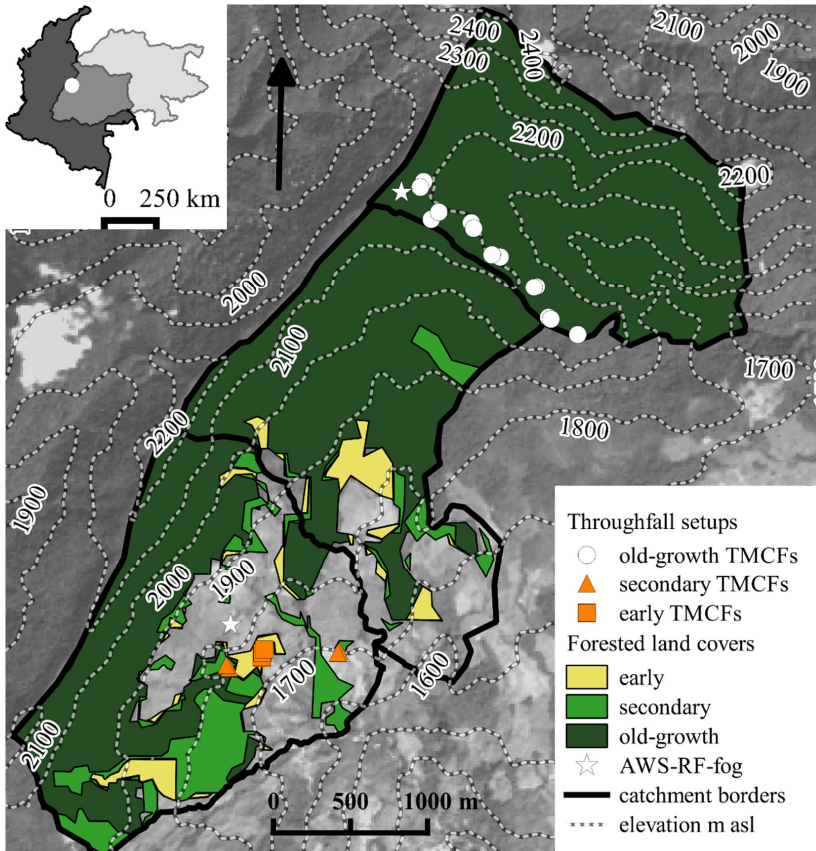


Figure 4.2. Map of study area and experimental setup. The inset map shows the Orinoco river basin (light grey) and its overlap with Colombia (dark grey). The white dot represents the study area, enlarged on the main map. This map shows: 1) Land cover classification: old-growth TCMFs, secondary TCMFs, and early TCMFs. 2) Location of the through-fall setups in each land cover type. 3) Location of the AWSs, rainfall and fog gauges. 4) Elevation contours and 5) Catchment borders. The background image is the band 8 (15m resolution) of a Landsat 8 image taken on December 25th, 2013.

4.2.2 Meteorological data

Meteorological data were collected with two Davis Vantage Pro2-plus automated weather stations (AWS; Figure 4.2). One AWS was located at a lower elevation (1819 m asl) on a grassland site at 2 m from the ground (72.907 E, 5.231 N; AWS₁₈₁₉). The second AWS was located at higher elevation (2148 m asl) at 17 m above the ground in a scaffolding tower surrounded by a forest canopy of c.16 m. Therefore, the meteorological station was 1 m above the surrounding canopy (72.897 E, 5.257 N; AWS₂₁₄₈). Both stations recorded the following mean daily data on a Weatherlink datalogger at 10 minute intervals: shortwave incoming radiation (Vantage-Pro2 6450 Solar pyranometer); relative humidity, air temperature, wind speed (large cup anemometer); and barometric pressure (Table 4.1).

Table 4.1. Mean daily values (\pm sd) of meteorological data at the two Automated Weather Stations (AWS_{elevation in m asl}).

	AWS ₁₈₁₉	AWS ₂₁₄₈
Short-wave incoming solar radiation (W m^{-2})	134.1 \pm 64.6	104.9 \pm 48.6
Measured/expected clear-sky solar radiation	0.41	0.32
Relative humidity (%)	92.3 \pm 4.6%	96.3 \pm 3.9
Air temperature ($^{\circ}\text{C}$)	16.6 \pm 0.9	14.7 \pm 0.8
Barometric pressure (kPa)	82.8 \pm 0.3	79.9 \pm 0.2
Wind speed (m s^{-1})	1.4 \pm 0.4	0.6 \pm 0.2

We used the Penman–Monteith model (Monteith, 1965) assuming a single layered canopy with zero stomatal resistance to estimate PE at each AWS elevation (PE₁₈₁₉= 1670 mm y⁻¹ and PE₂₁₄₈= 858 mm y⁻¹). Setting the canopy resistance to zero in the Penman-Monteith equation provides a good approximation of the evaporation rate from a completely wet canopy (Gash et al., 1980). This is likely a common condition in TMCFs. The required expected solar radiation at the study area was estimated from extra-terrestrial solar

radiation derived from solar geometry (Donatelli et al., 2006) and the clear sky transmissivity was estimated through the Thornton and Running (1999) model. In addition, we estimated the PE quantiles and the mean seasonal differences from each AWS elevation. PE_{1819} quantiles were more evenly distributed compared to the PE_{2148} quantiles, where the occurrence of clear sky days were rare (Figure 4.3). Analysis of the seasonal mean differences showed that even though PE was higher in the dry season than in the wet season at both elevations, PE_{2148} showed less pronounced seasonal differences in comparison to PE_{1819} (Figure 4.3).

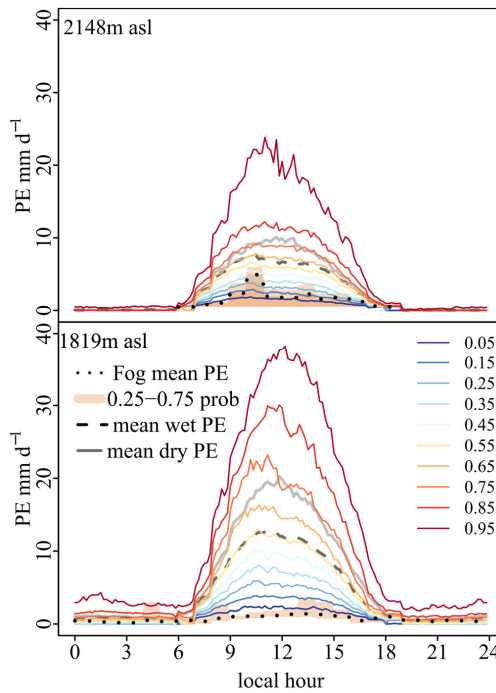


Figure 4.3. Diurnal cycles of potential evaporation at two elevations. Top panel: potential evaporation at 2148 m asl, Bottom panel: potential evaporation at 1819 m asl. Potential Evaporation (PE) quantiles (mm d^{-1}) are estimated by the Penman-Monteith model. We also plotted the mean wet and dry season PE and the 0.25 and 0.75 PE quantiles during observed fog events.

We installed two Decagon ECRN-100 rainfall gauges at 2 m above the ground. Data from each gauge were recorded at 10 minute intervals on a Decagon EM50 data logger. One rainfall gauge was located at 2148 m asl on a large clearing ($>900 \text{ m}^2$) inside the forest (RS₂₁₄₈; Figure 4.2). The other was located on a grassland at 1819 m asl (RS₁₈₁₉). We applied the Førlund and Hanssen-Bauer (1996) wind correction model to rainfall data. Wind data were obtained from the closest AWS. RS₂₁₄₈ ($13.9 \pm 19.0 \text{ mm d}^{-1}$) had higher mean daily values in contrast to RS₁₈₁₉ ($12.0 \pm 18.9 \text{ mm d}^{-1}$) agreeing with the previously reported positive correlation along elevation (Chapter 2). During the wet season RS₁₈₁₉ had a lower mean daily rainfall ($17.6 \pm 21.8 \text{ mm d}^{-1}$) and slightly longer dry spells ($<0.2 \text{ mm h}^{-1}$; $7.6 \pm 9.8 \text{ h}$) compared to RS₂₁₄₈ ($18.3 \pm 20.6 \text{ mm d}^{-1}$ and $6.7 \pm 6.8 \text{ h}$). These differences became larger during the dry season (RS₁₈₁₉: $3.2 \pm 7.3 \text{ mm d}^{-1}$ and $22.8 \pm 46.9 \text{ h}$; RS₂₁₄₈: $4.8 \pm 11.0 \text{ mm d}^{-1}$ and $13.2 \pm 12.0 \text{ h}$). This suggests that less severe dry season conditions occur at the higher elevation.

Next to the rainfall gauges we set up a cylindrical Juvik type fog collector (Juvik and Nullet, 1995) with a diameter of 21 cm and height of 60 cm with a circular greenhouse UV resistant plastic of 141 cm diameter on top to avoid rainfall inputs but without avoiding wind driven drizzle (horizontal precipitation). Each fog collector had a funnel-hose-rubber lid connection to a Decagon ECRN-100 rainfall gauge. Data from each gauge were recorded at 10 minute intervals on a Decagon EM50 data logger. All were positioned with the top at 2 m from the ground and were located on the side of the rainfall gauges avoiding up- and downwind positions in relation to the rainfall gauges. Data from fog collectors have to be interpreted with caution due to repeated failures in the connection system and occasional failures of the rain gauges. Furthermore, since fog gauge performance depends on wind speed (Frumau et al., 2011, Villegas et al., 2008) and given the fact that the high elevation wind speed was less than half of the wind speed of the low

elevation site (due to differences in upwind land cover, forest vs grassland; Chapter 2), we expect our measurements to underestimate the actual amount of water intercepted from fog. Therefore, we only use the data by aggregating it to hourly intervals to establish the relation between fog occurrence and PE. Fog occurrence measured by the fog gauge at the lower elevation showed that 75% of the daytime fog events were associated with inferred PE_{1819} values $<3.6 \text{ mm d}^{-1}$ whereas night-time fog events mainly occurred at PE_{1819} values $<2.95 \text{ mm d}^{-1}$ (Figure 4.3). At the higher elevation the inferred PE_{2148} values during daytime fog events were higher ($<6 \text{ mm d}^{-1}$) compared to the lower elevation events, whilst we did not record any nocturnal fog event (Figure 4.3), potentially due to low mean night-time wind speed ($<0.5 \text{ m s}^{-1}$; Chapter 2). Overall, these results corroborate the elusiveness of the fog signal as a function of insolation and/or relative humidity (Brauman et al., 2010).

4.2.3 Through-fall data

We recorded TF data for OGFs using six stainless steel ‘V’ shaped troughs of 30 cm wide and 400 cm length. These troughs were set up in two groups of three troughs each. Within each group the troughs were placed at a minimum distance of 5 m from each other. For SECFs and EARFs we built ‘U’ shape troughs using half 10.4 cm diameter PVC pipes of 200 cm length. Three ‘U’ shape troughs were used for SECFs and two ‘U’ shape troughs for EARFs. Each trough was connected to a 6506H UNIDATA 50 ml tipping bucket. Data were recorded on Starlogger 6004D UNIDATA every ten minutes. To prevent clogging from leaves and other canopy debris we covered the troughs with a 3 cm eye plastic mesh. Troughs were cleaned every 15 days. Missing data due to system failures were excluded from the analyses. To include the forest cover heterogeneity we moved the troughs to different sites. TF data were always collected inside the studied forests and not close to any forest border nor on ridges (distance $>200 \text{ m}$). In the OGFs we sampled 60

different sites, in SECFs we sampled 24 sites and in EARFs, we sampled 16 sites. Every time the gauges were moved we estimated the troughs' inclination, as topography and rocky soils prevented from keeping these values constant, and performed the corresponding corrections to estimate the effective horizontal sampling area. Mean water depth to produce a tip for 'V' shaped troughs was 0.073 ± 0.001 mm and for 'U' shaped troughs was 0.422 ± 0.014 mm. The implications of these differences will be considered in the comparison of the inferred fog's effects for the high elevation OGFs and low elevation SECFs and EARFs. We also kept the sites' disturbance to a minimum and re-calibrated the tipping buckets. TF/P ratios were estimated by averaging TF data at each 10 minute time step from all TF gauges in the same forest cover and excluding data when the gauges were failing. We then added all the averaged TF values and all the P values and estimated the TF_{total}/P_{total} per forest cover. We also estimated the median and corresponding error bounds from the TF/P ratios for each of the sampled sites to assess the variability as a function of forest cover. Error bounds give roughly a 95% confidence interval for the difference between two medians (McGill et al., 1978).

In addition, we measured the Vegetative Cover Fraction (VCF) for each trough through hemispherical photographs taken from the troughs' centre point. These photographs were taken with a Sigma 8mm f/3.5 EX DG circular fish-eye lens (180 degree field of view) mounted on a Canon EOS rebel Ti LSR camera. To evaluate VCF differences between the forest covers, we also took hemispherical photographs every 10 m along transects in each of the main forested covers (OGFs=186 data points, SECFs=182 data points, EARFs=117 data points). The hemispherical photographs were processed with the CAN-EYE v6 3.13 software (Weiss and Baret, 2014). Photography processing included calibrating the camera-lens system according to the procedure described in the CAN-Eye software's manual, classifying the photograph pixels into canopy or open sky and

establishing the proportion of canopy pixels. The classification threshold was established on a per photograph basis. The measured distribution of VCF did not agree well with the measured LAI. In contrast to the previously discussed LAI's for the three land covers, EARFs' mean VCF (0.93 ± 0.05) was higher than OGFs' (0.83 ± 0.10) and SECFs' (0.87 ± 0.06). However, the standard deviation in the measured VCF from OGFs suggests that differences were not significant. Both LAI and canopy gaps can increase with stand age (Brown and Lugo, 1990; Clark, 1996) and forests subjected to selective logging, such as the OGFs in the study area, are expected to have more canopy gaps (Clark, 1996).

4.2.4 Rutter model evaluation

The Rutter numerical rainfall interception model (Rm; Rutter et al., 1971; Rutter et al., 1975) was originally developed to analyse rainfall interception on a Corsican pine forest but has been widely applied to various forest types worldwide (Muzylo et al., 2009). The Rm approach simplifies the canopy by representing it as a single or bulk canopy layer. This matches the extent to which the canopy water balance terms were measured. In this study we used Rm as a tool to integrate our data and to provide a better insight on the canopy interception process. More specifically, we used it to: a) identify periods during which the observed TF could not be attributed to rainfall; identified by a zero signal in the simulated TF, and b) to have an approximation of the effects of contrasting PE under varying fog conditions on actual evaporation and in the wet and dry canopy frequency. Furthermore, we excluded stemflow because previous studies have found stemflow to be generally low for TMCFs (1-2% of measured P; Bruijnzeel et al., 2011a), likely due to the large storage capacity of epiphytes (Ah-Peng et al., 2017). The implications of this are further addressed in the discussion of our results.

Table 4.2. Rutter model components and the evaporation modules. Rainfall (P; mm), Vegetative cover fraction (VCF), Intercepted rainfall (I; mm), Evaporation (E; mm), Potential Evaporation (PE; mm), Canopy stored water (C; mm), Canopy storage capacity (S; mm), Drainage (D; mm), Drainage rate when S=C (D0, mm time-step⁻¹), time-step (t; minutes), drainage parameter (b), through-fall (TF; mm).

Rutter model components	
Intercepted rainfall	$I = P * VCF$
Linear Evaporation (E)	$E = PE * (C/S)$ when $C < S$
	$E = PE$ when $C > S$
Modified non-linear evaporation (E _{nl})	$E_{nl} = PE * [2(C/S) - (C/S)^2]$ when $C < S$
	$E_{nl} = PE$ when $C > S$
Drainage	$D = D0 * e^{b(C-S)}$ when $C > S$
	$D = 0$ when $C < S$
Integrated drainage over time steps. Water stored in the canopy after drainage for each time step	$C_{t1} = \ln(e^{-bC_{t0}} + t b D0 * e^{-b*S}) * b^{-1}$
Change in the amount of water stored in the canopy	$dc/dt = I - E - D$
Through-fall	$TF = P * (1 - VCF) + D$
S, D0 and b	Model parameters, identified by optimization of the NSE between observed and simulated TF, using the Levenberg-Marquardt optimization algorithm

In Rm, water input to the canopy is defined by the proportion of rainfall that is intercepted by the canopy (I in mm per time step). The proportion of rainfall that will pass through the canopy without being intercepted is defined by the open spaces of the canopy. A good approximation of open spaces in the canopy is 1-VCF (vegetative cover fraction) of the canopy (e.g. Gash et al., 1995). Consequently, the remaining rainfall proportion is assumed to be intercepted by the canopy. Water leaves the canopy by evaporation (E in mm per time step) and drainage (D in mm per time step; Table 4.2). In the original model

version (Rutter et al., 1971) D is calculated from the amount of water stored in the canopy (C in mm), the drainage rate (D_0 in mm per time step), the canopy water storage capacity (S in mm) and an empirical parameter (b ; Table 4.2). A modification was later introduced in which D is set to 0 when $C < S$ to prevent drainage when C becomes 0 (Calder, 1977). We followed the suggestion by Rutter et al. (1971) to estimate C after drainage by integrating the drainage term and calculating the change in C due to drainage for each time step (Table 4.2). This model considers a linear relation between evaporation and the C/S ratio. When C is equal or larger than S , evaporation is equal to PE , but once C becomes less than S , PE is reduced as a function of the C/S ratio. However, conflicting evidence has emerged on this relationship (Klassen, 2001). Schellekens et al. (1999), for example, found that both the Rutter and Gash models severely underestimated the observed interception loss, likely due to underestimating evaporation. Therefore, we modified the calculation of evaporation by applying a nonlinear relationship that results in an enhanced evaporation rate shortly after rainfall (R_m-E_{nl} ; Table 4.2).

From the required input variables to constrain the Rutter model, we measured P , TF and VCF , and estimated PE from the observed meteorological parameters. In addition, we estimated the three parameters (S , D_0 and b) by optimizing the Nash-Sutcliffe Efficiency Index (NSE; Nash and Sutcliffe, 1970) comparing the observed and simulated TF in 10 minute temporal resolution over observation periods without missing data. For this optimization we used the Levenberg-Marquardt optimization algorithm (Levenberg, 1944; Marquardt, 1963; Table 4.2; Appendix 4A) instead of the usually employed TF and P regression method (*i.e.* Jackson, 1975) because it does not only require identifying a minimum rainfall intensity threshold to fill the canopy but also a fairly arbitrary selection of a regression line on the upper bounds of the data dispersion. The optimization was done for both Rutter model versions: R_m and R_m-E_{nl} . For all comparisons between NSE

and model parameters the error bounds corresponded to the boxplot notches which give roughly a 95% confidence interval for the difference in two medians (McGill et al., 1978).

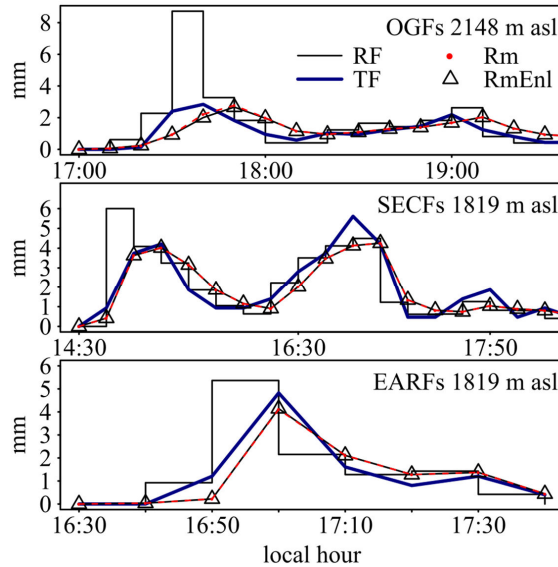


Figure 4.4. Simulated and observed through-fall for three selected cases. Top panel: rainfall recorded in old-growth forests (OGFs) in May 5, 2015. Middle panel: rainfall event recorded in secondary TMCFs (SECFs) in June 25, 2015; Bottom panel: rainfall event recorded in early succession TMCFs (EARFs) in May 5, 2015. Simulations are done using the standard Rutter model (Rm) and the Rutter model with non-linear evaporation (Rm-Enl).

Despite differences in the evaporation calculations in the employed Rutter models, both models performed equally well in terms of the NSE ($Rm=0.627 \pm 0.053$; $Rm-E_{nl}=0.628 \pm 0.053$). Therefore, model performance was not significantly improved by the non-linear evaporation introduced by E_{nl} . This is further illustrated in Figure 4.4 which shows a comparison of the simulated and observed TF for three specific events for each forest cover type. In fact, simulation differences were almost imperceptible and there were no significant differences in the optimized median parameter values between models (Rm : $S=2.2 \pm 1.2$ mm; $D0=0.39 \pm 0.11$ mm h^{-1} ; $b=0.74 \pm 0.14$; $Rm-E_{nl}$: $S=1.5 \pm 0.9$ mm;

$D_0=0.38 \pm 0.19 \text{ mm h}^{-1}$; $b=0.72 \pm 0.14$). This result suggests that the model parameters can compensate each other and thus cannot easily be interpreted as physical properties. Furthermore, the selected specific events for each forest cover (7 h in total) shown in Figure 4.4 also support a fairly good model performance in relation to observed TF. Given these results on model performance we selected the Rm- E_{nl} model for further analyses on the canopy water balance, as it addresses the underestimating of evaporation by the Rutter model (Schellekens et al., 1999). OGFs had a higher median NSE (0.628 ± 0.053), than SECFs (0.485 ± 0.010) and EARFs (0.544 ± 0.164 ; Figure 4.5). The inferred parameter values for OGFs ($S= 2.92 \pm 1.17 \text{ mm}$; $D_0= 0.53 \pm 0.24 \text{ mm h}^{-1}$; $b= 0.53 \pm 0.11$) and SECFs ($S= 1.64 \pm 2.33 \text{ mm}$; $D_0= 0.36 \pm 0.39 \text{ mm h}^{-1}$; $b= 0.83 \pm 0.26$) suggest that the dynamics in canopy rainfall interception for these two forest covers is very similar with larger storage and drainage rates compared to EARFs' low S and D_0 estimates ($S= 0.33 \pm 0.51 \text{ mm}$; $D_0= 0.06 \pm 0.34 \text{ mm h}^{-1}$; $b= 0.93 \pm 0.83$; Figure 4.5).

4.2.5 Impact of temporal resolution on fog water input estimate (RQ1)

TF data reported in the literature were collected at different temporal resolutions. This likely has a strong effect on the estimates of additional water inputs by fog. To evaluate this effect, we aggregated the 10 minute data in hourly and daily time-steps for the shared time series between forest covers. We then followed the same averaging procedure for the TF data per time step as described in Section 4.2.3. The data time series were partitioned for each temporal resolution and forest cover between data when $P > TF$ and data when $TF > P$ (represented in the lower halves and upper halves, respectively, in the panels of Figure 4.6; Appendix 4A).

The difference between TF and P when $TF > P$ was assumed to represent the additional water inputs by fog to the system (TF_{add}). Afterwards, we established the proportion of

TF_{add} in relation to total measured P (P_{total}) for each temporal resolution. We also verified that the TF_{total}/P_{total} remained constant across the different temporal resolutions.

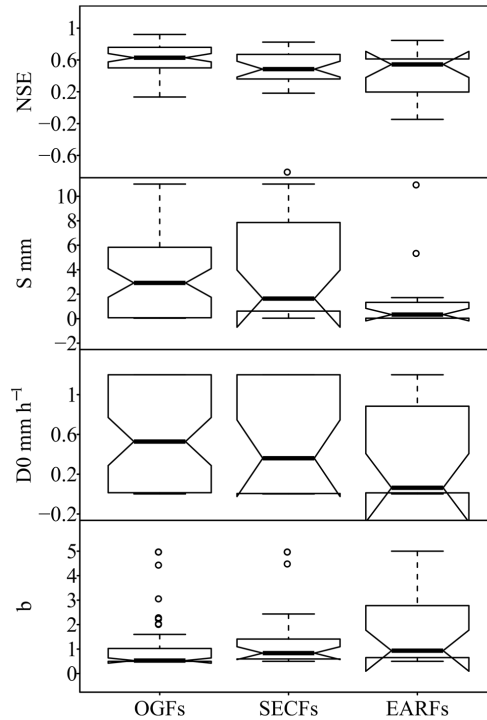


Figure 4.5. Performance of the Rutter model and distribution of the optimized parameters. Model results are for the Rm model with non-linear evaporation for each land cover: OGFs, SECFs and EARFs. From top panel to bottom panel: 1) Nash-Sutcliffe Efficiency Index-NSE; 2) canopy storage-S; 3) drainage at saturation-D0; and 4) drainage parameter-b.

4.2.6. Canopy water balance partitioning under different fog conditions (RQ2)

Evaporation depends on the amount of canopy water available to fulfil PE water demands and thus, it will also determine the dry and wet (dry/wet) canopy frequency. However, measuring evaporation and dry/wet canopy frequencies directly was not feasible due to the remote and steep character of the site, and budget limitations. Alternatively, Rutter model simulations can be used to estimate dry/wet canopy frequencies and also to assess

the potential effect of higher (clear skies) and lower (overcast skies) solar radiation levels on the canopy water balance of each forest cover. Our approach therefore consisted of a sensitivity analysis performed by forcing the 0.5, 0.25, 0.55, 0.75 and 0.95 quantiles from the estimated PE time series (Section 4.2.2; Figure 4.3) for the two studied elevations on Rm-Enl for each site using the optimized parameters. We compared the simulated E/TF ratios and the dry/wet canopy frequency (dry when $C=0$; wet when $C>0$) within and between the forest covers (Appendix 4A). We also estimated the PE/TF ratio from our observed TF and estimated PE to use it as a reference value.

4.2.7 Fog water inputs from fog-only events (RQ3)

Fog events occurring without rainfall are not always detected by the fog gauges given their dependence on fog water content and wind speed (Villegas et al., 2008). Observed TF when there is no rainfall could represent the water inputs by fog events, but these TF observations could also be caused by canopy storage drip. Therefore, simulated TF can allow us to discriminate between fog drip events and canopy drainage after rainfall. For all sites we extracted the recorded fog drip when the simulated TF was equal to zero to estimate the input of fog water and proportion of days with fog at the three forest covers. Given that TF gauges presented failures on different moments we excluded missing data from the daily mean estimates per forest cover. To estimate this mean monthly water inputs by fog we multiplied daily mean values of fog water input by the number of days per month, assuming that fog inputs during the days with observations were representative for the entire month (Appendix 4A).

4.2.8. Fog water inputs during rainfall (RQ4)

The co-occurrence of fog and rainfall is common in the Orinoco TMCs (Chapter 2). This limits quantifying the fog effect on canopy interception. Usually, this effect is only quantified when TF exceeds P. However, this would neglect those specific events where

fog, despite contributing to fill the canopy water storage, does not necessarily cause TF to exceed P. This, either because the canopy storage is not completely full and/or because evaporation is also withdrawing water from the canopy. In order to detect the fog signal during rainfall events we selected rainfall events that were preceded by three dry hours and that lasted for at least forty minutes. Then we evaluated the TF/P ratio at the first four ten-minute time steps of rainfall (40 minutes; t_0 : from 0 to 10 minutes; t_1 : from 10 to 20 minutes; t_2 : from 20 to 30 minutes; t_3 : from 30 to 40 minutes) between the wettest/foggiest months and the driest months for each of the forest covers, identified from Section 4.2.7 (Appendix 4A). We excluded intermediate months from the analysis.

4.3. Results

4.3.1 Mean observed through-fall to precipitation ratios

TF_{total}/P_{total} data revealed small differences between the forest covers. OGFs had the highest TF_{total}/P_{total} ratio (77%), followed by SECFs (74%) and EARFs (73%; Table 4.3) but median TF_{total}/P_{total} differences between forest covers indicate that these are not significant (OGFs= 77±3%; SECFs=68±6%; EARFs=69±10%). The OGFs' TF_{total}/P_{total} values are close to the mean TF of 81±11% reported by Bruijnzeel et al. (2011a) for lower montane cloud forests. SECFs' TF_{total}/P_{total} values agreed with the 75% reported by Hölscher et al. (2011) for mid successional TMCFs but were lower than the >80% reported for the Mexican secondary TMCFs (Holwerda et al., 2010). To our knowledge, only Hölscher et al. (2011) and Pryet et al. (2012) have reported TF/P observations for early successional/shrubby TMCFs. Their mean TF/P ratios for early successional TMCFs are very different: 115% in Pryet et al. (2012) and 69% in Hölscher et al. (2011). These results, even though comparable to the expected values according to other studies, do not provide information on the potential amounts of additional water inputs by fog.

4.3.2 Impact of temporal resolution on fog water input estimates

The analysis of data aggregation to coarser temporal resolutions shows that there is generally a decrease in the monthly and total TF_{add}/P_{total} ratio and an increase in the intercepted rainfall in all forest covers (Figure 4.6 and Table 4.3). The differences in estimated TF_{add}/P_{total} from the 10 minute to the daily temporal resolution between forest covers were 0.2 in OGFs (10 minute $TF_{add}/P_{total}= 0.23$), 0.15 in SECFs (10 minute $TF_{add}/P_{total}= 0.16$) and 0.18 in EARFs (10 minute $TF_{add}/P_{total}= 0.20$). Expressed in absolute rainfall amounts these values translate into considerable TF_{add} differences of 1268 mm in OGFs, 817 mm in SECFs and 1013 mm in EARFs (Table 4.3). Therefore, when using longer temporal resolutions most additional water inputs become unnoticeable (<0.03). However, it is important to consider that the 10 minute resolution is detailed enough to separate the canopy wetting period and post rainfall dripping because drainage after rainfall ceases will cause TF to be larger than P . Thus, the additional water inputs are likely overestimated through the quantification of both the true additional water inputs by fog and the post rainfall drip. Using the hourly temporal resolution data, the water balance during rainfall events is better represented, whereas using the daily temporal resolution data will result in diurnal variations in meteorological conditions that easily obscure the additional water inputs.

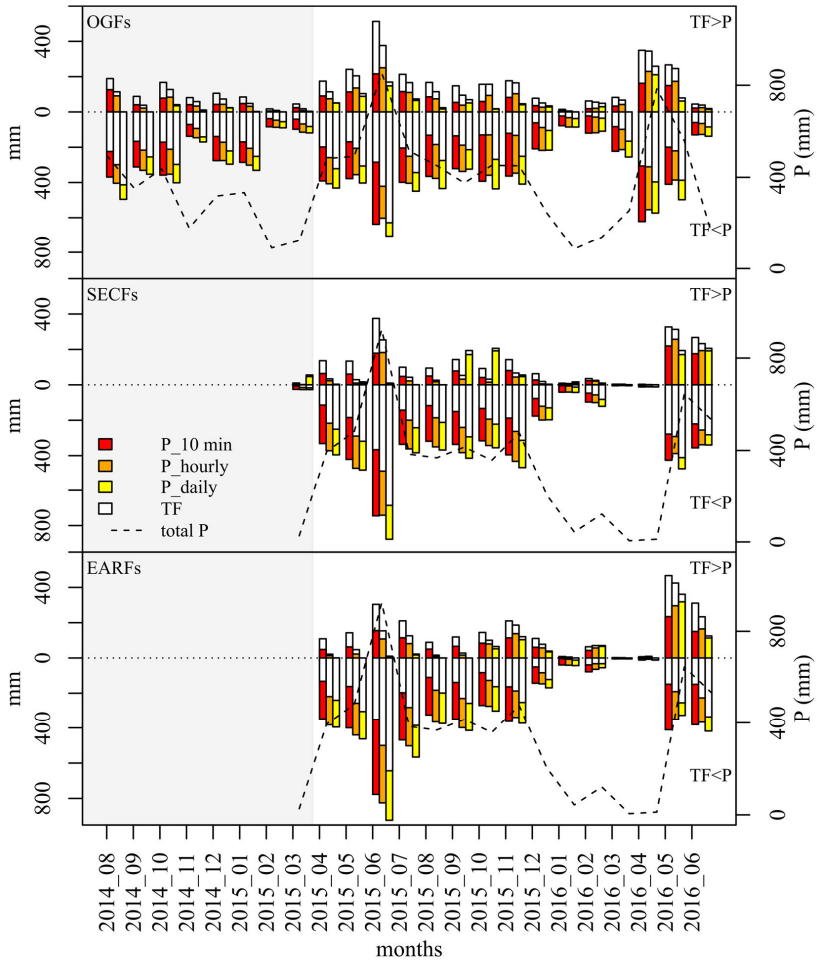


Figure 4.6. Separation of rainfall events into those with lower through-fall (TF) than rainfall (P) and those with higher TF than P at different temporal resolutions. Data is shown in monthly totals. The evaluated temporal resolutions were: 10 minutes, hourly and daily. Data plotted in the bottom half of each panel is when P exceeded TF and data plotted in the upper half of each panel is when TF exceeded P. Top panel: Old-growth TMCFs (OGFs), middle panel: Secondary TMCFs (SECFs), and bottom panel: Early succession TMCF (EARFs). Total monthly P is on the right side axis. The grey area represents the data excluded from the analysis in Table 4.3.

Table 4.3. Temporal resolution effect on estimating additional water inputs for each forest cover. We partitioned P and TF time series per forest cover in different temporal resolutions (10 minutes, hourly and daily) in two groups: when $P > TF$ (inter) and when $TF > P$ (add). We show total P and TF amounts and their absolute difference for each group and the additional TF ratio (TF_{add}) to total measured rainfall (Pt). In the last column we present the TF_{total}/P_{total} ratio.

Forest	10 minutes			hourly			daily			TF_{total}/P_{total}		
	P (mm)	TF (mm)	abs diff	P (mm)	TF (mm)	abs diff	TF_{add}/P_t	P (mm)	TF (mm)		abs diff	TF_{add}/P_t
O add	1244	2689	1445	1397	2202	805	0.23	821	998	177	0.03	0.77
G inter	5040	2131	2909	4892	2618	2274	0.13	5468	3821	1647	0.01	0.74
S add	1049	1926	877	827	1140	313	0.06	427	487	60	0.01	0.74
C inter	4314	2031	2283	4536	2817	1719	0.06	4936	3471	1465	0.01	0.74
E add	1185	2299	1114	1047	1503	456	0.08	714	815	101	0.02	0.73
A inter	4369	1734	2635	4507	2530	1977	0.20	4841	3218	1623	0.02	0.73

4.3.3 Canopy water partitioning under contrasting PE conditions

The observed TF values were typically lower than the simulated TF (Figure 4.7). This can be caused by multiple reasons: model underestimates of E, ignoring the role of stemflow which could potentially be more significant than reported for TMCFs (1-2%; Bruijnzeel et al., 2011a), or missing sources of water, caused by an overflow of the tipping bucket before or during tipping, specially under high-intensity rainfall. However, forcing inferred PE in the model within its quantile range at each elevation provides information to address our second research question by analysing fog's relative influence on the canopy water balance by partitioning rainfall inputs into TF and E and by determining the dry/wet canopy frequency (Figure 4.7). The increase in the simulated E/TF median between the 0.05 PE quantile (foggiest PE) and the 0.95 PE quantile (clear skies) was 0.21 for OGFs, 0.25 for SECFs and 0.17 for EARFs. The similar increase in E/TF for OGFs and SECFs did not reflect the strong PE differences with elevation (c.f. Figure 4.3). The inferred larger difference in E/TF between SECFs and EARFs, both exposed to similar meteorological conditions, was thus likely more related to difference in the canopy storage (Figure 4.7). This was further supported by the dry/wet canopy analysis in which EARFs had a longer dry canopy frequency than SECFs for all analysed PE quantiles. This would result in a reduced E from the PE.

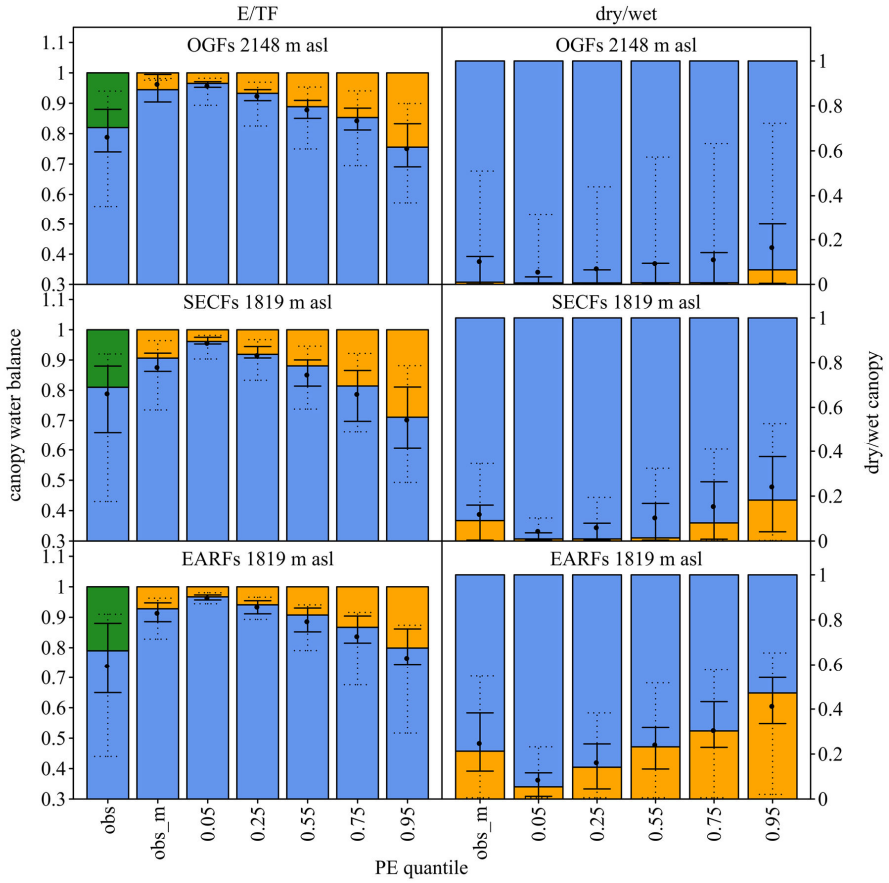


Figure 4.7. Influence of fog on the water balance partitioning into median through-fall and evaporation and dry/wet canopy frequency. Results originate from simulations employing estimated potential evaporation (PE) for the observed meteorological time series (obs_m), and simulations forced with the PE quantiles from higher to lower fog influence (0.05, 0.25, 0.55, 0.75, 0.95; x-axes). Plots on the left show the simulated evaporation/through-fall ratio (E/TF; orange/blue) and plots on the right show the simulated canopy dry/wet frequency (orange/blue). The measured water balance in terms of PE (in green) and TF (blue) is also shown. Solid error bars are the 0.25 and 0.75 of the distribution and dotted error bars are the 0.05 and 0.95 of the distribution. The dots represent the mean values. Top panels: High elevation old-growth forest (OGFs 2148 m asl); middle panels: Low elevation secondary TMCFs (SECFs 1819 m asl); and bottom panels: Low elevation early succession TMCFs (EARFs 1819 m asl)

4.3.4 Fog water inputs by fog-only events

The model simulations were used to separate drainage after rainfall from fog drip caused by interception. This allows to quantify the fog water inputs by fog-only events and address our third research question. Results indicated differences in fog water inputs by fog-only events between forest covers (Figure 4.8). These differences have an associated uncertainty due to differences in the minimum tipping water depth of the TF gauges in OGFs (0.07 mm tip^{-1}) and SECFs/EARFs (0.4 mm tip^{-1}). TF gauges in OGFs are more sensitive to fog inputs and have a lower influence of residual water stored in the tipping bucket from previous rainfall, whereas TF gauges in SECFs and EARFs are less sensitive to fog inputs and have a larger influence of residual water (from 0.00 to 0.39 mm) stored in the tipping bucket from previous rainfall. However, a random distribution of residual water in the TF gauges can be safely assumed throughout the study period and between gauges. Days with fog-only events were on average more frequent at OGFs than at SECFs and EARFs, except during the dry season. However, the measurement records for SECFs and EARFs were shorter than for OGFs preventing us from comparing the fog inputs on the 2014-2015 dry season. According to both rainfall and PE data the 2015-2016 measured dry season was evidently more severe than the 2014-2015 dry season. This is likely due to the influence of the strong 2015-2016 El Niño event (Jiménez-Muñoz et al., 2016; Figure 4.8). Nevertheless, at least for the strong dry season, fog-only water measurements suggested a lowering in the condensation level increasing the inputs of fog water at the lower elevation forest sites. In relation to water inputs by fog from fog-only events, OGFs showed a range between $0.2 \text{ mm month}^{-1}$ in the driest months to more than 20 mm month^{-1} during the wettest month. Throughout the study period from August 2014 to May 2016 (22 months) OGFs had 147.3 mm of water inputs by fog drip (equal to 80 mm y^{-1}), representing 1.6% of the total water inputs (9313 mm). However, our estimates are conservative given that we are only considering water inputs from fog-only events

and exclude fog water inputs during rainfall events. SECFs tended to have slightly higher fog inputs than EARFs, but even in the months with higher fog inputs, this never exceeded 10 mm month⁻¹. Throughout the study period total fog inputs from fog-only events for SECFs and EARFs (April 2015 to May 2016, excluding April 2016) were 79.5 mm and 45.4 mm. This represents 1.5% and 0.8% of the total water inputs (5363 mm and 5554 mm), respectively. The small differences in the percentage of fog water inputs in relation to P_{total} for OGFs and SECFs agreed well with the small differences detected between Mexican old growth and secondary TMCFs (Holwerda et al., 2010). However, there is no coincidence between OGFs and SECFs in the months with the highest fog water inputs. Therefore, the elevation differences between the two forest covers in our study area are also an important factor. In terms of seasonality, OGFs fog inputs were related to monthly rainfall. However, the months with highest rainfall were not necessarily the months with higher fog frequency or inputs (Figure 4.8).

4.3.5 Fog water inputs during rainfall

In the previous section we only quantified the fog that dripped from the canopy after filling the canopy storage. In this section, we approach our fourth research question by quantifying the role of fog in partially filling the storage during the first forty minutes of rainfall. For this approach we chose the foggiest and least foggy months according to the analysis of the data discussed in the previous section (Table 4.4). As rainfall progressed there was a gradual increase in the TF/P proportion for all forest covers as expected by the gradual saturation of the canopy water storage (Figure 4.9). In OGFs the contrasts in the median TF/P between rainfall events during the least foggy months ($t_2=0.23\pm 0.05$; $t_3=0.36\pm 0.07$) and the foggiest months ($t_2=0.37\pm 0.06$; $t_3=0.64\pm 0.08$) were strongly significant (*sensu* Chambers et al., 1983).

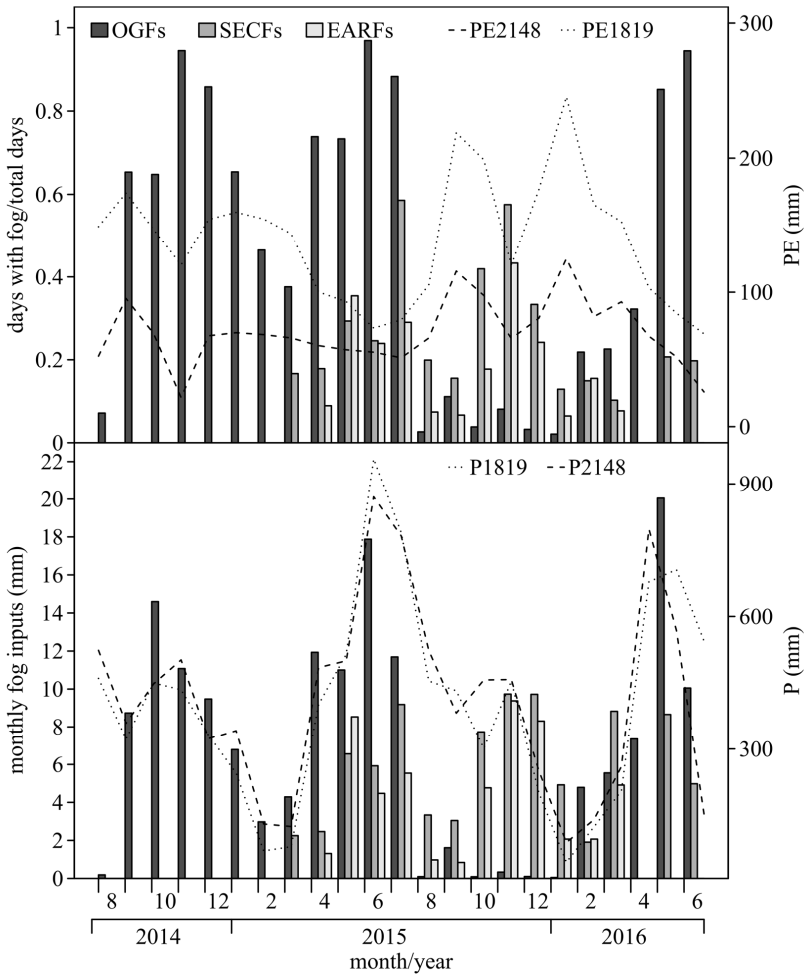


Figure 4.8. Through-fall due to fog. The top panel shows the monthly proportion of days with fog occurrence at each main forest covers (OGFs, SECFs and EARFs) and the monthly potential evaporation (PE) estimated at both elevations: 2148 m asl and 1819 m asl. The bottom panel shows monthly fog inputs and rainfall measured at 1819 m asl and 2148 m asl. Note that data for OGFs was collected from August 2014, whilst data for SECFs and EARFs was collected from in April 2015, and had no data on April 2016. Data for all forest covers were collected until June 12, 2016.

Table 4.4. The foggiest and least foggy months (MFM and LFM) chosen per forest cover (Old-growth TCMF-OGFs; Secondary TCMF-SECFs; Early succession TCMF-EARFs) for the analyses on the fog effects during rainfall.

	Selected Months
OGFs - MFM	Oct-2014, Nov-2014, Apr-2015, May-2015, Jun-2015, Jul-2015, May-2016, Jun-2016
OGFs - LFM	Aug-2014, Aug-2015, Sep-2015, Oct-2015, Nov-2015, Dec-2015, Jan-2016
SECFs - MFM	Jul-2015, Oct-2015, Nov-2015
SECFs - LFM	Sep-2015, Jan-2016, Feb-2016, Mar-2016
EARFs - MFM	May-2015, Jul-2015, Nov-2015, Dec-2015
EARFs - LFM	Aug-2015, Aug-2015, Jan-2016, Mar-2016, May-2016

Even though there were rainfall events in both the foggiest and less foggy months when TF strongly exceeded P these were most common during t_3 in the foggiest months (Figure 4.9). In the case of SECFs, median differences in TF/P between the foggiest months and the least foggy months became significant only after 30 minutes (t_3) of rainfall (foggiest months= 0.70 ± 0.12 ; least foggy months= 0.19 ± 0.20). In the case of EARFs, no significant evidence of fog influence was observed in the TF/P ratio when comparing foggiest with least foggy months. These results likely reflect the higher fog interception capacity of SECFs in comparison to EARFs. Notice that the median values for all forest covers in both the foggiest and least foggy months were below the 1:1 TF/P ratio. This implies that this fog effect would pass unnoticed with the usual TF/P per rainfall event approach that only considers a fog influence for those events where TF exceeds P.

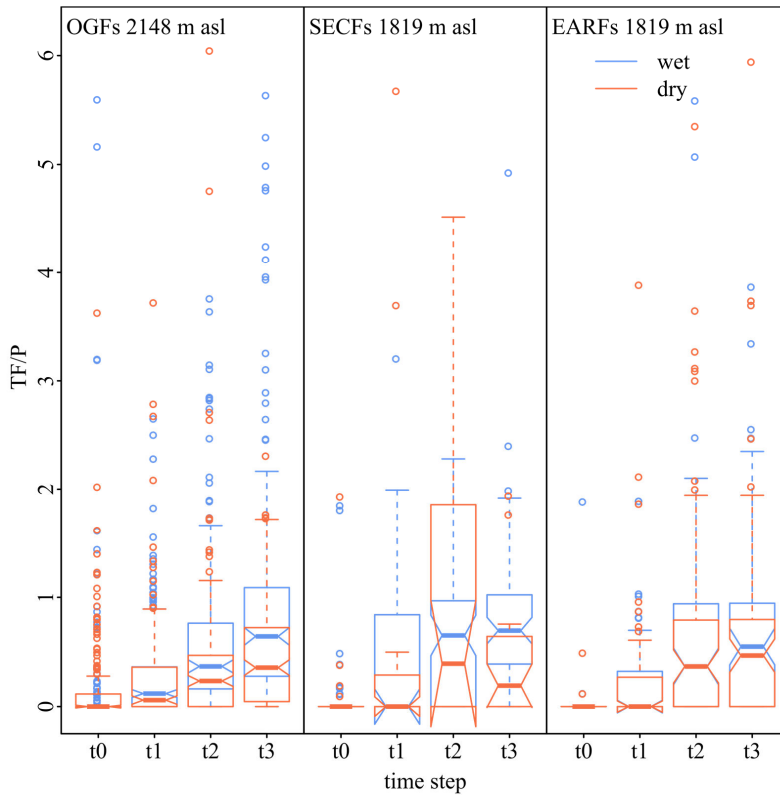


Figure 4.9. Evolution of through-fall/rainfall ratios during the onset of rainfall in the foggiest and least foggy months. Left panel: old growth TMCFs (OGFs), middle panel: secondary TMCFs (SECFs) and right panel: early succession TMCFs (EARFs). Time steps indicate the first four 10 min time steps of each rainfall event.

In Table 4.5 we list the means and standard errors of P intensities and PE values of both the foggiest (wet) and least foggy months (dry) to evaluate if they can influence the TF/P differences described previously. In OGFs, differences in P intensities were smaller than the error bounds, except in the first 10 min when P was highest in the least foggy month compared to the foggiest month. Differences in PE during rainfall were not significantly different whereas antecedent PE_{1h} and PE_{dry} were higher in the least foggy months. Higher antecedent PE leads to drier canopies, thus influencing the initial TF/P values. However,

it does not explain the tendency of TF/P differences becoming larger as P progressed. In SECFs, P_{10} differences between the foggiest and least foggy months were smaller than the error bounds. Afterwards, P_{11} and P_{12} had higher values in the foggiest months, and P_{13} was larger in the least foggy months. These P variations are not reflected in the TF/P patterns depicted in Figure 4.9. Differences in PE during the preceding dry period between the foggiest months and the least foggy months varied. Whilst PE_{1h} was higher in the foggiest months, PE_{dry} was higher in the least foggy months. In this case, PE_{dry} can be more relevant for reducing the water stored in the canopy and thus influencing observed TF/P differences. Potentially wetter canopies can lead to the observed tendency of higher TF/P in the foggiest months. In EARFs, P_{10} were higher in the least foggy months compared to the foggiest months, whereas differences in P_{t_2} were larger in the least foggy months. These variations were not reflected in the observed TF/P patterns. In addition, PE differences were smaller than the error bounds, suggesting that PE was not relevant to explain the observed TF/P ratios.

Table 4.5. Seasonal and elevation differences in mean rainfall and mean potential evaporation of through-fall during analysed rainfall events at the three dominant forested land covers. Rainfall at the four analysed 10 minute time steps (P_{t_0} to t_3 in mm) and potential evaporation during the rainfall event (PE_{RF} in mm), one hour before the rainfall event (PE_{1h}) and for the whole dry period before the rainfall event (PE_{dry}).

	OGFs 2148 m asl		SECFs 1819 m asl		EARFs 1819 m asl	
	Wet (n=294)	Dry (n=237)	Wet (n=87)	Dry (n=33)	Wet (n=80)	Dry (n=68)
P_{t_0}	0.66±0.04	0.88±0.06	0.86±0.14	0.79±0.19	0.68±0.08	0.96±0.16
P_{t_1}	1.84±0.13	1.74±0.13	1.97±0.26	1.02±0.16	1.74±0.22	1.77±0.23
P_{t_2}	2.09±0.15	2.02±0.15	1.94±0.24	1.17±0.31	2.11±0.22	1.53±0.18
P_{t_3}	1.68±0.13	1.61±0.15	2.34±0.30	4.07±0.84	2.50±0.34	2.18±0.36
PE_{RF}	0.033±0.005	0.032±0.01	0.07±0.01	0.04±0.01	0.034±0.004	0.040±0.005
PE_{1h}	0.073±0.002	0.083±0.002	0.12±0.01	0.06±0.02	0.06±0.01	0.07±0.01
PE_{dry}	0.50±0.03	1.06±0.08	1.50±0.15	2.64±0.42	1.60±0.30	1.4±0.16

4.4. Discussion

The interaction between the vegetation and the atmosphere in TMCFs is modulated by multiple processes that are highly sensitive to fog. Despite that the fog's influence on canopy interception is widely acknowledged, quantifying its effects has been generally approached following a 'black-box' or input/output approach that neglects these processes. Thus, we analysed the fog's influence on each process separately, namely evaporation (RQ2), and fog interception during fog-only events (RQ3) and during foggy rainfall events (RQ4; Figure 4.1). While our analysis is based on TF data, we employed the Rutter model to infer canopy water storage dynamics. The Rutter model generally performed well, but the estimates of the parameter values (S , D_0 and b) constrained only by TF data do not necessarily represent the physical canopy characteristics they intend to due to their compensatory character (Vrugt et al., 2003). Therefore, using these inferred parameter values to define and compare canopy characteristics of different forests (or studies) can be misleading. However, the running water balance principle of the Rutter model suggest that the water storage and release from the canopy is properly represented, and thus, it can provide insights on the canopy water dynamics.

Another important factor when evaluating the canopy water balance of TMCFs from TF observations is their temporal resolution. Water inputs by fog interception, identified when $TF > P$ can be overestimated using high temporal resolutions (< 10 min) that separate the canopy wetting ($TF < P$) and post rainfall dripping ($TF > P$) phases during P events. In contrast, using lower temporal resolutions ($> \text{day}$) underestimate fog water inputs by mixing rainfall events with and without fog, and fog-only events which can all happen within a day. Therefore, an intermediate temporal resolution (hourly) achieves a better compromise in aggregating rainfall-canopy phases and accounting for daily meteorological variations. The estimates of water inputs by fog interception in the hourly

resolution (TF_{add}/P_{total}) ranged from 0.08 to 0.13 (Table 4.3). These numbers reflect fog effects on the canopy water balance only when $TF > P$, however, other fog effects might pass unnoticed with this approach.

The effect of fog on reducing actual evaporation (E) was further investigated by forcing on TF simulations the different quantiles of estimated PE from meteorological data. Contrasts in E/TF between foggy and fogless conditions ranged from 0.17 to 0.25 (Figure 4.7). The canopy of OGFs had the lowest dry canopy frequency, thus, it tended to have enough available water to fulfil a fog-reduced PE (Figure 4.3). This inferred dry canopy frequency agreed well with the observations in other TMCFs and this shows that the canopy (including associated epiphytes) requires long dry-spells of up to eight days to dry (Tobón et al., 2011; Mulligan et al., 2011). The relative rareness of having dry canopy conditions in OGFs and SECFs also indicates that there is a limited applicability of interception models that assume a dry canopy between rainfall events to study canopy water balances in TMCFs (*e.g.* the Gash model). At the other end, the canopy of EARFs was subjected to a higher PE and it was more frequently dry with the lack of available water in the canopy, limiting E . Higher PE values increase E (OGFs vs SECFs), but if the canopy dries, E is reduced (SECFs vs EARFs). The higher water availability in the canopy of SECFs compared to EARFs' is most likely related to a more complex canopy with a higher epiphyte load in more developed secondary forests. Furthermore, in terms of the canopy energy budget, the transition from a wet to a dry canopy increases the sensible heat fluxes (*e.g.* Holwerda et al., 2016, Ray et al., 2006). This is particularly important in TMCFs when considering the downwind effects of these energy fluxes to favour fog conditions (Lawton et al., 2001).

The analyses to quantify fog inputs showed that fog drip during fog-only events do not represent a significant input to the catchments' water budgets (from 0.8 to 1.6% of

measured P; Figure 4.8 and Figure 4.10). These values are similar to the 1.4% reported in the relatively less exposed Jamaican forests (Hafkenscheid, 2000), to the fog contribution of 0.8% in Peruvian TMCFs (Gómez-Peralta et al., 2008) and to the <2% in Mexican TMCFs (Holwerda et al., 2010). However, the additional water inputs by fog during rainfall events are likely more relevant. For example, in OGFs, TF/P after 30 min of rainfall was 0.28 to 0.51 times higher in the foggiest months than in the least foggy months (Figure 4.9). Furthermore, a higher TF/P does not always imply a TF>P, thus, it can be overlooked in the estimates that only consider as water inputs by fog interception the additional TF values when TF>P. However, our approach does not allow to estimate total fog inputs during all rainfall events. Thus, the uncertainty around these estimates remains considerable. For example, if we assume that the minimum estimated fog inputs were those derived from fog-only events and the maximum fog inputs are likely those estimated when TF>P in the hourly time resolution (Table 4.3), the potential range in total water inputs by fog relative to total rainfall for each forest cover is: 1.7% to 12.8% in OGFs; 1.5% to 5.8% in SECFs, and 0.8% to 8.2% in EARFs (Figure 4.10).

In the case of high elevation OGFs, where fog tended to follow the seasonal rainfall (Figure 4.8), the potential underestimation of water inputs to these TMCFs is only relevant during the wet season. This contrasts to other TMCFs under oceanic influence, where fog water inputs are highly relevant during the dry season (*e.g.* Goldsmith et al., 2013). A larger water contribution by fog at the low elevation SECFs and EARFs compared to the high elevation OGFs during the sampled dry season, suggests a seasonal downward shift of fog along the elevation gradient (Figure 4.8). However, with only one year of data we cannot know if this is a typical dry season phenomenon, especially considering that the dry season intensity is highly variable between years (Chapter 3).

Nevertheless, fog inputs are likely too low to explain the reported missing water inputs in the dry season (Chapter 2).

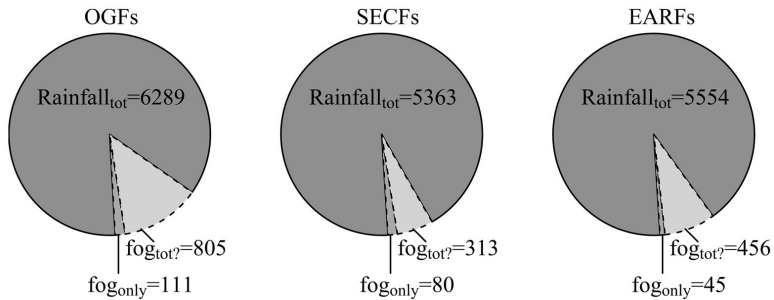


Figure 4.10. Contribution of fog to total water inputs per forest cover over the study period. Each pie-chart shows: estimated fog inputs during fog only events (fog_{only}; Section 4.3.4); maximum potential fog inputs estimated from the hourly time resolution when TF is larger than P (fog_{tot?}; Section 4.3.1), which include the fog_{only} inputs; and total measured rainfall (Rainfall_{tot}). Units are mm totals over the shared study period for all forest covers (April 1, 2015 to June 12, 2016).

From a catchment perspective, the fog effects we have described suggest that the higher elevations sustain overall wetter conditions in contrast to lower elevations subjected to a relatively smaller influence of fog. A higher moisture in the system can potentially translate into a larger contribution of water to streamflows. Even though additional fog water inputs represented a low proportion of total rainfall similar to other TMCFs (*e.g.* Gómez-Peralta et al., 2008; Hafkenscheid, 2000; Holwerda et al., 2010), fog plays a key role in reducing PE, and thus E, and in having a more frequently wet canopy. Furthermore, TF is enhanced during foggy rainfall events in contrast to fogless rainfall events.

The individual processes that have been evaluated in detail in this study have associated uncertainties that together explain the difficulty to close a water budget in TMCF catchments (*e.g.* Chapter 2; Clark et al., 2014; Muñoz-Villers et al., 2012). First, with only two measurement sites to provide the observations to infer PE along the elevation

gradient we can only assume a linear dependence of PE along elevation. Second, we simplified forest covers in three major categories that are likely far from being homogeneous. A more detailed canopy characterization of the different forest covers, with the collection of micrometeorological data along the vertical gradient and stemflow data would allow to use more realistic, albeit complex, canopy interception and potential evaporation models suitable for multilayered canopies. However, this also requires more sophisticated experimental setups that are not easy to install and maintain in TMCFs which are often remote and inaccessible. Given the current concerns about climate and water availability changes in time, it is perhaps more pertinent to have simpler, more robust and affordable monitoring systems that can stay operational for longer time periods.

4.5. Conclusions

Quantifying the effects that fog has on the canopy water budget from through-fall (TF) data is highly challenging. However, depending on the temporal resolution of the observations, first order estimates are achievable. Our analysis showed that the temporal resolution of data (RQ1) affects estimates on water inputs by fog. Data collected in daily or longer time periods average out fog effects by combining foggy and clear sky conditions. This is an important consideration when comparing fog's influence across TMCFs that were studied based on datasets using different temporal resolutions.

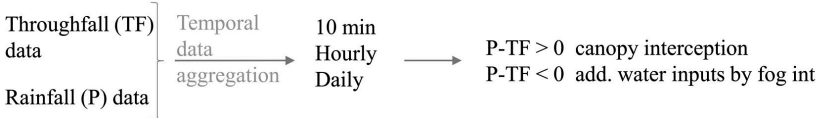
We then evaluated fog's influence on each process separately, namely evaporation (RQ2) and fog interception during fog-only events (RQ3) and during foggy rainfall events (RQ4). Fog water inputs from fog only events represent a very low percentage of total rainfall (1.6% max). However, our results demonstrate that fog effects on the canopy water balance are in fact important to sustain the hydrology of TMCFs. For example, the contrast in potential evaporation between fog and fogless conditions increase the E/TF

ratios up to 0.25. We also showed that TF is significantly enhanced during rainfall events co-occurring with fog, despite the fact that these events are not always associated with TF being higher than P. Therefore, studies that only account for the fog effects when TF exceeds P underestimate fog inputs. A reduction in fog persistence would not only have an impact on the amount of water reaching the ground but also on the canopy energy budget.

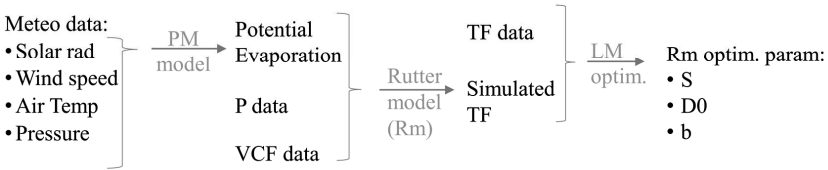
Extrapolating these evaluated effects of fog on the canopy water budget to the catchment water budget remains challenging due to associated uncertainties in the data collection system and analysis, and in the extrapolation of the point measurements to the catchment scale. Nevertheless, results show that higher elevations likely provide a larger contribution of water to streamflow due to stronger fog effects than the forests at the low elevations. In this way, our observations contribute to ongoing efforts to unravel and close the water balance of TMCF catchments.

Appendix 4A

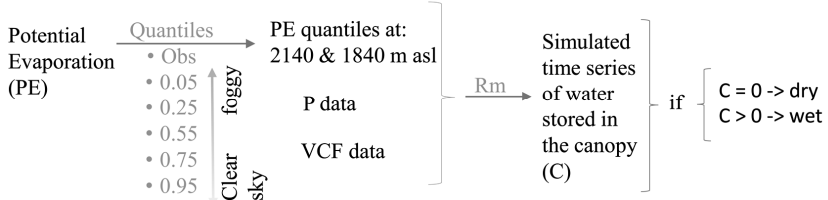
Temporal resolution impact analysis



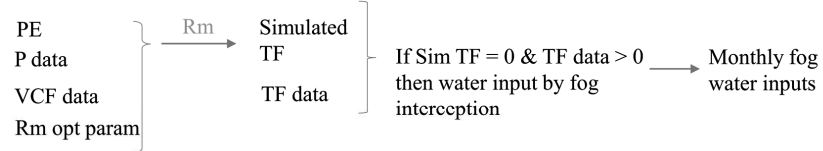
Estimating the Rutter model parameters



Fog effects on Potential Evaporation



Water inputs by fog interception



Fog water inputs during rainfall

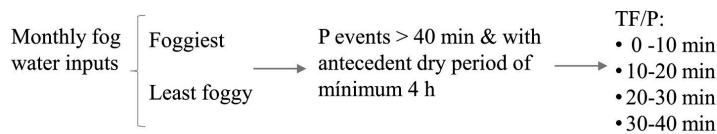


Figure 4A. Flow diagram of the data analyses employed to answer the research questions. Abbreviations not explained in the diagram: additional water inputs by fog interception (add.water inputs by fog int), Penman-Monteith model (PM model), Vegetative Cover Fraction (VCF), Levenberg-Marquardt optimization (LM optim), Rutter model optimized parameters (Rm optim. param.), canopy sotrage (S), Drainage rate when C = S (D0), and Rutter model drainage parameter (b).



CHAPTER 5

Synthesis

Chapter 5

Synthesis

This thesis aims to better understand the hydrological functioning of Tropical Montane Cloud Forests (TMCFs) in the unique setting of the seasonal Orinoco River basin headwaters located in the Colombian eastern Andes. Such enhanced understanding is fundamental to evaluate the impact of land-use and climate change on TMCFs' hydrology. To accomplish this, a hydro-meteorological monitoring system was setup in 2013 covering three headwater TMCF catchments with contrasting land covers. The observational data that were collected were analysed and used to address the following research questions (RQs):

- RQ1. What is the hydro-meteorological spatio-temporal variability in the three neighbouring catchments with different forest covers?
- RQ2. To what extent can variations in streamflow between catchments be explained by the differences in forest cover?
- RQ3. What is the hydrological role of TMCFs' organic layers in water storage and release under land-use and climate changes?
- RQ4. What is the role of fog presence and interception on the canopy water balance on three successional TMCFs' regeneration stages?

The answers to these RQs provided novel information on continental TMCFs' hydrological functioning with a unique upwind land cover compared to other studied TMCFs. This chapter aims to synthesize and integrate the information gained in addressing the individual research questions in chapters 2, 3 and 4. First, the effect of seasonal and spatial hydro-meteorological variability on streamflows is addressed (RQ1). Then, the effects of the different land covers found in each catchment on streamflow

behaviour (RQ2) are discussed and the information gained by addressing the first and second research questions is integrated to understand their combined effect on the catchments' observed water budgets. Afterwards, the two main threats for TMCFs' hydrological functioning, namely, the increased occurrence of extreme dry seasons and land-cover change affecting streamflow are discussed from the soil (RQ3) and canopy interception (RQ4) perspectives. At the end of the section the main conclusions that can be drawn from this research are highlighted.

5.1. Seasonal and spatial hydro-meteorological variability effects on streamflows

TMCFs are considered key ecosystems for hydrological regulation despite their narrow distribution that is constrained by fog persistence (Zadroga, 1981). The unique interactions between TMCFs and fog suggest that forest clearance could decrease streamflows, contrary to the expected increase in streamflow following deforestation described for other tropical forests (Calder, 2002). However, empirical evidence for a decrease in streamflow following TMCFs' deforestation is inconsistent (*e.g.* Bruijnzeel, 2006; Muñoz-Villers, 2008). The main challenge is to unveil the spatio-temporal hydro-meteorological variations and their interactions with the various forest covers found in a catchment area. In this way, compensation effects on streamflow generation between higher and lower fog persistence areas and contrasting land covers can be assessed. The three studied headwater catchments span from 1600 m to 2300 m asl in an area of approximately 10.2 km². Despite the fairly small size of these catchments the spatio-temporal variation in hydro-meteorological variables, coupled with land cover contrasts between catchments, lead to distinct streamflow behaviour (Chapter 2). From a spatial perspective the higher elevations of these TMCF catchments receive larger rainfall inputs and experience lower potential evaporation than the lower elevations. Furthermore, the elevation contrasts are enhanced during the dry season and imply that at the higher

elevations seasonality is less pronounced than at the lower elevations (Figures 2.4 and 4.3). Similar patterns in precipitation and evaporation along the elevation gradients have also been described in Bolivian and Ecuadorian eastern Andean TMCFs (Schawe et al., 2011; Emk, 2007). However, a first order comparison among eastern Andean TMCFs located downwind of the Amazon basin forested lowlands and TMCFs located downwind of the seasonally flooded savannahs of the Orinoco River basin, indicated that this site experiences higher rainfall in the wet season and drier conditions during the dry season. This pattern likely reflects the strong seasonal moisture contrast of the seasonally flooded savannahs compared to the more seasonally stable moisture conditions of the Amazon forests (*e.g.* Kim et al., 2012).

The described hydro-meteorological gradients along elevation coupled with the elevation distribution of the studied catchments and their different land covers influence streamflow behaviour. Thus, direct comparisons of catchments that only focus on land-cover contrasts without acknowledging their distribution along the elevation gradient, can be misleading. The fact that the most forested catchment (FOR) area is mainly found at the higher elevation compared to the intermediately forested catchment (INT) and the less forested catchment (DEF), had a notable effect on the water saturation of each of these catchments. Evidence for a higher water saturation at the higher elevation was found in both soil moisture data and canopy wetness frequency estimates. More specifically, soil moisture was persistently higher, even during the dry season, at the higher elevation forest site compared to the lower elevation grasslands and forests sites (Chapter 3). Additionally, the simulated occurrence of having a wet canopy was higher for the old-growth forests at the higher elevation compared to early succession and secondary lower elevation forests (Chapter 4). The higher water saturation at the higher elevations was reflected in the observed differences in streamflow between the studied catchments. First,

higher streamflow values were recorded during both the wet and the dry seasons in FOR compared to INT and DEF (Chapter 2). Second, slightly higher rainfall-streamflow responses in FOR were also recorded during the dry season compared to those of the other two catchments. Third, during the dry season the elevation contrasts between catchments (FOR being located generally higher than INT and INT being located higher than DEF) were reflected in the dry season streamflows (Chapter 2). This confirms that dry season streamflows were largely determined by the higher water inputs at the higher elevations, despite that inferred direct water inputs by fog were relatively low (Chapter 4). Fourth, DEF's delayed response in streamflow to rainfall during the dry season likely reflected a drier system that during rainfall events would first fill its water storage reservoir before reaching the streambed (Chapter 2).

5.2. Land-cover effects on streamflows

From a land-cover perspective, forests have a complex canopy and a thick soil organic layer, while grasslands have a comparatively simpler canopy and no organic layer. These differences in soil and canopy properties translate into a larger water storage in forests compared to the grasslands. Even though canopy-storage values were optimized in the process-based continuous water-balance Rutter model (Rutter et al., 1971; Rutter et al., 1975; Rutter and Morton 1977), and thus have to be interpreted with caution, the water-storage estimates of the forest canopy (from 0.3 mm to 2.9 mm; Chapter 4) were smaller than those observed in the organic layers (from 35 mm to 59 mm; Chapter 3). This difference highlights the hydrological importance of these organic layers. A larger water storage in forests implies a more tortuous path for precipitation to reach the streambed and this delays the rainfall-runoff responses. Thus, wet season rainfall-streamflow responses in FOR and INT were slower and less pronounced than in DEF (Chapter 2). This is in agreement with the results from other studies on forests around the world,

including TMCFs, where deforested catchments have faster rainfall-streamflow responses (e.g. TMCFs: Muñoz-Villers and McDonnell, 2013; Muñoz-Villers and McDonnell, 2012; Roa-García et al., 2011; other forests: Bruijnzeel, 2004 and Zhao et al., 2012). However, note that in contrast to most of these studies, the differences in rainfall-streamflow responses in this study are mainly explained by the key hydrologic role of organic layers and not by the deterioration of infiltration capacities in deforested areas, for which no evidence was found (Chapter 3).

Additional information regarding the combined effect of land cover and elevation on streamflow can be retrieved from the observation that INT had a lower streamflow compared to DEF during the wet season. The area covered by lower elevation forest found in INT has a larger canopy interception capacity compared to that of DEF's lower elevation grassland cover. A higher potential evaporation at the lower elevations, due to both higher temperatures and incoming radiation, cause the forest canopies of the secondary and early succession stages to lose larger amounts of intercepted water than the higher elevation forests. This will more readily empty the canopy-water storage. In fact, simulations with the Rutter model that compare the frequency of having a dry canopy of secondary and early succession forests, showed that early succession forests are more frequently dry than secondary forests (Chapter 4). Additionally, transpiration is also expected to be higher, given that leaf wetness is likely less frequent compared to the higher elevations (following Letts and Mulligan, 2005). This all together likely explains why INT had the lowest wet season streamflow.

5.3. Closing the water budgets

The water budgets of the studied catchments suggested additional water inputs (Chapter 2) that were varying seasonally. During the dry season daily estimated missing sources of water reached up to 50% of incoming rainfall, while during the wet season these

missing sources were up to 10%. According to the estimated additional water inputs by fog interception obtained by the classical approach of identifying the events when through-fall exceeded rainfall, the expected annual contribution of fog interception ranges between 6 to 13% of incoming rainfall (Chapter 4). Therefore, this additional water input is too small to explain the missing sources of water necessary to close the water budget during the dry season. A potential source of the missing water is the soil water storage as suggested by Clark et al. (2014) for Peruvian TMCFs. In Chapter 3 the water storage and release from the organic layers was estimated by combining soil data and the Hydrus-1D modelling system. The observed presence of about 77% of the root biomass in the organic layer indicated that this is a highly dynamic hydrological component where most of the water uptake for transpiration takes place. Water passing through this organic layer to the mineral soils will most likely find its way to the streamflow channel.

In order to integrate the collected hydrometeorological data, including soil moisture, a simple hydrological model was developed. This simple hydrological model was constrained by monthly observed rainfall and soil moisture, and inferred potential evaporation (Table 5.1) and was used to infer streamflow. The inferred streamflow for each catchment showed a fairly good agreement with the observed streamflow (from June 2014 to May 2015; Figure 5.1). The integration of soil moisture in this model largely reduced the amounts of missing water inputs compared to those estimated from the rainfall-streamflow analysis in Chapter 2. In addition, after the dry season, the estimated streamflow tends to be overestimated in all catchments. This suggests that recharge takes place at the beginning of the wet season after the soil moisture storage largely contributed to sustain dry season baseflows. In a per catchment perspective, the streamflow inferred with the simple water balance model for FOR consistently underestimates observed streamflow after the rainiest month, whereas in the less forested catchments (INT and

DEF) the inferred streamflow tends to be slightly higher than the observed. This is likely caused by higher water inputs at the highest elevations in FOR and lower water inputs at the lowest elevations in DEF and INT. A monitoring system that covers the full elevation range is required to better represent the spatial variation of all hydro-meteorological variables along the elevation gradient.

5.4. Dry season effects on moisture

Given anticipated climate change, evaluating and monitoring its potential impacts on the hydrological functioning of ecosystems such as TMCFs is highly relevant. Climate change in the Northern Andes is expected to enhance seasonality with a larger probability of extreme events (Magrin et al., 2014). Changes in local and upwind temperature and atmospheric moisture conditions affect the cloud condensation level (Still et al., 1999; Ray et al., 2006), especially in continental TMCFs (van der Molen et al., 2006). This is particularly important for TMCFs, given the fog's key role in defining their hydrological functioning (Oliveira et al., 2014). For example, the assessment of the fog effects on the canopy-water balance showed that under clear-sky conditions evaporation can increase up to 20% compared to foggy conditions (Chapter 4)

Table 5.1. Description of the hydrological model. This model is constrained by monthly mean rainfall (P), potential evaporation (PE), and soil moisture gains and losses (Sm_{gain} ; Sm_{loss}). For the time-series where fog input estimates (P_{fog}) were available they were also used as input. It estimates through-fall (TF), runoff (RO) and streamflow (Q).

Case 1. Wet canopy	Case 2. Dry canopy	Case 3. P underestimation or PE overestimation
$P-PE = TF$ when $P > PE$	If $P < PE$ then $PE-P = PE_{soil}$	$P-PE = TF$ when $P > PE$
$TF-Sm_{gain} = RO$ when $TF > Sm_{gain}$	$RO=0$	If $TF < Sm_{gain}$ then $RO=0$
$Sm_{loss}+RO = Q$	$Sm_{loss}-PE_{soil} = Q$	$Sm_{loss}=Q$
When there are P_{fog} estimates: $P+P_{fog}-PE=TF$		

According to the Rutter model simulations, this increase in evaporation lead to a more frequently dry canopy, especially at lower elevations. This reduced canopy wetness is expected to result in an increase in the sensible heat flux (Holwerda et al., 2016) and such changes in the partitioning of surface energy fluxes can influence the moisture and heat content of the atmosphere (van der Molen et al., 2006).

From a soil-moisture perspective, several studies indicated that TMCFs' transpiration is not limited by soil moisture during the dry season (Tanaka et al., 2003, Giambelluca et al., 2009, Wallace and McJannet, 2010). However, during the 2015-2016 dry season, likely influenced by the relative strong 2015 El Niño (Jiménez-Muñoz et al., 2016), soil moisture reached minimum values for the three years of observational data. Simulations with the Hydrus-1D model suggest that this severe 16-day dry period potentially reduced soil moisture enough to affect plant transpiration (Chapter 3). Such situation was not detected in the previous mild dry season (2014-2015). Identifying the occurrence of extreme dry seasons is particularly relevant given the reported vulnerability of TMCFs to drought (Oliveira et al., 2014). The simulations also assessed if the organic layers could potentially provide an advantage to sustain plant transpiration under extreme dry conditions. Results indicated that profiles with organic layers had a larger variability in the reduction in transpiration in comparison to profiles without the organic layer. This implies that under severe dry conditions, at least some forest patches would be better suited to cope with these conditions.

5.5. Land-cover change impacts on streamflows

The hydrological interactions between the vegetation and the atmosphere largely determine streamflows. Therefore, land-cover changes resulting either from land use change or natural disturbances lead to changes in streamflows. Under seasonal climates, like the one in the Orinoco River basin, variability in streamflow mainly follows the

precipitation patterns (*e.g.* Holwerda et al., 2016). One important additional cause for seasonal variation in hydrological processes can be leaf shedding from deciduous species (*e.g.* Goldsmith et al., 2011). However, no deciduous species were observed in the study area. An additional cause of contrasting seasonal variation in hydrological processes between different land-covers are the differential physiological controls of transpiration by plant species under water stress conditions (Holwerda et al., 2016; Motzer, 2005). TMCFs' species are highly susceptible to hydraulic failure thus their stomatal behaviour is highly conservative under high vapour pressure deficits (Jane and Green, 1985; Motzer, 2005). Therefore, TMCFs' water use during dry periods will probably be lower than non-TMCF vegetation (*e.g.* sugar cane; Holwerda et al., 2016). Although water use by grasslands compared to that of TMCFs has not been directly assessed, analyses from soil moisture depletion rates during dry spells in both TMCFs and grasslands show that they are both highly variable throughout time (Chapter 2). Nevertheless, water use is not the only hydrological process that is altered by land-cover change. For example, the contrast in water storages between grasslands and forests is key in defining the direction of change following land-cover change. A reduced water storage in grasslands compared to forests explain why streamflows in deforested catchments tend to be larger and have stronger rainfall-streamflow responses than those of forested catchments (Crespo et al., 2011; Roa-García et al., 2011). However, the hydrologic role of the organic layer as a large water-storage compartment has not been previously considered and the results presented here suggest that their removal after slash-and-burn practices could actually play a more relevant role in increasing rainfall-streamflow responses following deforestation, than for example the impact of reduced canopy water storage (Chapter 3). In the case of TMCFs with low fog-water inputs, like the ones found in the studied area (Chapter 4), the decrease in canopy fog interception by deforestation is not expected to be larger than the expected

decrease in interception losses due to deforestation. In addition, fog (at least at the higher elevations) generally follows the rainfall patterns. This implies that additional water input by fog water interception during the dry season are very low. In summary, deforestation of TMCFs likely results in higher rainfall-streamflow responses and even though it could potentially increase streamflows, the reduction in water storage within the catchments would lead to overall drier conditions.

After land abandonment (either grassland or croplands) or natural disturbances, regeneration will take place. However, the regeneration processes can be intentionally interrupted in certain areas due to rotational crop practices that are common in the studied area. This implies that a fairly constant proportion of the catchment is in an early successional stage. Consequently, assessing the restoration of hydrological processes along the multiple regeneration stages is of great interest. In addition, considering land-cover distribution along the elevation range is important. Eighty two percent of old-growth forests are found at the higher elevations (>1900 m asl), whereas most intervened areas are found at the lower elevations (<1900 m asl; secondary forests: 68%, early succession forests: 86%, and grasslands: 92%). Overall, regeneration of TMCFs at the higher and lower elevations will likely gradually reduce rainfall-streamflow responses with an increase in stand age. This assertion is based on a gradual increase in canopy and soil complexity in terms of canopy vertical structure and epiphyte colonization, and organic layer development. However, the latter was not found to be correlated to land-cover probably due to the further influence of slope in the accumulation of organic matter. In parallel, the increase in canopy complexity is also likely to favour fog water interception, especially at the higher elevations. Such higher fog persistence with its effect on reducing evaporation (and also transpiration) will prevent a severe increase in water use as forest recovers. Therefore, water contributions to streamflow are not expected to

decrease as forest recovers at the higher elevations. In contrast, forest recovery at the lower elevations is more likely to increase water use and, consequently, reduce streamflows. In terms of the catchment water budget, the final effects on streamflow will depend on the balance between the hydrological dynamics at higher and lower elevations. Nevertheless, as mentioned before, a forested catchment with a larger water storage will generally be wetter than a deforested catchment. This is also relevant when considering the importance of the upwind land covers to determine fog water inputs.

5.6. Conclusions

Through this research the understanding on TMCs' hydrological functioning in the Orinoco River basin has been improved, allowing to evaluate the land-use and climate-change impacts on their hydrology. More specifically, I present the main conclusions in relation to each of the research questions:

RQ1. From a spatial perspective, TMCs at higher elevations receive larger rainfall inputs and experience lower potential evaporation than the TMCs at lower elevations. Furthermore, the elevation contrasts are enhanced during the dry season and imply that at the higher elevations seasonality is less pronounced than at the lower elevations.

RQ2. Contrasts in canopy and soil water storage (mainly due to the presence/absence of organic layers) between the studied land covers in conjunction with their distribution within the catchments largely define streamflows. For example: a) deforested areas favour higher rainfall-streamflow responses, b) forested areas at the lower elevations have higher evaporation and lower throughfall, thus contributing less to streamflow generation, and c) high elevation forest cover has a lower potential evaporation and has an overall higher fog interception capacity due to a complex canopy and a larger soil water storage, thus, contributing more to streamflow generation.

RQ3. The organic layers represent a large water storage that potentially reduce rainfall-streamflow responses and provide higher water availability for plant water use even in dry seasons.

RQ4. Additional water inputs by fog interception are not particularly significant in terms of sustaining streamflows. However, fog's effect in reducing potential evaporation is highly relevant to sustain canopy and soil moisture conditions. A reduction in the persistence of fog conditions would enhance evaporation up to 20% and thus lead to a decrease in streamflows.



CHAPTER 6

Outlook

Chapter 6

Outlook

6.1. Future Research

This research has provided new information on the hydrological functioning of Tropical Montane Cloud Forests (TMCFs) in the Orinoco, and various approximations on the spatio-temporal variability of the hydrological processes within the catchments. This information further facilitates to parameterize hydrological models useful to acquire insights on the potential land-cover and climate change effects on the water yields of the studied catchments. However, the validation of such models can benefit from a longer time series, especially regarding streamflow measurements. Unfortunately, streamflow measurements were interrupted due to weir damage and a frequent change in the streambed caused by land-slides in all catchments. The applied weir set-up in these highly dynamic environments should be reconsidered. One alternative to explore is to create dummy weirs above the actual measuring weir to function as sediment and boulder deposits, which would have to be subjected to periodical sediment removals. However, there is no guarantee that under extreme events they could prevent sediments from depositing in the measuring weir. Another alternative is to not use weirs but to make use of natural occurring stream channels that create critical flow conditions. In this case, a detailed description of the wetted area and of the streambed along with monitoring changes in these specific features would be required. The advantage of this alternative measurement strategy is that sediments continue their way downstream instead of depositing in the measuring sector as was also corroborated in the intermediate forested catchment. Independent of the chosen alternative methods regarding weir set-up, frequent streamflow measurements by the dilution method are required to rigorously consider uncertainty in flow data of highly dynamic streambeds as suggested by McMillan et al.

(2010). Achieving a suitable streamflow gauging system would enable long term streamflow analyses essential to assess the role of the different processes involved in the hydrological functioning of catchments like those studied in the presented study. Given the integrating character of streamflow data of the multiple spatially variable hydrological processes within the catchment, streamflow recession analysis could provide novel insights on such processes (*e.g.* Kirchner, 2009).

In addition to employing streamflow data to infer the catchment's hydrological processes, an improved data collection setup would be needed to increase the spatial resolution of the moisture distribution along the elevation gradient and record how this gradient shifts throughout the seasons. More ambitiously, such an improved setup should also address the topographical effects on the moisture elevation gradient. With only two automated weather stations it was possible to distinguish first-order differences in the moisture gradient along elevation but a more realistic non-linear relation of meteorological variables with elevation could not be identified (Bendix et al., 2008a). Furthermore, even though geospatial models were employed to infer topographic effects on solar radiation and wind speed conditions, these models require more point measurements to be properly validated. This is particularly relevant in TMCs where it is widely recognized that the fog interception processes are spatially variable and related to topography (Berry et al., 2016; Bruijnzeel et al., 2011b). This brings up the fog measuring issue and its effects on evaporation. The fog gauging method performed very poorly, partly due to poorly sealed connections on the setup and also to its dependence on wind speed (Villegas et al., 2008), being relatively low in the study area. The inferred fog frequency based on fog's effect in reflecting solar radiation and in throughfall data provided first order approximations. However, there is ample space for improvement. On the one hand, fog fluxes can be determined using more direct, albeit expensive and complex, methods such as eddy

covariance (*e.g.* Burkard et al., 2003). In a less sophisticated fashion, vertically distributed weather stations covering from the understory to the turbulent layer over the canopy could provide proxies to the atmospheric conditions under fog influence (*e.g.* Dietz et al., 2007) and better evaporation estimates. On the other hand, more accessible (budget wise) alternatives to quantify fog persistence have been recently proposed, such as the use of time-lapse photography along elevation gradients coupled with meteorological measurements (Bassiouni et al., 2017). Further refinement can lead to more sophisticated algorithms that could allow to extract more information from the photographs on fog characteristics. Under realistic budget limitations it is a major challenge to find an optimal compromise between high detail information from a few, or even single, point measurements or less detailed information with a broader coverage of the catchment's spatial heterogeneity. At the end, an important consideration is that under current land-cover and climate change pressures it is highly relevant to sustain a monitoring setup capable of recording long term data to detect changes in fog persistence and quantifying the effects of these changes on TMCF hydrological processes.

There should also be enough attention for below-ground hydrological processes, which are also highly relevant as was demonstrated in this study. Ground water monitoring coupled with a more detailed distribution of soil depth and soil texture variability with depth enable the use of 2D and 3D water flow modelling systems. This should result in a more realistic representation of the soil water flow. Furthermore, water use by the different land cover types being present within the catchments was approximated by the potential evapotranspiration estimated through the Penman-Monteith model included in the Hydrus-1D software and constrained by default values commonly applied for reference land cover types that do not necessarily represent TMCFs' conditions. Consequently, direct measurements of plant water use, such as sap flow measurements

(*e.g.* Eller et al., 2015) could improve our knowledge on the soil-vegetation-atmosphere interactions and how they respond to extreme drought conditions.

From a broader perspective, in Chapter 2 the potential influence of the unique upwind moisture conditions of the seasonally flooded savannahs on the observed seasonal hydro-meteorological patterns at the TCMF elevation gradient was discussed. The observations from TCMFs on the Orinoco River basin were compared to those measured for other TCMFs located further south in the eastern Andes downwind of Amazon forests. However, much more research is required to understand the extent to which these contrasting upwind conditions determine seasonal shifts in the cloud condensation level of eastern Andean TCMFs, and how potential upwind land-cover changes in the lowlands can affect fog persistence in TCMFs. To gain better insight on the potential lowland-mountain ecosystem feedbacks, hydro-meteorological data is needed. According to my knowledge there is no hydro-meteorological data available from the seasonally flooded savannahs. A first approach could rely on the application of other data sources derived from remotely sensed data. With these data, it is feasible to explore, through regional modelling experiments, the influence of the lowlands seasonality on the regional climate including the TCMFs' downwind areas. For example, this approach was used for analysing the effect of seasonal Sudanese wetlands in the Nile River basin climatology (Mohamed et al., 2006). The results from such a modelling exercise should provide basic information to define the further research direction. Hopefully, such more detailed and improved follow-up studies will be conducted before the Orinoco River basin seasonally flooded savannahs are modified by the ambitious National plans to transform this natural ecosystem into a major biofuel crop area (Pardo-Vargas et al., 2015).

6.2. Connecting with decision-making processes

In the synthesis the potential land-cover and climate-change impacts on TCMF hydrological functioning were discussed. Some of these impacts can be mitigated by local or regional policies, whereas others are outside of the local/regional decision making scope. If these latter impacts are not addressed nationally or internationally, they should be adapted to, coped with or simply accepted. This thesis research was motivated by the desire to close knowledge gaps to improve decision-making processes. As a first contribution to do so, I present a diagram with the potential actions that can be undertaken by different decision-making levels regarding land-use and climate change and their expected effects in TCMFs' conservation (Figure 6.1). For example, the hydro-meteorological and ecological monitoring along this specific elevation range is crucial to track and better understand the intra-annual seasonal variability, the long-term successional dynamics and the already noticed changes in climate and its consequences. Given that the climate-change projections for the area depict a more pronounced seasonality, local administrations should soon reinforce both their flooding and fire control strategies, and consider potential impacts on agricultural and livestock production. Additional information, on which the diagram (Figure 6.1) is based, was mainly derived from a better understanding of the historic drivers of land-use change and their evolution through time. By understanding the drivers that have modulated people's relation with the forests it is possible to identify the consequences of those changing relations on forest cover and to assess the deforestation risks in the study area. To do so, historical land-cover change was analysed through Landsat imagery from the 1980's till 2015 (Quintana-Linares, 2017), conducting a quantitative and qualitative analysis on proximate or direct and underlying causes of change (following Geist and Lambin, 2002). In an MSc thesis study by Quintana-Linares (2017, being conducted under my supervision), a geostatistic

approach was used to address the proximate deforestation causes and interviews were used to identify the underlying causes. This resulted in a time-line of key events that modified people's land-use practices. Results showed that recent deforestation rates in Chámeza varied over time. Among the main proximate drivers of change were soil type, slopes and distance from urban centres and roads. People preferred to use flatter and more accessible areas and to conserve forests in steeper inaccessible areas. This corresponds to the findings of Sandel and Svenning (2013) of worldwide patterns of deforestation in mountainous terrains.

The main underlying driver that induced forest recovery was violence derived from the internal armed conflict in Colombia. In contrast to other Colombian regions, peace was established by the military forces around 2003. Thus, this analysis on the main drivers of deforestation for this municipality already includes a post-conflict scenario that has lasted for over a decade. Before the conflict resulted in the displacement of people around 1998, deforestation rates were higher than forest recovery rates. Once the conflict threatened people's lives, forcing them to first abandon the rural areas and then the municipality, forest recovery rates became larger than deforestation rates. As soon as the conflict ended the pattern reversed. However, recent trends suggest a reduced deforestation. When interviewees were asked about the future of forests, they all agreed that the forest-colonization interests were already declining before the conflict reached Chámeza, and now very few people are willing to go through the efforts and investments of colonizing remote mountains. In fact, one of the limitations of such colonization is the lack of manual labour. This lack is partly caused by the displacement or forced recruitment of young people by illegal armed groups, and partly due to the global trend of lack of interest by young adults in sustaining a rural lifestyle (White, 2012). Furthermore, current fruit crops and cattle ranching subsidies involve clear rules that forbid beneficiaries to cut down

forests. Nevertheless, many land owners still have large extents of forests from which they would gain more profits if they were grasslands. However, through the more widespread media reach, they learned about payments for ecosystem services, and stories about big companies interested in buying forested areas. Nevertheless, there is little in-depth understanding of how these opportunities work. As land owners are becoming older and younger generations are less keen in rural life styles, the risk of a turnover in land-ownership are apparent. The current peace situation, along with structural infrastructure improvements (*i.e.* the pavement of the main road) likely attract new investors interested in buying (forest) land. If policies on deforestation are ambiguous, if successors are absent or exploitation is difficult, unnecessary risks emerge when the protection of forests is left in the hands of new investors (*e.g.* Humphries, 1998).

The implementation of a conservation policy can combine restrictions on deforestation with the promotion of alternative uses to provide additional benefits to forest-land owners, similar to the conservation policies implemented in Costa Rica (Calvo-Alvarado et al., 2009). This can change the current, rather indifferent view they have on forests. For example, environmental compensations from infrastructure projects or water use by oil companies in the Cusiana River basin, or carbon and biodiversity conservation markets can be used to implement conservation agreements or to fund the transition from traditional practices, such as the slash and burn, to increased productivity of already deforested areas. The implementation of such conservation agreements also rely on the evidence provided on the key hydrological role of these TMCFs and of their vulnerability to climate and land-use changes. Even smaller enterprises that address to some extent these aspects on the causes and consequences for local environmental change, like the implementation of this research project, has affected the way people perceive forests. The seemingly ‘inexplicable’ interests of outsiders on the local forest ignited their curiosity

on the potential use that these forests have, not only as water regulators but also as income generators. Throughout the project over eighteen local inhabitants (men and women) have been employed and small leasing fees for the grassland areas occupied by the monitoring setups were paid. The project received more than 100 visitors, who required services for food, board, transportation and field guides. Furthermore I have participated in municipal events, like the peace week and the farmer's day, and attended annual meetings with the municipal council to share the results and insights that resulted from this research. Thus, such scientific research project can indeed not only play a key role as knowledge generator but also serves to introduce and enhance awareness about these aspects of land-use decisions and consequences for the environment, as well as to be in itself an alternative conservation strategy.

From a regional policy perspective, the local municipal administrations responsible for the management of the landscapes that contain TMCFs have to press for the departmental and national government and the regional environmental authorities to recognize the key role these forests play in local and regional scale water regulation. This should also include the potential vulnerability of these forest to changes in the upwind (seasonally flooded) savannahs, regional climates and local land use that all alter the hydrologic regimes (Figure 6.1). Any prospects to promote the afforestation of the savannahs and/or draining them has potentially serious consequences for downwind ecosystems, especially through the effects on streamflow during the dry season.

Also, plans to explore and exploit oil in the area exist but they are currently suspended due to the current low international oil prices. Such plans are authorized nationally but require recommendations from regional environmental authorities. These recommendations should explicitly consider the consequences for environmental services provided by these forests that will be threatened by deforestation for infrastructure and

by indirect socio-economic impacts (i.e. increases in population, employment and income; Viña and Cavelier, 1999). Understanding the role of the forests, assessing their vulnerabilities and evaluating the impacts of land-use plans require good monitoring networks, environmental datasets, integrated modelling approaches and future scenarios. This strongly stresses the importance of research activities like those explored in this PhD project

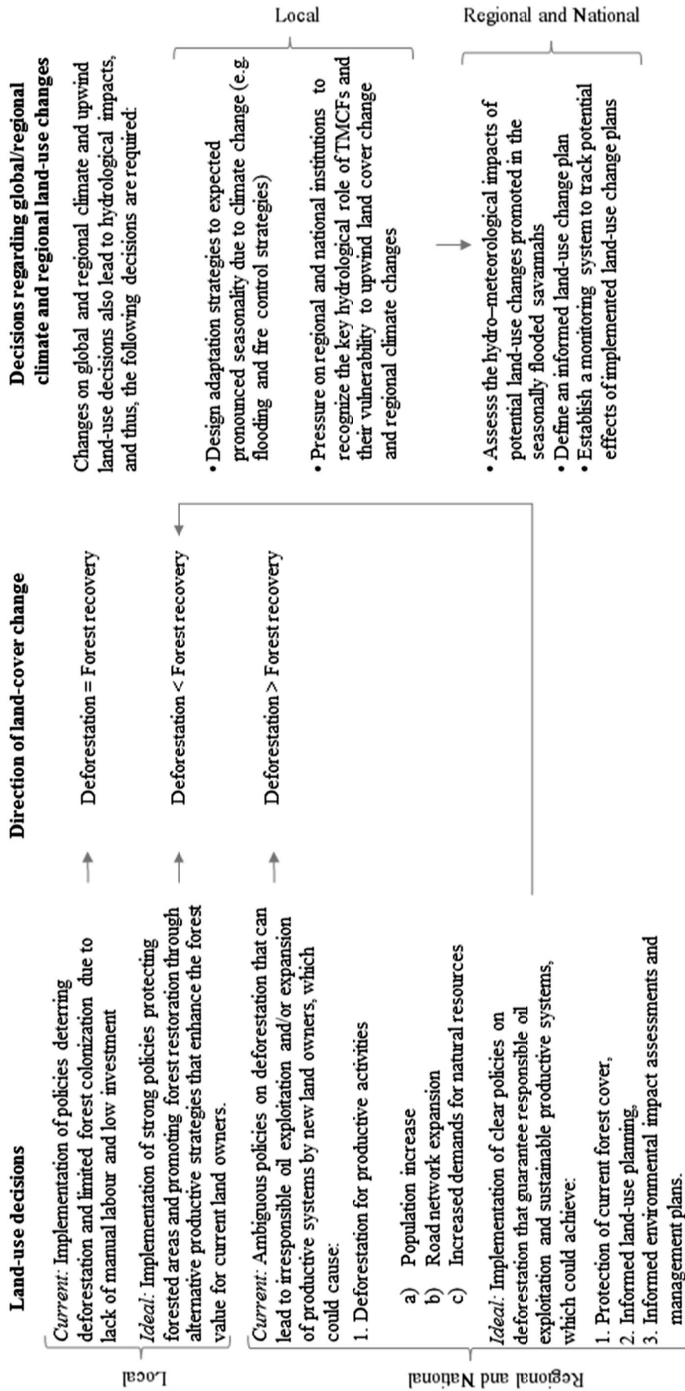


Figure 6.1. Diagram illustrating how land-use and climate-change related decisions, from the local to the national level, determine TMCFs' conservation and hydrological impacts. The diagram is divided horizontally into current and ideal land-use decisions (on the left), the consequent direction of land-cover change (the middle), and decisions on global/regional climate and regional land-use change (on the right). Vertically each section is divided into local and regional/national decisions

Summary

This thesis was framed within the increasing concern on water availability and in the belief that proper land-use management decisions and climate change adaptation plans can only be effective if they have a clear scientific basis. Therefore, this thesis aimed to improve our understanding on the hydrological functioning of Tropical Montane Cloud Forests (TMCFs) in the unique setting of the seasonal Orinoco River basin headwaters located in the Colombian eastern Andes. This understanding is fundamental to evaluate the impact of land-use and climate changes on TMCFs' hydrology. Despite that hydrological processes largely depend on specific site conditions, the findings of this research are not only relevant for the specific study site, but also to broaden our knowledge regarding key processes in other TMCFs. Furthermore, along the development of this research different methodological approaches were employed. These approaches were suitable to confront common logistic challenges in complex environments such as TMCFs. To accomplish the research aim, a hydro-meteorological monitoring system was set up in 2013. This system covered three headwater TMCF catchments with contrasting land covers. The observational data that were collected, were analysed and used to parameterize a model to address the following research questions (RQs):

- RQ1. What is the hydro-meteorological spatio-temporal variability in the three neighbouring catchments with different forest covers?
- RQ2. To what extent can variations in streamflow between catchments be explained by the differences in forest cover?
- RQ3. What is the hydrological role of TMCFs' organic layers in water storage and release under land-use and climate changes?
- RQ4. What is the role of fog presence and interception on the canopy water balance on three successional TMCFs' regeneration stages?

In the introduction (Chapter 1) the scientific and socio-environmental context in which this research took place was provided. The main objective and the research questions of this PhD study were addressed in chapters 2-4. Chapter 2 described the observed spatial and temporal variability in hydro-meteorological variables (RQ1) and provided a detailed analysis of the corresponding hydrological responses of soil moisture and streamflow in three neighbouring catchments with contrasting land cover (RQ2). The uncertainties associated with these RQs, their methods and setups were also assessed. Results revealed a positive relation of fog/rainfall with elevation that became more pronounced during the dry season. Therefore, hydrological responses were modulated by the interaction of land cover and elevation. During the wet season the deforested catchment had higher rainfall-streamflow responses compared to the catchments with larger forest covers. During the dry season the catchments' elevation distribution largely determined streamflow values, caused by a larger contribution to streamflow from the higher elevations. Overall, results also evidenced a missing water source that could be potentially related to the contribution of soil water storages to streamflow and/or to the unquantified water inputs by fog.

In Chapter 3 the role of the organic layer in TCMF water storage for different land-cover and climate conditions (RQ3) was assessed by combining field and laboratory data with modelling. First, the organic layer water retention curves were determined from field samples and the water retention curves for mineral soils were estimated from texture data. This allowed to quantify the storage capacity of the organic and mineral layers and assess the potential land-use and climate change impacts on TCMFs' soil moisture dynamics. From the land-use change perspective, the water storage capacity loss by slash-and-burn deforestation practices was estimated. These estimates show that the storage loss ranges from 35 to 59 mm when TCMFs are converted to pastures. This is an order of magnitude larger than the estimated TCMFs' canopy storage capacity (2 to 5 mm). Therefore, the

higher peak flow observations in deforested catchments might not only be explained by a decreasing canopy water storage capacity but also likely due to a decreasing soil water storage. From the climate change perspective, the effect of contrasting dry season conditions on soil moisture and transpiration were evaluated using the Hydrus 1-D water-flow model. Also, the sensitivity of these hydrological variables to uncertainties in saturated hydraulic conductivity were assessed. Although transpiration was not limited by soil moisture during the mild dry season, it was affected during the severe dry season and continued to decline under the expected prolongation of dry spells due to climate change. The results highlighted the key role of the organic layer in TMCFs' hydrological functioning and call for an increased focus on the role of organic soils when evaluating effects of land-use and climate changes on TMCFs' hydrology.

In Chapter 4, fog's effect on the canopy water budget of three TMCF successional stages (RQ4) was assessed by combining hydro-meteorological data on a high temporal resolution (*i.e.* 10 minutes) with modelling. This approach allowed to quantify the fog effects on the canopy-water balance. More specifically, the fog effects in reducing evaporation and in enhancing water inputs through fog interception by the canopy were addressed during fog events without rainfall and during foggy rainfall events. Simulation results indicated that fog can reduce evaporation by up to 20%. In addition, the forest canopy at the high elevations seldom reach dry canopy conditions, whereas these are more common at the low elevation forests. Differences in dry canopy frequencies likely also translate into a different energy partitioning in latent and sensible heat. Furthermore, fog water input estimates during fog-only events, even though higher at the higher elevation, are probably insignificant (from 0.8% to 1.6% of measured rainfall), but this input of fog water can become more relevant during foggy rainfall events (from 5.8% to 12.8% of measured rainfall). Additional to the fog trends along the elevation gradient, variable fog-

vegetation interactions were controlled by differences in canopy water storages as a function of forest cover. Each evaluated process has associated uncertainties, which together cumulatively explain why closing a water budget in TMCF catchments is limited by data collection methods that probably do not capture all relevant fog effects. In addition, this study indicated that the temporal resolution of measured rainfall and through-fall, combined with the compensating effects of canopy parameters estimated by the Rutter canopy-rainfall interception model, pose an additional challenge to understand and quantify the role of fog inputs in TMCFs' water budgets.

In Chapter 5 the results from the individual chapters were integrated to improve the understanding on TMCFs' hydrological functioning and the hydrological impacts of land-use and climate changes. In Chapter 6, the main challenges to further develop the monitoring system that was used in this research were discussed. This chapter finalizes with suggestions on how the outcomes of this thesis, coupled with preliminary analyses on the main land-use change drivers in the recent past, can be used to provide scientific support to decision-making processes on resource governance and climate-change adaptation plans under the study area's socio-environmental context.

References

- Ah-Peng, C., Williamson-Cardoso, A., Flores, O., West, A., Wilding, N., Strasberg, D., Hedderson, T.A.J., 2017. The role of epiphytic bryophytes in interception, storage, and the regulated release of atmospheric moisture in a tropical montane cloud forest. *J. Hydrol.*, 548, 665–673.
- Alkama, R., Cescatti, A., 2016. Biophysical climate impacts of recent changes in global forest cover. *Science*, 351, 600–604.
- Alpert, P., 1986. Mesoscale indexing of the distribution of orographic precipitation over high mountains. *J. Clim. Appl. Meteorol.*, 25, 532–545
- Anderson-Teixeira, K.J., Snyder, P.K., Twine, T.E., Cuadra, S. V., Costa, M.H., DeLucia, E.H., 2012. Climate-regulation services of natural and agricultural ecoregions of the Americas. *Nat. Clim. Chang.*, 2, 77–181.
- Andréassian, V., 2004. Waters and forests: from historical controversy to scientific debate. *J. Hydrol.*, 291, 1–27.
- Arriaga, F.J., Lowery, B., Mays, M.D., 2006. A fast method for determining soil particle size distribution using a laser instrument. *Soil Sci.*, 171, 663–674.
- Balthazar, V., Vanacker, V., Molina, A., Lambin, E.F., 2015. Impacts of forest cover change on ecosystem services in high Andean mountains. *Ecol. Indic.*, 48, 63–75.
- Bassiouni, M., Scholl, M.A., Torres-Sanchez, A.J., Murphy, S.F., 2017. A method for quantifying cloud immersion in a tropical mountain forest using time-lapse photography. *Agric. For. Meteorol.*, 243, 100–112.
- Beckers, E., Pichault, M., Pansak, W., Degré, A., Garré, S., 2016. Characterization of stony soils' hydraulic conductivity using laboratory and numerical experiments. *Soil*, 2, 421–431.
- Bendix, J., Rollenbeck, R., Richter, M., Fabian, P., Emck, P., 2008a. Climate, In: Beck, E., Bendix, J., Kottke, I., Makeschin, F., Mosandl, R., Gradients in a tropical mountain ecosystem of Ecuador. Springer, Berlin Heidelberg, pp. 63–74
- Bendix, J., Rollenbeck, R., Fabian, P., Emck, P., Richter, M., Beck, E., 2008b. Climate Variability: temporal heterogeneities, In: Beck, E., Bendix, J., Kottke, I., Makeschin, F., Mosandl, R. (Eds.), Gradients in a Tropical Mountain Ecosystem of Ecuador, Ecological Studies. Springer Berlin Heidelberg, Berlin, Heidelberg, pp. 281–290.
- Benner, J., Vitousek, P.M., Ostertag, R., 2010. Nutrient cycling and nutrient limitation in tropical montane cloud forests. In: Bruijnzeel, L.A., Scatena, F.N., Hamilton, L.S. (Eds.), Tropical Montane Cloud Forests. Cambridge University Press, Cambridge, pp. 90–100
- Beniston, M., 2003. Climatic Change in Mountain Regions: A Review of Possible Impacts. *Clim. Chang.*, 59, 5–31.
- Berry, Z.C., Gotsch, S.G., Holwerda, F., Muñoz-Villers, L.E., Asbjornsen, H., 2016. Slope position influences vegetation-atmosphere interactions in a tropical montane cloud forest. *Agric. For. Meteorol.*, 221, 207–218.
- Beven, K., Germann, P., 1982. Macropores and water flow in soils. *Water Resour. Res.*, 18, 1311–1325.

- Bockheim, J.G., Gennadiyev, A.N., 2000. The role of soil-forming processes in the definition of taxa in Soil Taxonomy and the World Soil Reference Base. *Geoderma*, 95, 53–72.
- Bogner, C., Engelhardt, S., Zeilinger, J., Huwe, B. 2008. Visualization and analysis of flow patterns and water flow simulations in disturbed and undisturbed tropical soils. In: Beck, E., Bendix, J., Kottke, I., Makeschin, F., Mosandl, R., Gradients in a tropical mountain ecosystem of Ecuador. Springer, Berlin Heidelberg, pp. 387–396.
- Böhner, J., Antonic, O., 2009. Land-Surface Parameters Specific to Topo-Climatology. In T. Hengl, & H. I. Reuter (Eds.), *Geomorphometry: Concepts, Software, Applications*, pp. 195–226. Elsevier Science.
- Bonan, G.B., 2008. Forests and climate change: forcings, feedbacks, and the climate benefits of forests. *Science*, 320, 1444–1449.
- Bonell, M., 2005. Runoff generation in tropical forests. In: Bonell, M., Bruijnzeel, L.A., (Eds.), *Forests, water and people in the humid tropics: past, present and future hydrological research for integrated land and water management*. Cambridge University Press, Cambridge, pp. 314–406.
- Bonell, M., 2010. The impacts of global change in the humid tropics: selected rainfall-runoff issues linked with tropical forest-land management. *Irrig. Drain. Syst.*, 24, 279–325.
- Bos, M.G., 1989. *Discharge measurement structures*, Third ed. International Institute for Land reclamation and Improvement, Wageningen.
- Brauman, K.A., Freyberg, D.L., Daily, G.C., 2010. Forest structure influences on rainfall partitioning and cloud interception: A comparison of native forest sites in Kona, Hawai'i. *Agr. Forest. Meteorol.*, 150, 265–275.
- Brown, S., Lugo, A.E., 1990. Tropical secondary forests. *J. Trop. Ecol.*, 6, 1–32.
- Brown, A.E., Zhang, L., McMahon, T.A., Western, A.W., Vertessy, R.A., 2005. A review of paired catchment studies for determining changes in water yield resulting from alterations in vegetation. *J. Hydrol.*, 310, 28–61.
- Bruijnzeel, L.A. (Ed), 2006. *Hydrological impacts of converting tropical montane cloud forest to pasture, with initial reference to northern Costa Rica*. Final technical report for project R7991, DFID Forestry research programme. Amsterdam, The Netherlands: VU University Amsterdam.
- Bruijnzeel, L.A., 1989. Forestation and dry season flow in the tropics: A closer look. *J. Trop. For. Sci.*, 3, 229–243
- Bruijnzeel, L.A., 2001. Hydrology of tropical montane cloud forests: a reassessment. L. use water. *Resour. Res.*, 1, 1–18.
- Bruijnzeel, L.A., 2004. Hydrological functions of tropical forests: not seeing the soil for the trees? *Agric. Ecosyst. Environ.*, 104, 185–228
- Bruijnzeel, L.A., Eugster, W., Burkard, R., 2006. Fog as a hydrologic input. *Encyclopedia of hydrological sciences*. John Wiley & Sons. Chapter 38, 559–582.
- Bruijnzeel, L.A., Kappelle, M., Mulligan, M., Scatena, F.N., 2011a. Tropical montane cloud forests: state of knowledge and sustainability perspectives in a changing world. In: Bruijnzeel, L.A., Scatena, F.N., Hamilton, L.S. (Eds.), *Tropical Montane Cloud Forests*. Cambridge University Press, Cambridge, pp. 691–740.

- Bruijnzeel, L.A., Mulligan, M., Scatena, F.N., 2011b. Hydrometeorology of tropical montane cloud forests: emerging patterns. *Hydrol. Process.*, 25, 465–498.
- Bruijnzeel, L.A., Veneklaas, E.J., 1998. Climatic conditions and tropical montane forest productivity: the fog has not lifted yet. *Ecology*, 79, 3–9.
- Burkard, R., Bützberger, P., Eugster, W., 2003. Vertical fogwater flux measurements above an elevated forest canopy at the Lägeren research site, Switzerland. *Atmos. Environ.*, 37, 2979–2990.
- Bussmann, R.W., Wilcke, W., Richter, M., 2008. Landslides as Important Disturbance Regimes — Causes and Regeneration. In: Beck, E., Bendix, J., Kottke, I., Makeschin, F., Mosandl, R., Gradients in a tropical mountain ecosystem of Ecuador. Springer, Berlin Heidelberg, pp. 319–330.
- Buytaert, W., Cuesta-Camacho, F., Tobón, C., 2011. Potential impacts of climate change on the environmental services of humid tropical alpine regions. *Glob. Ecol. Biogeogr.*, 20, 19–33.
- Calder, I.R., 1977. A model of transpiration and interception loss from a spruce forest in Plynlimon, central Wales. *J. Hydrol.*, 33, 247–265.
- Calder, I.R., 2002. Forests and hydrological services: reconciling public and science perceptions. *Land use and water resources research*, 2, 1–12.
- Calder, I.R., 2007. Forests and water-Ensuring forest benefits outweigh water costs. *For. Ecol. Manage.*, 251, 110–120.
- Calvo-Alvarado, J., McLennan, B., Sánchez-Azofeifa, A., Garvin, T., 2009. Deforestation and forest restoration in Guanacaste, Costa Rica: Putting conservation policies in context. *Forest Ecol. Manag.*, 258, 931–940.
- Campbell, C.S., Campbell, G.S., Cobos, D.R., Bissey, L.L., 2009. Calibration and evaluation of an improved low-cost soil moisture sensor. Available at: [Http://Www.Decagon.Com/Education/Calibration-and-Evaluation-of-an-Improved-Low-Cost-Soil-Moisture-Sensor-13492-01-an/](http://www.decagon.com/education/calibration-and-evaluation-of-an-improved-low-cost-soil-moisture-sensor-13492-01-an/) 1–13.
- Célleri, R., Feyen, J., 2009. The Hydrology of Tropical Andean Ecosystems: Importance, Knowledge Status, and Perspectives. *Mt. Res. Dev.* 29, 350–355.
- Chambers, J.M., Cleveland, W.S., Kleiner, B., 1983. Graphical methods for data analysis. Belmont, Wadsworth International Group.
- Chaves, J., Neill, C., Germer, S., 2008. Land management impacts on runoff sources in small Amazon watersheds. *Hydrol.*, 12, 1099–1085.
- Chu, H.S., Chang, S.C., Klemm, O., Lai, C.W., Lin, Y.Z., Wu, C.C., Lin, J.Y., Jiang, J.Y., Chen, J., Gottgens, J.F., Hsia, Y.J., 2014. Does canopy wetness matter? Evapotranspiration from a subtropical montane cloud forest in Taiwan. *Hydrol. Process.* 28, 1190–1214.
- Clark, D.B., 1996. Abolishing virginity. *J. Trop. Ecol.*, 12, 735–739.
- Clark, K.E., Torres, M.A., West, A.J., Hilton, R.G., New, M., Horwath, A.B., Fisher, J.B., Rapp, J.M., Robles Caeres, A., Malhi, Y., 2014. The hydrological regime of a forested tropical Andean catchment. *Hydrol. Earth Syst. Sci.* 18, 5377–5397.
- Cong, Z., Lü, H., Ni, G., 2014. A simplified dynamic method for field capacity estimation and its parameter analysis. *Water Sci. Eng.* 7, 351–362.

- Conrad, O., Bechtel, B., Bock, M., Dietrich, H., Fischer, E., Gerlitz, L., Wehberg, J., Wichmann, V., Böhner, J., 2015. System for Automated Geoscientific Analyses (SAGA) v. 2.1.4, *Geosci. Model Dev.*, 8, 1991–2007.
- Corripio, J. G., 2003. Vectorial algebra algorithms for calculating terrain parameters from DEMs and the position of the sun for solar radiation modelling in mountainous terrain. *Int. J. Geogr. Inf. Sci.*, 17, 1–23.
- Crespo, P.J., Feyen, J., Buytaert, W., Bücker, A., Breuer, L., Frede, H.-G., Ramírez, M., 2011. Identifying controls of the rainfall–runoff response of small catchments in the tropical Andes (Ecuador). *J. Hydrol.*, 407, 164–174.
- Crockford, R.H., Richardson, D.P., 2000. Partitioning of rainfall into through-fall, stemflow and interception: effect of forest type, ground cover and climate. *Hydrol. Process.*, 14, 2903–2920.
- Dane, J.H., Hopmans, J.W., 2002. Water retention and storage. In: Dane, J.H., Topp, G.C., Madison, W., Davidson, R. (Eds.), *Methods of Soil Analysis. Part 4. SSSA*, pp. 671–673.
- DeFries, R., Eshleman, K.N., 2004. Land-use change and hydrologic processes: a major focus for the future. *Hydrol. Process*, 18, 2183–2186.
- Dietz, J., Leuschner, C., Hölscher, D., Kreilein, H., 2007. Vertical patterns and duration of surface wetness in an old-growth tropical montane forest, Indonesia. *Flora*, 202, 111–117
- Donatelli, M., Carlini, L., Bellocchi, G., 2006. A software component for estimating solar radiation. *Environ. Model. Softw.*, 21, 411–416.
- Dunne, K.A., Willmott, C.J., 1996. Global Distribution of Plant-extractable Water Capacity of Soil. *Int. J. Climatol.*, 16, 841–859.
- Durack, P.J., Wijffels, S.E., Matear, R.J., 2012. Ocean salinities reveal strong global water cycle intensification during 1950 to 2000. *Science*, 336, 455–458.
- Eller, C.B., Burgess, S.S.O., Oliveira, R.S., 2015. Environmental controls in the water use patterns of a tropical cloud forest tree species, *Drimys brasiliensis* (Winteraceae). *Tree Physiol.*, 35, 387–399.
- Eller, C.B., Lima, A.L., Oliveira, R.S., 2013. Foliar uptake of fog water and transport belowground alleviates drought effects in the cloud forest tree species, *Drimys brasiliensis* (Winteraceae). *New Phytol.*, 199, 151–162.
- Ellison, D., Futter, M.N., Bishop, K., 2012. On the forest cover-water yield debate: From demand- to supply-side thinking. *Glob. Chang. Biol.*, 18, 806–820.
- Ellison, D., Morris, C.E., Locatelli, B., Sheil, D., Cohen, J., Murdiyarso, D., Gutierrez, V., Van Noordwijk, M., Creed, I.F., Pokorny, J. and Gaveau, D., 2017. Trees, forests and water: Cool insights for a hot world. *Glob. Environ. Chang.*, 43, 51–61.
- Emck, P., 2007. A climatology of south Ecuador-with special focus on the major Andean ridge as Atlantic-Pacific climate divide. PhD Thesis. Friedrich-Alexander-Universität Erlangen-Nürnberg (FAU), Naturwissenschaftliche Fakultät.

- Esquivel-Muelbert, A., Baker, T.R., Dexter, K., Lewis, S.L., Steege, H. ter, Lopez-Gonzalez, G., Mendoza, A.M., Brienen, R., Feldpausch, T.R., Pitman, N., Alonso, A., van der Heijden, G., Peña-Claros, M., Ahuite, M., Alexiades, M., Dávila, E.Á., Murakami, A.A., Arroyo, L., Aulestia, M., Balslev, H., Barroso, J., Boot, R., Cano, A., Moscoso, V.C., Comiskey, J., Dallmeier, F., Daly, D., Dávila, N., Duivenvoorden, J., Montoya, A.J.D., Erwin, T., Fiore, A. Di, Fredericksen, T., Fuentes, A., García-Villacorta, R., Gonzales, T., Guevara, J.E.A., Coronado, E.N.H., Huamantupa-Chuquimaco, I., Killeen, T., Malhi, Y., Mendoza, C., Mogollón, H., Jørgensen, P.M., Montero, J.C., Mostacedo, B., Nauray, W., Neill, D., Vargas, P.N., Palacios, S., Cuenca, W.P., Camacho, N.C.P., Peacock, J., Phillips, J.F., Pickavance, G., Quesada, C.A., Ramírez-Angulo, H., Restrepo, Z., Rodriguez, C.R., Paredes, M.R., Sierra, R., Silveira, M., Stevenson, P., Stropp, J., Terborgh, J., Tirado, M., Toledo, M., Torres-Lezama, A., Umaña, M.N., Urrego, L.E., Martinez, R.V., Gamarra, L.V., Vela, C., Torre, E.V., Vos, V., von Hildebrand, P., Vriesendorp, C., Wang, O., Young, K.R., Zartman, C.E., Phillips, O.L., Cornejo, F., 2016. Seasonal drought limits tree species across the Neotropics. *Ecography*, 40, 618-629.
- Feddes, R.A., Kowalik, P., Kolinska-Malinka, K., Zaradny, H., 1976. Simulation of field water uptake by plants using a soil water dependent root extraction function. *J. Hydrol.*, 31, 13-26.
- Fleischbein, K., Wilcke, W., Goller, R., Boy, J., Valarezo, C., Zech, W., Knoblich, K., 2005. Rainfall interception in a lower montane forest in Ecuador: effects of canopy properties. *Hydrol. Process.*, 19, 1355-1371.
- Fodor, N., Sándor, R., Orfanus, T., Lichner, L., Rajkai, K., 2011. Evaluation method dependency of measured saturated hydraulic conductivity. *Geoderma*, 165, 60-68.
- Førland, E., Hanssen-Bauer, I., 1996. Manual for operational correction of Nordic precipitation data. Norwegian Meteorol. Inst. Report 24/96 KLIMA, p. 66.
- Frahm, J.-P., Gradstein, S.R., 1991. An Altitudinal Zonation of Tropical Rain Forests Using Byrophytes. *J. Biogeogr.*, 18, 669-678.
- Frumau, K.F., Burkard, R., Schmid, S., Bruijnzeel, L.A., Tobón, C., Calvo-Alvarado, J.C., 2011. A comparison of the performance of three types of passive fog gauges under conditions of wind-driven fog and precipitation. *Hydrol. Process.*, 25, 374-383.
- Gash, J.H.C., 1979. An analytical model of rainfall interception by forests. *Q. J. Roy. Meteor. Soc.*, 105, 43-55.
- Gash, J.H.C., Lloyd, C.R., Lachaud, G., 1995. Estimating sparse forest rainfall interception with an analytical model. *J. Hydrol.*, 170, 79-86.
- Gash, J.H.C., Wright, I.R., Lloyd, C.R., 1980. Comparative estimates of interception loss from three coniferous forests in Great Britain. *J. Hydrol.*, 48, 89-105.
- Geist, H. J., Lambin, E. F., 2002. Proximate Causes and Underlying Driving Forces of Tropical Deforestation. *BioScience*, 52, 143.
- Gentry, A.H., 1988. Changes in plant community diversity and floristic composition on environmental and geographical gradients. *Ann. Mo. Bot. Gard.*, 75, 1-34.

- Gerold, G., Schawe, M., Bach, K., 2008. Hydrometeorologic, pedologic and vegetation patterns along an elevational transect in the montane forest of the Bolivian Yungas. *Die Erde.*, 139, 141–168.
- Ghimire, C.P., Bruijnzeel, L.A., Lubczynski, M.W., Bonell, M., 2014. Negative trade-off between changes in vegetation water use and infiltration recovery after reforestation degraded pasture land in the Nepalese Lesser Himalaya. *Hydrol. Earth Syst. Sci.* 18, 4933–4949.
- Giambelluca, T.W., DeLay, J.K., Nullet, M.A., Scholl, M.A. and Gingerich, S.B., 2011. Canopy water balance of windward and leeward Hawaiian cloud forests on Haleakalā, Maui, Hawai'i. *Hydrol. Process.*, 25, 438–447.
- Giambelluca, T.W., Gerold, G., 2011. Hydrology and Biogeochemistry of Tropical Montane Cloud Forests, In: Levia, D.F., Carlyle-Moses, D., Tanaka, T. (Eds.), *Forest Hydrology and Biogeochemistry, Ecological Studies*. Springer Netherlands, Dordrecht, pp. 221–259.
- Giambelluca, T.W., Martin, R.E., Asner, G.P., Huang, M., Mudd, R.G., Nullet, M.A., DeLay, J.K., Foote, D., 2009. Evapotranspiration and energy balance of native wet montane cloud forest in Hawai'i. *Agric. For. Meteorol.* 149, 230–243.
- Girardin, C.A.J., Malhi, Y., Aragão, L.E.O.C., Mamani, M., Huaraca-Huasco, W., Durand, L., Feeley, K.J., Rapp, J., Silvia-Espejo, J.E., Silman, M., Salinas, N., Whittaker, R.J., 2010. Net primary productivity allocation and cycling of carbon along a tropical forest elevational transect in the Peruvian Andes. *Glob. Chang. Biol.*, 16, 3176–3192.
- Goldsmith, G.R., Matzke, N.J., Dawson, T.E., 2013. The incidence and implications of clouds for cloud forest plant water relations. *Ecol. Lett.*, 16, 307–314.
- Gómez-Peralta, D., Oberbauer, S.F., McClain, M.E., Philippi, T.E., 2008. Rainfall and cloud-water interception in tropical montane forests in the eastern Andes of Central Peru. *Forest Ecol. Manag.*, 255, 1315–1325.
- Gotsch, S.G., Asbjornsen, H., Holwerda, F., Goldsmith, G.R., Weintraub, A.E., Dawson, T.E., 2014. Foggy days and dry nights determine crown-level water balance in a seasonal tropical montane cloud forest. *Plant, Cell Environ.*, 37, 261–272.
- Grayson, R.B., Western, A.W., Chiew, F.H., Blöschl, G., 1997. Preferred states in spatial soil moisture patterns: Local and nonlocal controls. *Water Resour. Res.*, 33, 2897–2908.
- Grieve, I.C., Proctor, J., Cousins, S.A., 1990. Soil variation with altitude on Volcan Barva, Costa Rica. *CATENA*, 17, 525–534.
- Grubb, P., 1977. Control of forest growth and distribution on wet tropical mountains: with special reference to mineral nutrition. *Annu. Rev. Ecol. Syst.*, 8, 83–107
- Guillod, B.P., Orlowsky, B., Miralles, D., Teuling, A.J., Blanken, P.D., Buchmann, N., Ciais, P., Ek, M., Findell, K.L., Gentine, P., Lintner, B.R., 2014. Land-surface controls on afternoon precipitation diagnosed from observational data: uncertainties and confounding factors. *Atmos. Chem. Phys.*, 14, 8343–8367
- Hafkenscheid, R.L., 2000. Hydrology and biogeochemistry of tropical montane rain forests of contrasting stature in the Blue Mountains, Jamaica. PhD Thesis, Vrije Universiteit, Amsterdam, The Netherlands, pp. 302.

- Hamilton, S.K., Sippel, S.J., Melack, J.M. 2002. Comparison of inundation patterns among major South American floodplains. *J. Geophys. Res.*, 107, 8038.
- Hartanto, H., Prabhu, R., Widayat, A.S., Asdak, C., 2003. Factors affecting runoff and soil erosion: plot-level soil loss monitoring for assessing sustainability of forest management. *For. Ecol. Manage.*, 180, 361–374.
- Haurwitz, B., 1948. Isolation in relation to cloud type. *J. Meteorol.*, 5, 110–113
- Hertel, D., Leuschner, C., Holscher, D., 2003. Size and Structure of Fine Root Systems in Old-growth and Secondary Tropical Montane Forests (Costa Rica). *Biotropica*, 35, 143–153.
- Herwitz, S.R., 1985. Interception storage capacities of tropical rainforest canopy trees. *J. Hydrol.*, 77, 237–252
- Hidalgo, H.G., D.R. Cayan, and Dettinger, M.D., 2005. Sources of Variability of Evapotranspiration in California. *J. Hydrometeorol.*, 6, 3–19.
- Hijmans, R.J., Cameron, S.E., Parra, J.L., Jones, P.G., Jarvis, A., 2005. Very high resolution interpolated climate surfaces for global land areas. *Int. J. Climatol.*, 25, 1965–1978.
- Hildebrandt, A., Eltahir, E.A., 2008. Using a horizontal precipitation model to investigate the role of turbulent cloud deposition in survival of a seasonal cloud forest in Dhofar. *J. Geophys. Res.: Biogeosci.*, 113, G04028.
- Hölscher, D., Köhler, L., Kappelle, M., Leuschner, Ch., 2011. Ecology and use of old-growth and recovering montane oak forests in the Corsillera de Talamanca, Costa Rica. In: Bruijnzeel, L.A., Scatena, F.N., Hamilton, L.S. (Eds.), *Tropical Montane Cloud Forests*. Cambridge University Press, Cambridge, pp.610–617
- Hölscher, D., Köhler, L., van Dijk, A.I., Bruijnzeel, L.S., 2004. The importance of epiphytes to total rainfall interception by a tropical montane rain forest in Costa Rica. *J. Hydrol.*, 292, 308–322
- Holwerda, F., Alvarado-Barrientos, M.S., González-Martínez, T.M., 2016. Surface energy exchange in a tropical montane cloud forest environment: Flux partitioning, and seasonal and land cover-related variations. *Agr. Forest. Meteorol.*, 228, 13–28.
- Holwerda, F., Bruijnzeel, L.A., Muñoz-Villers, L.E., Equihua, M., Asbjornsen, H., 2010. Rainfall and cloud water interception in mature and secondary lower montane cloud forests of central Veracruz, Mexico. *J. Hydrol.*, 384, 84–96.
- Hooke, R.L., Martín-Duque, J.F., 2012. Land transformation by humans: A review. *GSA Today*, 12, 4–10.
- Hu, J., Riveros-Iregui, D.A., 2016. Life in the clouds: are tropical montane cloud forests responding to changes in climate? *Oecologia*, 180, 1061–1073.
- Hu, W., Shao, M., Wang, Q., She, D., 2012. Effects of measurement method, scale, and landscape features on variability of saturated hydraulic conductivity. *J. Hydrol. Eng.*, 18, 378–386.
- Hudson R, Fraser J., 2002. Alternative methods of flow rating in small coastal streams. Forest Research Extension Note EN-014 (Hydrology). Vancouver Forest Region.

- Humphries, S., 1998. Milk cows, migrants, and land markets: unraveling the complexities of forest-to-pasture conversion in Northern Honduras. *Econ Dev Cult Change.*, 47, 95-124.
- Huwe, B., Zimmermann, B., Zeilinger, J., Quizhpe, M., Elsenbeer, H., 2008. Gradients and patterns of soil physical parameters at local, field and catchment scales. In: Beck, E., Bendix, J., Kottke, I., Makeschin, F., Mosandl, R., Gradients in a tropical mountain ecosystem of Ecuador. Springer, Berlin Heidelberg, pp. 375–386
- IGAC, 2014. Estudio General de Suelos y Zonificación de Tierras: Departamento de Casanare. Imprenta nacional de Colombia, Bogotá, pp. 416.
- Ilek, A., Kucza, J., Szostek, M., 2015. The effect of stand species composition on water storage capacity of the organic layers of forest soils. *Eur. J. For. Res.*, 134, 187–197.
- Jackson, L.J., 1975. Relationships between rainfall parameters and interception by tropical forest. *J. Hydrol.*, 24, 215–238
- Jackson, R.B., Carpenter, S.R., Dahm, C.N., McKnight, D.M., Naiman, R.J., Postel, S.L., Running, S.W., 2001. Water in a changing world. *Ecol. Appl.*, 11, 1027–1045.
- Jane GT, Green TGA. 1985. Patterns of stomatal conductance in six evergreen tree species from a New Zealand cloud forest. *Bot. Gaz.*, 146, 413–420.
- Jarvis, A., Mulligan, M., 2011. The climate of cloud forests. *Hydrol. Process.*, 25, 327–343.
- Jiménez-Muñoz, J.C., Mattar, C., Barichivich, J., Santamaría-Artigas, A., Takahashi, K., Malhi, Y., Sobrino, J.A., van der Schrier, G., 2016. Record-breaking warming and extreme drought in the Amazon rainforest during the course of El Niño 2015–2016. *Sci. Rep.*, 6.
- Juvik, J.O., Nullet, D., 1995. Comments on “A Proposed Standard Fog Collector for Use in High-Elevation Regions.” *J. Appl. Meteorol.*, 34, 2108–2110.
- Kapos, V., Tanner, E. V., 1985. Water relations of Jamaican upper montane rain forest trees. *Ecology*, 66, 241–250.
- Keim, R.F., Tromp-van Meerveld, H.J., McDonnell, J.J., 2006. A virtual experiment on the effects of evaporation and intensity smoothing by canopy interception on subsurface stormflow generation. *J. Hydrol.*, 327, 352–364
- Keith, D.M., Johnson, E.A., Valeo, C., 2010. Moisture cycles of the forest floor organic layer (F and H layers) during drying. *Water Resour. Res.*, 46, W07529.
- Khain, A.P., 2009. Notes on state-of-the-art investigations of aerosol effects on precipitation: a critical review. *Environ. Res. Lett.*, 4, 015004. Kim, Y., Knox, R.G., Longo, M., Medvigy, D., Hutya, L.R., Pyle, E.H., Wofsy, S.C., Bras, R.L., Moorcroft, P.R., 2012. Seasonal carbon dynamics and water fluxes in an Amazon rainforest. *Glob. Chang. Biol.*, 18, 1322–1334.
- Kirchner, J. W., 2009. Catchments as simple dynamical systems: Catchment characterization, rainfall-runoff modeling, and doing hydrology backward. *Water Resour. Res.*, 45, W02429.
- Klaassen, W., 2001. Evaporation from rain-wetted forest in relation to canopy wetness, canopy cover, and net radiation. *Water Resour. Res.*, 37, 3227–3236

- Knapp, A.K., Beier, C., Briske, D.D., Classen, A.T., Luo, Y., Reichstein, M., Smith, M.D., Smith, S.D., Bell, J.E., Fay, P.A., Heisler, J.L., Leavitt, S.W., Sherry, R., Smith, B., Weng, E., 2008. Consequences of more extreme precipitation regimes for terrestrial ecosystems. *BioScience*, 58, 811–821.
- Lambin, E.F., Turner, B.L., Geist, H.J., Agbola, S.B., Angelsen, A., Bruce, J.W., Coomes, O.T., Dirzo, R., Fischer, G., Folke, C., George, P.S., Homewood, K., Imbernon, J., Leemans, R., Li, X., Moran, E.F., Mortimore, M., Ramakrishnan, P.S., Richards, J.F., Skånes, H., Steffen, W., Stone, G.D., Svedin, U., Veldkamp, T.A., Vogel, C., Xu, J., 2001. The causes of land-use and land-cover change: moving beyond the myths. *Glob. Environ. Chang.*, 11, 261–269.
- Latrubesse, E.M., Stevaux, J.C., Sinha, R., 2005. Tropical rivers. *Geomorphology*, 70, 187–206.
- Lawton, R.O., Putz, F.E., 1988. Natural disturbance and gap-phase regeneration in a wind-exposed tropical cloud forest. *Ecology*, 69, 764–777
- Lawton, R.O., Nair, U.S., Pielke, R.A., Welch, R.M., 2001. Climatic impact of tropical lowland deforestation on nearby montane cloud forests. *Science*, 294, 584–587.
- Letts, M.G., Mulligan, M., 2005. The impact of light quality and leaf wetness on photosynthesis in north-west Andean tropical montane cloud forest. *J. Trop. Ecol.* 21, 549–557.
- Letts, M.G., Roulet, N.T., Comer, N.T., Skarupa, M.R., Versegny, D.L., 2000. Parametrization of peatland hydraulic properties for the Canadian land surface scheme. *Atmosphere-Ocean*, 38, 141–160.
- Leuschner, C., Wiens, M., Harteveld, M., Hertel, D., Tjitrosemito, S., 2006. Patterns of Fine Root Mass and Distribution along a Disturbance Gradient in a Tropical Montane Forest, Central Sulawesi (Indonesia). *Plant Soil*, 283, 163–174.
- Levenberg, K., 1944. A method for the solution of certain non-linear problems in least squares. *Q. Appl. Math.*, 2, 164–168.
- Magrin, G.O., Marengo, J.A., Boulanger, J.-P., Buckeridge, M.S., Castellanos, E., Poveda, G., Scarano, F.R., Vicuña, S., 2014. Central and South America, in: Barros, V.R., Field, C.B., Dokken, D.J., Mastrandrea, M.D., Mach, K.J., Bilir, T.E., Chatterjee, M., Ebi, K.L., Estrada, Y.O., Genova, R.C., Girma, B., Kissel, E.S., Levy, A.N., MacCracken, S., Mastrandrea, P.R., White, L.L. (Eds.), *Climate Change 2014: Impacts, Adaptation, and Vulnerability. Part B: Regional Aspects. Contribution of Working Group II to the Fifth Assessment Report of the Intergovernmental Panel of Climate Change*. Cambridge University Press, Cambridge, United Kingdom and New York, NY, USA, pp. 1499–1566.
- Makarieva, A.M., Gorshkov, V.G., 2007. Biotic pump of atmospheric moisture as driver of the hydrological cycle on land. *Hydrol. Earth Syst. Sci. Discuss.*, 11, 1013–1033.
- Malmer, A., Murdiyarmo, D., Sampurno Bruijnzeel, L.A., Ilstedt, U., 2010. Carbon sequestration in tropical forests and water: A critical look at the basis for commonly used generalizations. *Glob. Chang. Biol.*, 16, 599–604.
- Marquardt, D.W., 1963. An algorithm for least-squares estimation of nonlinear parameters. *SIAM J. Appl. Math.*, 11, 431–441.

- Masih, I., Maskey, S., Uhlenbrook, S., Smakhtin, V., 2011. Assessing the Impact of Areal Precipitation Input on Streamflow Simulations Using the SWAT Model. *J. Am. Water Resour. Assoc.*, 47, 179–195.
- McDonnell, R.A., 2008. Challenges for integrated water resources management: How do we provide the knowledge to support truly integrated thinking?. *Int. J. Water Resour. D.*, 24, 131–143.
- McGill, R., Tukey, J.W., Larsen, W.A., 1978. Variations of box plots. *Am. Stat.*, 32, 12–16
- McInnes, K.L., Erwin, T.A., Bathols, J.M., 2011. Global Climate Model projected changes in 10 m wind speed and direction due to anthropogenic climate change. *Atmos. Sci. Lett.*, 12, 325–333.
- McMillan, H., Freer, J., Pappenberger, F., Krueger, T., Clark, M., 2010. Impacts of uncertain river flow data on rainfall-runoff model calibration and discharge predictions. *Hydrol. Process.*, 24, 1270–1284.
- McMillan, H., Krueger, T., Freer, J., 2012. Benchmarking observational uncertainties for hydrology: Rainfall, river discharge and water quality. *Hydrol. Process.*, 26, 4078–4111.
- McVicar, T.R., Körner, C., 2013. On the use of elevation, altitude, and height in the ecological and climatological literature. *Oecologia*, 171, 335–337.
- McVicar, T.R., Li, L., Van Niel, T.G., Zhang, L., Li, R., Yang, Q., Zhang, X., Mu, X., Wen, Z., Liu, W., Zhao, Y., Liu, Z., Gao, P., 2007a. Developing a decision support tool for China's re-vegetation program: Simulating regional impacts of afforestation on average annual streamflow in the Loess Plateau. *For. Ecol. Manage.*, 251, 65–81.
- McVicar, T.R., Van Niel, T.G., Li, L., Hutchinson, M.F., Mu, X., Liu, Z., 2007b. Spatially distributing monthly reference evapotranspiration and pan evaporation considering topographic influences. *J. Hydrol.*, 338, 196–220.
- McVicar, T.R., Van Niel, T.G., Li, L.T., Roderick, M.L., Rayner, D.P., Ricciardulli, L., Donohue, R.J., 2008. Wind speed climatology and trends for Australia, 1975–2006: Capturing the stilling phenomenon and comparison with near-surface reanalysis output. *Geophys. Res. Lett.*, 35, L20403.
- McVicar, T.R., Van Niel, T.G., Roderick, M.L., Li, L.T., Mo, X.G., Zimmermann, N.E., Schmatz, D.R., 2010. Observational evidence from two mountainous regions that near-surface wind speeds are declining more rapidly at higher elevations than lower elevations: 1960–2006. *Geophys. Res. Lett.*, 37, L06402.
- Meade, R., 1994. Suspended sediments of the modern Amazon and Orinoco rivers. *Quat. Int.*, 21, 29–39.
- Mejía, H.G., 2008. La geología de la región del transecto Sumapaz (Cordillera Oriental de Colombia), In: van der Hammen, T. (Ed.), La Cordillera Oriental Colombiana Transecto Sumapaz. Schweizerbart Science Publishers, Stuttgart, Germany, pp. 25–57.
- Mejía, J.F., Mesa, O.J., Poveda, G., Veléz, J., Hoyos, C.D., Mantilla, R.I., Barco, J., Cuartas, A., Montoya, M., Botero, B., 1999. Distribución espacial y ciclos anual y semianual de la precipitación en Colombia. *Dyna.*, 127, 7–24.

- Miller, C., Davenport, A., 1998. Guidelines for the calculation of wind speed-ups in complex terrain. *J. Wind Eng. Ind. Aerodyn.*, 74, 189–197.
- Minasny, B., Hartemink, A.E., 2011. Predicting soil properties in the tropics. *Earth-Science Rev.*, 106, 52–62.
- Minasny, B., McBratney, A.B., 2003. Integral energy as a measure of soil-water availability. *Plant and Soil*, 249, 253–262.
- Mohamed, Y.A., Savenije, H.H.G., Bastiaanssen, W.G.M., van den Hurk, B.J.J.M., 2006. New lessons on the Sudd hydrology learned from remote sensing and climate modeling. *Hydrol. Earth Syst. Sci.*, 10, 507–518.
- Monteith, J.L., 1965. Evaporation and environment. In: *The State and Movement of Water in Living Organisms*. In: Proceedings of the 19th symposium Soc. Exp. Biol., Swansea 1964. Academic Press, for the Society for Experimental Biology, UK, pp. 205–234.
- Monteith, J.L., 1981. Evaporation and surface temperature. *Q. J. R. Meteorol. Soc.*, 107, 1–27.
- Mosquera, G. M., Céleri, R., Lazo, P. X., Vaché, K. B., Perakis, S. S., Crespo, P., 2016. Combined use of isotopic and hydrometric data to conceptualize ecohydrological processes in a high-elevation tropical ecosystem. *Hydrol. Process.*, 30: 2930–2947.
- Motzer, T., 2005. Micrometeorological aspects of a tropical mountain forest. *Agric. For. Meteorol.*, 135, 230–240.
- Motzer, T., Munz, N., Küppers, M., Schmitt, D., Anhof, D., 2005. Stomatal conductance, transpiration and sap flow of tropical montane rain forest trees in the southern Ecuadorian Andes. *Tree Physiol.*, 25, 1283–93.
- Mualem, Y., 1976. A new model for predicting the hydraulic conductivity of unsaturated porous media. *Water Resour. Res.*, 12, 513–522.
- Mulligan, M., 2011. Modeling the tropics-wide extent and distribution of cloud forest and cloud forest loss, with implications for conservation priority. In: Bruijnzeel, L.A., Scatena, F.N., Hamilton, L.S. (Eds.), *Tropical Montane Cloud Forests*. Cambridge University Press, Cambridge, pp. 14–38.
- Mulligan, M., Burke, S.M., 2005. FIESTA: Fog Interception for the Enhancement of Streamflow in Tropical Areas, 174 pp. <http://www.ambiotek.com/fiesta>
- Mulligan, M., Jarvis, A., González, J., Bruijnzeel, L.A., 2011. Using “biosensors” to elucidate rates and mechanisms of cloud water interception by epiphytes, leaves, and branches in a sheltered Colombian cloud forest. In: Bruijnzeel, L.A., Scatena, F.N., Hamilton, L.S. (Eds.), *Tropical Montane Cloud Forests*. Cambridge University Press, Cambridge, pp. 249–260.
- Muñiz-Castro, M.-A., Williams-Linera, G., Benítez-Malvido, J., 2015. Restoring montane cloud forest: establishment of three Fagaceae species in the old fields of central Veracruz, Mexico. *Restor. Ecol.*, 23, 26–33.
- Muñoz-Villers, L.E., 2008. Efecto del cambio en el uso del suelo sobre la dinámica hidrológica y calidad del agua en el trópico húmedo del centro de Veracruz, México. Ph.D. thesis. Autonomous University of Mexico.

- Muñoz-Villers, L.E., Holwerda, F., Gómez-Cárdenas, M., Equihua, M., Asbjornsen, H., Buijnzeel, L.A., Marín-Castro, B.E., Tobón, C., 2012. Water balances of old-growth and regenerating montane cloud forests in central Veracruz, Mexico. *J. Hydrol.*, 462, 53–66.
- Muñoz-Villers, L.E., McDonnell, J.J., 2012. Runoff generation in a steep, tropical montane cloud forest catchment on permeable volcanic substrate. *Water Resour. Res.*, 48, 3543–3560.
- Muñoz-Villers, L.E., McDonnell, J.J., 2013. Land use change effects on runoff generation in a humid tropical montane cloud forest region. *Hydrol. Earth Syst. Sci.*, 17, 3543–3560.
- Muzylo, A., Llorens, P., Valente, F., Keizer, J.J., Domingo, F., Gash, J.H.C., 2009. A review of rainfall interception modelling. *J. Hydrol.*, 370, 191–206.
- Nash, J.E., Sutcliffe, J.V., 1970. River flow forecasting through conceptual models part I-A discussion of principles. *J. Hydrol.*, 10, 282–290.
- Nobre, C.A., Sellers, P.J., Shukla, J., 1991. Amazonian deforestation and regional climate change. *J. Clim.*, 4, 957–988.
- Oliveira, R.S., Eller, C.B., Bittencourt, P.R.L., Mulligan, M., 2014. The hydroclimatic and ecophysiological basis of cloud forest distributions under current and projected climates. *Ann. Bot.*, 113, 909–920.
- Pardo-Vargas, L.E., Laurance, W.F., Clements, G.R., Edwards, W., 2015. The impacts of oil palm agriculture on Colombia's biodiversity: what we know and still need to know. *Trop. Conserv. Sci.*, 88, 828–845.
- Penna, D., Brocca, L., Borga, M., Dalla Fontana, G., 2013. Soil moisture temporal stability at different depths on two alpine hillslopes during wet and dry periods. *J. Hydrol.*, 477, 55–71.
- Peña-Arancibia, J.L., Zhang, Y., Pagendam, D.E., Viney, N.R., Lerat, J., van Dijk, A.I.J.M., Vaze, J., Frost, A.J., 2015. Streamflow rating uncertainty: Characterisation and impacts on model calibration and performance. *Environ. Model. Softw.*, 63, 32–44.
- Peralta, H., Ataroff, M., 2005. Hídrica en la selva nublada de la cuenca alta del río cusiana y un pastizal de reemplazo, cordillera oriental, Colombia, in: Ataroff, M., Silva, J.F. (Eds.), ICAE. Mérida, pp. 31–36.
- Piao, S., Friedlingstein, P., Ciais, P., de Noblet-Ducoudré, N., Labat, D., Zaehle, S., 2007. Changes in climate and land use have a larger direct impact than rising CO₂ on global river runoff trends. *Proc. Natl. Acad. Sci.*, 104, 15242–15247.
- Pielke, R.A., Adegoke, J., Beltrán-Przekurat, A., Hiemstra, C.A., Lin, J., Nair, U.S., Niyogi, D., Nobis, T.E., 2007. An overview of regional land-use and land-cover impacts on rainfall. *Tellus, Ser. B Chem. Phys. Meteorol.*, 59, 587–601.
- Ponette-González, A.G., Weathers, K.C., Curran, L.M., 2010. Water inputs across a tropical montane landscape in Veracruz, Mexico: synergistic effects of land cover, rain and fog seasonality, and interannual precipitation variability. *Glob. Chang. Biol.*, 16, 946–963.

- Poveda, G., Waylen, P.R., Pulwarty, R.S., 2006. Annual and inter-annual variability of the present climate in northern South America and southern Mesoamerica. *Palaeogeogr. Palaeoclimatol. Palaeoecol.*, 234, 3–27.
- Pryet, A., Dominguez, C., Tomai, P.F., Chaumont, C., d'Ozouville, N., Villacís, M., Violette, S., 2012. Quantification of cloud water interception along the windward slope of Santa Cruz Island, Galapagos (Ecuador). *Agr. Forest. Meteorol.*, 161, 94–106.
- Quintana-Linares, A.M., 2017. Impacto de las causas próximas y subyacentes en el cambio del bosque andino y altoandino del municipio de Chámeza (Casanare-Colombia). MSc thesis. Maestría de Manejo, Uso y Conservación del Bosque. Universidad Distrital Francisco José de Caldas. pp. 86.
- Rapp, J.M., Silman, M.R., 2012. Diurnal, seasonal, and altitudinal trends in microclimate across a tropical montane cloud forest. *Clim. Res.*, 55, 17–32.
- Ravina, I., Magier, J., 1984. Hydraulic conductivity and water retention of clay soils containing coarse fragments. *Soil Sci. Soc. Am. J.*, 48, 736–740.
- Ray, D.K., Nair, U.S., Lawton, R.O., Welch, R.M., Pielke, R.A., 2006. Impact of land use on Costa Rican tropical montane cloud forests: Sensitivity of orographic cloud formation to deforestation in the plains. *J. Geophys. Res.*, 111, D02108.
- Reichstein, M., Bahn, M., Mahecha, M.D., Kattge, J., Baldocchi, D.D., 2014. Linking plant and ecosystem functional biogeography. *Proc. Natl. Acad. Sci.*, 111, 13697–13702.
- Reinhardt, K., Smith, W.K., 2008. Impacts of cloud immersion on microclimate, photosynthesis and water relations of *Abies fraseri* (Pursh.) Poiret in a temperate mountain cloud forest. *Oecologia*, 158, 229–238.
- Roa-García, M.C., Brown, S., Schreier, H., Lavkulich, L.M., 2011. The role of land use and soils in regulating water flow in small headwater catchments of the Andes. *Water Resour. Res.*, 47, W05510
- Rodríguez, E., Morris, C.S., Belz, J.E., 2006. A Global Assessment of the SRTM Performance Verification Data Sets. *Photogramm. Eng. Remote Sens.*, 72, 249–260.
- Rodríguez-Iturbe, I., 2000. Ecohydrology: A hydrologic perspective of climate-soil-vegetation dynamics. *Water Resour. Res.*, 36, 3–9.
- Roman, L., Scatena, F.N., Bruijnzeel, L.A., 2011. Global and local variations in tropical montane cloud forest soils. In: Bruijnzeel, L.A., Scatena, F.N., Hamilton, L.S. (Eds.), *Tropical Montane Cloud Forests*. Cambridge University Press, Cambridge, pp. 77–89.
- Ronayne, M.J., Houghton, T.B., Stednick, J.D., 2012. Field characterization of hydraulic conductivity in a heterogeneous alpine glacial till. *J. Hydrol.*, 458, 103–109.
- Rubio-Rivas, P., 2008. Los suelos del transecto Sumapaz. In: van der Hammen, T. (Ed.), *La Cordillera Oriental Colombiana, Transecto Sumapaz. Studies on Tropical Andean Ecosystems*, Berlin-Stuttgart, pp. 59–142.
- Rudiyanto, Minasny, B., Setiawan, B. I., 2016. Further results on comparison of methods for quantifying soil carbon in tropical peats. *Geoderma*, 269, 108–111.

- Rutter, A.J., Kershaw, K.A., Robins, P.C. and Morton, A.J., 1971. A predictive model of rainfall interception in forests, I. Derivation of the model from observations in a plantation of Corsican pine. *Agr. Meteorol.*, 9, 367–384.
- Rutter, A.J., Morton, A.J., Robins, P.C., 1975. A predictive model of rainfall interception in forests. II. Generalization of the model and comparison with observations in some coniferous and hardwood stands. *J. Appl. Ecol.*, 12, 367–380.
- Rutter, A.J. and Morton, A.J., 1977. A predictive model of rainfall interception in forests. III. Sensitivity of the model to stand parameters and meteorological variables. *J. Appl. Ecol.*, 14, 567–588.
- Sandel, B., Svenning, J., 2013. Human impacts drive a global topographic signature in tree cover. *Nat. Commun.* 4, 2474.
- Scatena, F., Bruijnzeel, L., Bubba, P., Das, S., 2011. Setting the stage, In: L. A. Bruijnzeel et al. (Eds.) Tropical Montane Cloud Forests. International Hydrology Series. Cambridge: Cambridge University Press. pp. 3–13
- Schaap, M.G., Leij, F.J., van Genuchten, M.T., 2001. Rosetta: a Computer Program for Estimating Soil Hydraulic Parameters with Hierarchical Pedotransfer Functions. *J. Hydrol.*, 251, 163–176.
- Schawe, M., Gerold, G., Bach, K., 2011. Hydrometeorological patterns in relation to montane forest types along an elevational gradient in the Yungas of Bolivia. In: L. A. Bruijnzeel et al. (Eds.) Tropical Montane Cloud Forests. International Hydrology Series. Cambridge: Cambridge University Press. pp. 199–207
- Schawe, M., Glatzel, S., Gerold, G., 2007. Soil development along an altitudinal transect in a Bolivian tropical montane rainforest: Podzolization vs. hydromorphy. *Catena*, 69, 83–90.
- Schellekens, J., Scatena, F.N., Bruijnzeel, L.A., van Dijk, A.I.J.M., Groen, M.M.A., van Hogezaand, R.J.P., 2004. Stormflow generation in a small rainforest catchment in the Luquillo Experimental Forest, Puerto Rico. *Hydrol. Process.*, 18, 505–530.
- Schellekens, J., Scatena, F.N., Bruijnzeel, L.A., Wickel, A.J., 1999. Modelling rainfall interception by a lowland tropical rain forest in northeastern Puerto Rico. *J. Hydrol.*, 225, 168–184.
- Scholl, M., Eugster, W., Burkard, R., 2011. Understanding the role of fog in forest hydrology: stable isotopes as tools for determining input and partitioning of cloud water in montane forests. *Hydrol. Process.*, 25, 353–366.
- Sevruk, B., Zahlavova, L., 1994. Classification system of precipitation gauge site exposure: Evaluation and application. *Int. J. Climatol.*, 14, 681–689.
- Sheil, D., Murdiyarso, D., 2009. How Forests Attract Rain: An Examination of a New Hypothesis. *Bioscience*, 59, 341–347.
- Shukla, J., Nobre, C. and Sellers, P., 1990. Amazon deforestation and climate change. *Science*, 247, 1322–1325.
- Šimůnek, J., Šejna, M., Saito, H., Sakai, M., van Genuchten, M.T., 2013. The HYDRUS software package for simulating two-and three-dimensional movement of water, heat, and multiple solutes in variably-saturated media, Technical manual, version 4.16. Department of Environmental Sciences, University of California Riverside, Riverside, California.

- Slingo, J.M., 2007. The Development and Verification of a Cloud Prediction Scheme For the Ecmwf Model. *Q. J. R. Meteorol. Soc.*, 113, 899–927.
- Spracklen, D. V., Arnold, S.R., Taylor, C.M., 2012. Observations of increased tropical rainfall preceded by air passage over forests. *Nature*, 489, 282–285.
- Stallard, R., Koehnken, L., Johnsson, M., 1991. Weathering processes and the composition of inorganic material transported through the Orinoco River system, Venezuela and Colombia. *Geoderma*, 51, 133–165.
- Stevenson, P., Casas, L., 2008. Plantas del norte del municipio de Chámeza. In: Ramírez, B. (Ed), Informe Técnico “Levantamiento y análisis de información necesaria para la elaboración del plan de acción que permita obtener la declaratoria de área protegida del bosque ubicado al norte del municipio de Chámeza”. Asociación de Becarios de Casanare y Municipio de Chámeza, pp. 31–36
- Still, C., Foster, P., Schneider, S., 1999. Simulating the effects of climate change on tropical montane cloud forests. *Nature*, 398, 15–17.
- Suryatmojo, H., Fujimoto, M., Kosugi, K., Mizuyama, T., 2014. Runoff and soil erosion characteristics in different periods of an intensive forest management system in a tropical Indonesian rainforest. *Int. J. Sustain. Dev. Plan.*, 9, 830–846.
- Tanaka, N., Kuraji, K., Tantasirin, C., Takizawa, H., Tangtham, N., Suzuki, M., 2011. Relationships between rainfall, fog and throughfall at a hill evergreen forest site in northern Thailand. *Hydrol. Process.*, 25, 384–391.
- Tanaka, K., Takizawa, H., Tanaka, N., Kosaka, I., Yoshifuji, N., Tantasirin, C., Piman, S., Suzuki, M., Tangtham, N., 2003. Transpiration peak over a hill evergreen forest in northern Thailand in the late dry season: assessing the seasonal changes in evapotranspiration using a multilayer model. *J. Geophys. Res.: Atmos.*, 108, 4533.
- Tanner, E.V.J., 1977. Four montane rain forests of Jamaica: a quantitative characterization of the floristics, the soils and the foliar mineral levels, and a discussion of the interrelations. *J. Ecol.*, 883–918.
- Tanner, E.V.J., Vitousek, P.M., Cuevas, E., 1998. Experimental Investigation of Nutrient Limitation of Forest Growth on Wet Tropical Mountains. *Ecology*, 79, 10–22.
- Teuling, A.J., Taylor, C.M., Meirink, J.F., Melsen, L.A., Miralles, D.G., Van Heerwaarden, C.C., Vautard, R., Stegehuis, A.I., Nabuurs, G.J. and de Arellano, J.V.G., 2017. Observational evidence for cloud cover enhancement over western European forests. *Nat. Commun.*, 8.
- Teuling, A.J., Seneviratne, S.I., Stöckli, R., Reichstein, M., Moors, E., Ciais, P., Luyssaert, S., Van Den Hurk, B., Ammann, C., Bernhofer, C., Dellwik, E., 2010. Contrasting response of European forest and grassland energy exchange to heatwaves. *Nat. Geosci.*, 3, 722–727.
- Teuling, A.J., Uijlenhoet, R., Hupet, F., Van Loon, E.E., Troch, P.A., 2006. Estimating spatial mean root-zone soil moisture from point-scale observations. *Hydrol. Earth Syst. Sci. Discuss.*, 3, 1447–1485.
- Teuling, A. J., Uijlenhoet, R., van den Hurk, B., Seneviratne, S. I., 2009. Parameter sensitivity in LSMs: An analysis using stochastic soil moisture models and ELDAS soil parameters. *J. Hydrometeorol.*, 10, 751–765

- Thornton, P.E., Running, S.W., 1999. An improved algorithm for estimating incident daily solar radiation from measurements of temperature, humidity, and precipitation. *Agric. For. Meteorol.*, 93, 211–228.
- Tobón, C., Bruijnzeel, L.A., Frumau, K.F.A., Calvo-Alvarado, J.C., 2011. Changes in soil physical properties after conversion of tropical montane cloud forest to pasture in northern Costa Rica. In: Bruijnzeel, L.A., Scatena, F.N., Hamilton, L.S. (Eds.), *Tropical Montane Cloud Forests*. Cambridge University Press, Cambridge, pp. 502–515.
- Tobón, C., Köhler, L., Frumau, K.F.A., Bruijnzeel, L.A., Burkard, R. and Schmid, S., 2011. Water dynamics of epiphytic vegetation in a lower montane cloud forest: fog interception, storage and evaporation. In: Bruijnzeel, L.A., Scatena, F.N., Hamilton, L.S. (Eds.), *Tropical Montane Cloud Forests*. Cambridge University Press, Cambridge, pp. 261–267.
- Tomkins, K.M., 2014. Uncertainty in streamflow rating curves: methods, controls and consequences. *Hydrol. Process.*, 28, 464–481.
- USDA, 2010. *Keys to Soil taxonomy*, 11th ed. Blacksburg, Virginia.
- USGS, 2014. Shuttle Radar Topography Mission, 1 Arc Second scene SRTM1N05W073V3, Global Land Cover Facility, University of Maryland, College Park, Maryland, February 2000.
- Vachaud, G., Passerat de Silans, A., Balabanis, P., Vauclin, M., 1985. Temporal stability of spatially measured soil water probability density function. *Soil Sci. Soc. Am. J.*, 49, 822–828.
- van der Molen, M.K., Dolman, A.J., Waterloo, M.J., Bruijnzeel, L.A., 2006. Climate is affected more by maritime than by continental land use change: A multiple scale analysis. *Glob. Planet. Change*, 54, 128–149.
- Van der Ploeg, M.J., Appels, W.M., Cirkel, D.G., Oosterwoud, M.R., Witte, J.P., Van der Zee, S.E.A.T.M., 2012. Microtopography as a driving mechanism for ecohydrological processes in shallow groundwater systems. *Vadose Zone J.*, 11.
- Van Dijk, A.I.J.M., Peña-Arancibia, J.L., 2012. Land cover and water yield: inference problems when comparing catchments with mixed land cover. *Hydrol. Earth Syst. Sc.*, 16, 3461–3473.
- van Genuchten, M.T., 1980. A closed-form equation for predicting the hydraulic conductivity of unsaturated soils. *Soil Sci. Soc. Am. J.*, 44, 892–898.
- van Genuchten, M.T., 1985. Convective-dispersive transport of solutes involved in sequential first-order decay reactions. *Comput. Geosci.*, 11, 129–147.
- van Genuchten, M.T., Leij, F.J., Yates, S.R., 1991. The RETC code for quantifying the hydraulic functions of unsaturated soils. Robert S. Kerr Environmental Research Laboratory.
- Veihmeyer, F.J., Hendrickson, A.H. 1931. The moisture equivalent as a measure of the field capacity of soils. *Soil Sci.*, 32, 181–193.
- Veneklaas, E.J., Van Ek, R., 1990. Rainfall interception in two tropical montane rain forests, Colombia. *Hydrol. Process.*, 4, 311–326.

- Villegas, J.C., Tobón, C., Breshears, D.D., 2008. Fog interception by non-vascular epiphytes in tropical montane cloud forests: dependencies on gauge type and meteorological conditions. *Hydrol. Process.*, 22, 2484–2492.
- Vina, A., Cavelier, J., 1999. Deforestation rates (1938–1988) of tropical lowland forests on the Andean foothills of Colombia. *Biotropica*, 31, 31–36.
- Viviroli, D., Archer, D.R., Buytaert, W., Fowler, H.J., Greenwood, G.B., Hamlet, A.F., Huang, Y., Koboltschnig, G., Litaor, M.I., Lopez-Moreno, J.I., Lorentz, S., Schädler, B., Schreier, H., Schwaiger, K., Vuille, M., Woods, R., 2011. Climate change and mountain water resources: Overview and recommendations for research, management and policy. *Hydrol. Earth Syst. Sci.*, 15, 471–504.
- Viviroli, D., Dürr, H., 2007. Mountains of the world, water towers for humanity: Typology, mapping, and global significance. *Water Resour.*, 43, W07447.
- Viviroli, D., Weingartner, R., 2004. The hydrological significance of mountains: from regional to global scale. *Hydrol. Earth Syst.*, 8, 1016–1029.
- Vörösmarty, C.J., Green, P., Salisbury, J., Lammers, R.B., 2000. Global water resources: vulnerability from climate change and population growth. *Science*, 289, 284–288.
- Vrugt, J.A., Dekker, S.C., Bouten, W., 2003. Identification of rainfall interception model parameters from measurements of through-fall and forest canopy storage. *Water Resour. Res.*, 39, 1251–1259.
- Wagener, T., Sivapalan, M., Troch, P.A., McGlynn, B.L., Harman, C.J., Gupta, H. V., Kumar, P., Rao, P.S.C., Basu, N.B., Wilson, J.S., 2010. The future of hydrology: An evolving science for a changing world. *Water Resour. Res.*, 46, W05301.
- Wallace, J., McJannet, D., 2010. Processes controlling transpiration in the rainforests of North Queensland. *Aust. J. Hydrol.*, 384, 107–117.
- Walther, G.-R., Post, E., Convey, P., Menzel, A., Parmesan, C., Beebee, T.J.C., Fromentin, J.M., Hoegh-Guldberg, O., Bairlein, F., 2002. Ecological responses to recent climate change. *Nature*, 416, 389–395.
- Wechsler, S., Kroll, C., 2006. Quantifying DEM uncertainty and its effect on topographic parameters. *Photogramm. Eng.*, 72, 1081–1090.
- Weiss, M., Baret, F., 2014. CAN-EYE user manual
- White, B., 2012. Agriculture and the generation problem: rural youth, employment and the future of farming. *IDS Bull.*, 43, 9–19.
- Wilcke, W., Boy, J., Goller, R., Fleischbein, K., Valarezo, C., Zech, W., 2011. Effect of topography on soil fertility and water flow in an Ecuadorian lower montane forest. In: Bruijnzeel, L.A., Scatena, F.N., Hamilton, L.S. (Eds.), *Tropical Montane Cloud Forests*. Cambridge University Press, Cambridge, pp. 402–409
- Wilcke, W., Valladares, H., Stoyan, R., Yasin, S., Valarezo, C., Zech, W., 2003. Soil properties on a chronosequence of landslides in montane rain forest, Ecuador. *CATENA*, 53, 79–95.
- Wilcke, W., Yasin, S., Schmitt, A., Valarezo, C., Zech, W., 2008. Soils along the altitudinal transect and in catchments, In: Beck, E., Bendix, J., Kottke, I., Makeschin, F., Mosandl, R., *Gradients in a tropical mountain ecosystem of Ecuador*. Springer, Berlin Heidelberg, pp. 75–86.

- Williams, C.A., Reichstein, M., Buchmann, N., Baldocchi, D., Beer, C., Schwalm, C., Wohlfahrt, G., Hasler, N., Bernhofer, C., Foken, T., Papale, D., Schymanski, S., Schaefer, K., 2012. Climate and vegetation controls on the surface water balance: Synthesis of evapotranspiration measured across a global network of flux towers. *Water Resour. Res.*, 48, W06523.
- Wösten, J.H., Lilly, A., Nemes, A., Le Bas, C., 1999. Development and use of a database of hydraulic properties of European soils. *Geoderma*, 90, 169–185.
- Wösten, J.H.M., Pachepsky, Y.A., Rawls, W.J., 2001. Pedotransfer functions: bridging the gap between available basic soil data and missing soil hydraulic characteristics. *J. Hydrol.*, 251, 123–150.
- Wullaert, H., Pohlert, T., Boy, J., Valarezo, C., Wilcke, W., 2009. Spatial through-fall heterogeneity in a montane rain forest in Ecuador: Extent, temporal stability and drivers. *J. Hydrol.*, 377, 71–79.
- Yang, D., Ishida, S., Goodison, B.E., Gunther, T., 1999. Bias correction of daily precipitation measurements for Greenland. *J. Geophys. Res. Atmos.*, 104, 6171–6181.
- Yang, F., Zhang, G.-L., Yang, J.-L., Li, D.-C., Zhao, Y.-G., Liu, F., Yang, R.-M., Yang, F., 2014. Organic matter controls of soil water retention in an alpine grassland and its significance for hydrological processes. *J. Hydrol.*, 519, 3086–3093.
- Zadroga, F., 1981. The hydrological importance of a montane cloud forest area of Costa Rica. In: Lal, R., Russell, E.W. (Eds.), *Tropical Agricultural Hydrology*. Wiley, New York, pp. 59–73.
- Zevenbergen, L.W., Thorne, C.R., 1987. Quantitative analysis of land surface topography. *Earth Surface Processes and Landforms*, 12, 47–56.
- Zhang, L., Dawes, W.R., Walker, G.R., 2001. Response of mean annual evapotranspiration to vegetation changes at catchment scale. *Water Resour. Res.*, 37, 701–708.
- Zhang, R., 1997. Determination of Soil Sorptivity and Hydraulic Conductivity from the Disk Infiltrometer. *Soil Sci. Soc. Am. J.*, 61, 1024–1030.
- Zhao, F., Xu, Z., Zhang, L., 2012. Changes in streamflow regime following vegetation changes from paired catchments. *Hydrol. Process.*, 26, 1561–1573.
- Zimmermann, B., Elsenbeer, H., Moraes, J. De, 2006. The influence of land-use changes on soil hydraulic properties: implications for runoff generation. *For. Ecol.*, 222, 29–38.
- Zotz, G., Tyree, M.T., Patino, S., Carlton, M.R., 1998. Hydraulic architecture and water use of selected species from a lower montane forest in Panama. *Trees*, 12, 302–309.

Acknowledgements

Not a single outcome of this thesis would have been possible if I had not received the support from all the people that were involved throughout the process. In the University and in field I found the help and inspiration from family, friends, colleagues and even strangers to move forward in this extremely interesting and challenging period.

I begin by thanking Laurens, Ryan and Rik for their patience and for sharing with me their vast knowledge. I really appreciate the freedom and advice you gave me to design and developed this research that I imagined six years ago. Along the way, Martine and Lieke complemented the team and provided the extra knowledge to dive into the exciting realm of soils and modelling. I am very grateful to all members of the Water System and Global Change group; you were always there making sure I kept on track. Also to the people from HQWM and SLM groups for inviting me to participate in your inspiring writing weeks and lab meetings. To Harm Gooren and Eef Velthorst for their help in the soil labs and Paul Torfs for his great help with modelling and statistics. Life in Wageningen would not have been as wonderful if it was not for Lina K and Martin, Emma, Deborah, Somayeh, Zamira, Tanya, Dan, Long, Geoffrey and Marleen.

This project was possible thanks to the funding from Colciencias, Equión Energía and the municipality of Chámeza. Conrado Tobón, thank you very much for your help in guiding the proposal for Colciencias. From Equión Energía. I would also like to thank Germán García, Ricardo Sandoval, Alejandro Rodríguez, Marco Vinicio Cárdenas, Claudia Cifuentes and Rafael Calixto and Carlos Velasco. I sincerely thank all the council members of Chámeza and Dr. Jorge Iván for supporting this project.

Field work was extremely challenging and it demanded a lot of creativity and endurance. Without the ideas and help of Carlos Roa, Wilson Mendieta, William Amaya, Luis

Barahona, Sergio Estrada, Leonardo Becerra, Jesús Holguín, José, Reinel and Joselín Perez, Aulí Castañeda, Olivo Pérez, Norelia Barreto, Rolando and Marlon Zamudio and Fludelvía Echeverría, there would be no setup. Special thanks to all field assistants, who bared with me the long rainy days, the heavy loads and risks: Manuel Montaña, John Cubides, Andrés, Kevin, Dora, Angie, Yanet, Bayona, Carolina, Adelina, Melesio, Rossana, Milton, Yesid and Víctor. And to all that provided support in many other ways: Patricia Castañeda, Inés Barrera, Mauricio Vallejo, Pastor Piñeros, Luis Arturo Jimenez, Presentación, Brisas y Nelson, Luis Arturo Acosta, Maria Rosario Rodríguez, Siervo Moreno, Ema Vargas, Steven, Odilia and all other Chamezans that gave me a hand along the way.

In order for the project to keep running while I was either in the Netherlands or in Chámeza the continuous and unconditional help from my parents and Anita, and the directive and administrative team (Pili, Denis, Fabio, Christian and Nayibe) from ABC were fundamental. It always seemed as if I was in all places at once. I like boasting of my solution-finding abilities, but in reality no thought-of solution would have been possible if you were not there to give me a hand.

Sergio and Ana Cristina I am glad we are all going simultaneously through the same stages of life. This way we get to complain, celebrate and provide support to each other. Sergio, this project began the night we set up the first meteorological station, now it is almost over. Are you ready for the next stage? Ana S. thank you for your support and company in these last years, it has been very amusing! Cheita, Zania, Natalia, Nelsy, Marce, Andrea, Ivonne, Patricio, Jorge, Tere, Aspasia and Camilo, thanks for your constant support. To my mom and dad, you know all my achievements are always inspired by you.

About the Author



Name:	Beatriz Helena Ramírez Correal
Born:	18 September in Bogotá, Colombia
Bachelor of Science (1999-2004):	Biology, Universidad de los Andes
BSc thesis:	Seed dispersal of <i>Astrocaryum chambira</i> (Arecaceae) in two <i>terra firme</i> forests under different degree of antropic intervention at the indigenous community of Macedonia, Amazonas (Colombia).
Master of Science (2005-2007):	Ecology and Evolution, Institute for Biodiversity and Ecosystem Dynamics, Universiteit van Amsterdam (<i>cum laude</i>). Alban Programme and Nuffic-Huygens Scholarships.
MSc thesis:	Seedling performance on different flooding gradients in north eastern Colombian Amazonia
Work experience (2008-2013):	Head of the Biodiversity Area and Associate, Asociación de Becarios de Casanare-ABC, Colombia.
PhD (2013-2018):	Water Systems and Global Change, Wageningen University. Colciencias Scholarship.
PhD education:	See page 208



*Netherlands Research School for the
Socio-Economic and Natural Sciences of the Environment*

D I P L O M A

For specialised PhD training

The Netherlands Research School for the
Socio-Economic and Natural Sciences of the Environment
(SENSE) declares that

Beatriz Helena Ramirez Correal

born on 18 September 1981 in Bogotá, Colombia

has successfully fulfilled all requirements of the
Educational Programme of SENSE.

Wageningen, 30 January 2017

the Chairman of the SENSE board

Prof. dr. Huub Rijnaarts

the SENSE Director of Education

Dr. Ad van Dommelen

The SENSE Research School has been accredited by the Royal Netherlands Academy of Arts and Sciences (KNAW)



K O N I N K L I J K E N E D E R L A N D S E
A K A D E M I E V A N W E T E N S C H A P P E N



The SENSE Research School declares that Ms Beatriz Ramirez Correal has successfully fulfilled all requirements of the Educational PhD Programme of SENSE with a work load of 39.5 EC, including the following activities:

SENSE PhD Courses

- o Environmental research in context (2013)
- o Scales and dimensions of sustainability: A system perspective (2013)
- o Water and global change: Modelling semi-arid grazing systems (2013)
- o Research in context activity: 'Active participation in and communication around Chámeza's Peace Week: What am I willing to do for peace and how is this relevant for sustainable development?' (2014)

Other PhD and Advanced MSc Courses

- o Data management, Wageningen University (2013)
- o Introduction to R for statistical analysis, Wageningen University (2013)
- o Where there is little data: How to estimate design variables in poorly gauged basins, UNESCO-IHE (2014)
- o Authorship rights, Dirección Nacional del Derecho de Autor [*National Directorate of Copyright*] (2015)

External training at a foreign research institute

- o Training on the setup, installation and maintenance of hydro-meteorological equipment, Coltein Ltda, Bogotá, Colombia (2013)
- o Training on soil particle analysis through laser diffraction and water retention curves for organic soils, Wageningen University (2014)
- o Water Balance Simulation Model (WASIM) training, Technische Universität München (2015)

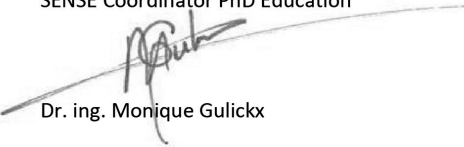
Management and Didactic Skills Training

- o Board member of Asociación de Becarios de Casanare ABC [*Association of Scholars of Casanare*], non-governmental organisation on education and communication of authentic development and environmental governance (2013-2016)
- o Supervising MSc student with fieldwork for thesis entitled 'Streamflow behaviour in tropical montane cloud forests in Chámeza, Colombia' (2014)
- o Supervising MSc student with thesis entitled 'Impact of the patterns and processes of change on forest cover at the municipal level' (2015)

Selection of Oral Presentations

- o *Hydro-meteorological functioning of the eastern Andean tropical montane cloud forests: Insight from a paired catchment study in the Orinoco river basin highlands*. European Geosciences Union (EGU) annual meeting 2016, 17-22 April 2016, Vienna, Austria
- o *Hydro-meteorological spatio-temporal variability in an eastern Andean tropical montane cloud forest (Orinoco river basin)*. Association for Tropical Biology and Conservation (ATBC) annual meeting, 18-23 June 2016, Montpellier, France

SENSE Coordinator PhD Education



Dr. ing. Monique Gulickx

The research described in this thesis was financially supported by Colciencias (Colombian Department for the Administration of Science, Technology and Innovation; Call 529-2011), Equion Energía (Solped: 14-01-2014-4000000215), Municipality of Chámeza (Cooperation agreement 004-2014) and Asociación de Becarios de Casanare-ABC.

Financial support from Wageningen University for printing this thesis is gratefully acknowledged

